
# COMPARATIVE STUDY OF DIFFERENT SPATIAL RESOLUTION DEM AND DIFFERENT GIS-BASED STATISTICAL MODELS FOR LANDSLIDE SUSCEPTIBILITY MAPPING AT OSSEY WATERSHED AREA IN BHUTAN

THONGLEY -

A Thesis Submitted to the Graduate School of Naresuan University
in Partial Fulfillment of the Requirements
for the Master of Science in (Geographic Information Science)
2020

# COMPARATIVE STUDY OF DIFFERENT SPATIAL RESOLUTION DEM AND DIFFERENT GIS-BASED STATISTICAL MODELS FOR LANDSLIDE SUSCEPTIBILITY MAPPING AT OSSEY WATERSHED AREA IN BHUTAN

THONGLEY -

A Thesis Submitted to the Graduate School of Naresuan University
in Partial Fulfillment of the Requirements
for the Master of Science in (Geographic Information Science)
2020

Thesis entitled "Comparative study of different spatial resolution DEM and different GIS-based statistical models for landslide susceptibility mapping at Ossey watershed area in Bhutan"

By THONGLEY -

has been approved by the Graduate School as partial fulfillment of the requirements for the Master of Science in Geographic Information Science of Naresuan University

**Oral Defense Committee**

..... Chair
(Associate Professor Dr. Chalermchai Pawattana, D.Eng.)

..... Advisor
(Assistant Professor Chaiwiwat Vansarochana, D. Tech Sci.)

..... Co Advisor
( Polpreecha Chidburee, Ph.D.)

..... Co Advisor
(Assistant Professor Wanwisa Pansak, Ph.D.)

..... Internal Examiner
(Associate Professor Pathana Rachavong)

**Approved**

.....
(Professor Paisarn Muneesawang, Ph.D.)

Dean of the Graduate School

| | |
|---|---|
| **Title** | COMPARATIVE STUDY OF DIFFERENT SPATIAL RESOLUTION DEM AND DIFFERENT GIS-BASED STATISTICAL MODELS FOR LANDSLIDE SUSCEPTIBILITY MAPPING AT OSSEY WATERSHED AREA IN BHUTAN |
| **Author** | THONGLEY - |
| **Advisor** | Assistant Professor Chaiwiwat Vansarochana, D. Tech Sci. |
| **Co-Advisor** | Polpreecha Chidburee, Ph.D. , Assistant Professor Wanwisa Pansak, Ph.D. |
| **Academic Paper** | Thesis M.S. in Geographic Information Science, Naresuan University, 2020 |
| **Keywords** | Landslide map, Spatial resolution DEM, GIS-Based statistical model |

## ABSTRACT

Landslide is one of the most frequent disasters at the Ossey watershed area in Bhutan causing inconvenience to the local people, financial losses, and claiming the lives of the people every year. This study aim to developing Landslide Susceptibility Mapping (LSM) at the Ossey watershed area in Bhutan and find the magnitude of impact of factors on the landslide by the factors. This study compares the accuracy of the different bivariate statistical models and the different spatial resolution on the accuracy of the LSM using various statistical methods.

The landslide inventory was done using the sentinel-2 imagery data, google earth image and field investigation. A total of 164 landslide locations were identified during landslide inventory of which 70% (115 landslide) were used for training datasets and the remaining 30% (49 locations) for the validation dataset. The LSM was developed using the fifteen factors which are derived from DEMs (ALOS PALSAR and SRTM), geological map of Bhutan, sentinel 2 data, digital topographic map of Bhutan, and rainfall data from Bhutan. All the influencing factors were resampled into three spatial resolutions namely to 12.5m, 30m, and 90m.

Three primary models were used to develop LSM which includes 1) Frequency Ratio (FR), 2) Index of Entropy (IOE), and 3) Weight of Evidence (WOE). The primary models were combined to form hybrid models which includes Frequency Ratio-Index of Entropy (FR-IOE), Index of Entropy, and Weight of Evidence (IOE-WOE), and Weight of Evidence and Frequency Ratio (WOE-FR). The LSM was developed using three different spatial resolutions for individual primary and hybrid models. All the LSM developed using various models were classified into five classes using the natural break classification to check area variation in different landslide zone.

The LSMs was validated using sensitivity, specificity, accuracy, Kappa index, Area Under the Curve (AUC), Root Mean Square Error (RMSE). The sensitivity shows degree of correctly classified landslide pixel, specificity shows degree of correctly classified non-landslide pixel, accuracy shows the proportion of correctly classified landslide and non-landslide pixel, kappa index shows the reliability of the models, AUC shows prediction rate and RMSE shows the relative error between the models. The WOE and its hybrid models shows better accuracy in all the validation parameters. The highest sensitivity (0.8095) corresponds to WOE, IOE-WOE and WOE-FR, highest accuracy for WOE-FR(0.7925), highest Kappa index for WOE-FR(0.5850), highest AUC for 0.8817(WOE and IOE-WOE), and the lowest RMSE for WOE(0.3722). This clearly shows that WOE is best model due to its superior accuracy. Moreover, when WOE is combined with other inferior models, it increases the accuracy.

Regarding the deviation of accuracy using different accuracy parameters, it was observed that finer spatial resolution is much better than the coarse spatial resolution with higher sensitivity, specificity, accuracy, kappa index, AUC and lower RMSE.

The results are expected to help researchers to understand how the accuracy deviates with the change in spatial resolution and to choose the best bivariate statistical analysis. The resultant maps are expected to provide a technical guide for the planners, decision-makers, and engineers for future developmental activities at the Ossey watershed area.

# ACKNOWLEDGEMENTS

Firstly, I would like to express my sincere gratitude to my advisor Assistant Professor Captain Dr. Chiwiwat Vansarochana, co-advisor Assistant Professor Dr. Wanwisa Pansak, and Dr. Polpreecha Chidburee for their valuable suggestions, encouragement, and inspiring motivation during the entire research period. This thesis would never be accomplished without their constant support and guidance throughout the research period.

My heartfelt gratitude goes to His Majesty the King of Bhutan and Naresuan University, Thailand for giving me the scholarship and financial support to pursue my postgraduate in Master of Science in Geographic Information Science. I also would like to thank the Royal University of Bhutan for granting me two years of study leave to undergo my studies.

Let me not forget to acknowledge Faculty of Agriculture, Natural Resources and Environment, the graduate school, Naresuan University and my colleagues for making a friendly environment during my stay at the university. I also would like to thank the Department of Geology and Mine of Bhutan, National Center for Hydrology and Meteorology of Bhutan, and other agencies for providing me the dataset for my research.

I would like to thank my mother, and relatives for their encouragement throughout my study period and of course my roommates for giving me moral supports and creating a friendly atmosphere. Finally, I would like to thank my wife for constant support, encouragement and most importantly her understanding and love.

THONGLEY -

# TABLE OF CONTENTS

**Page**

# List of Table

**Page**

# List of figures

**Page**

# LIST OF ABBREVIATIONS

| Abbreviation | Terms |
|---|---|
| LSM | Landslide susceptibility mapping |
| EM-DAT | Emergency Events Database |
| DEM | Digital Elevation Model |
| NAPA | National Adaptation Programme of Actions |
| FR | Frequency Ratio |
| IOE | Index of Entropy |
| WOE | Weight of Evidence |
| FR-IOE | Frequency Ratio-Index of Entropy |
| IOE-WOE | Index of Entropy-Weight of Evidence |
| WOE-FR | Weight of Evidence-Frequency Ratio |
| ROC | Receiver Operating Characteristic |
| AUC | Area Under the Curve |
| RMSE | Root Mean Square Error |
| TP | True Positive |
| FP | False Positve |
| TN | True Negative |
| FN | False Negative |
| NCHM | National Center for Hydrology and Meteorology |
| STRM | Shuttle Radar Topography Mission Digital Elevation Model |
| NASA | National Aeronautics and Space Administration |
| NGA | National Geospatial-Intelligence Agency |

| | |
|---|---|
| ESA | European Space Agency |
| GIS | Geographic Information System |
| GPS | Global Positioning System |
| DGM | Department of Geology and Mine |
| NLC | National Land Commission |
| TWI | Topographic Wetness Index |
| SPI | Stream Power Index |
| NDVI | Normalized Difference Vegetation Index |
| NDSI | Normalized Difference Soil Index |
| LULC | Land Use Land Cover |
| NIR | Near-Infrared |
| SWIR | Short Wave infrared |

# CHAPTER I
# INTRODUCTION

## 1.1 Background

Landslide is defined as the downward and outward movement of the slope-forming materials composed of natural rocks, soils, artificial fills, or a combination of these materials (Varnes, 1958). Landslide is the most complex natural geo-hazard which causes devastation, incurred millions of financial losses, and affects developmental activities especially in the steep and rugged terrain (Khan *et al.*, 2019). The landslide causes fatalities, tremendous property destruction, economic losses, and inconveniences (Wang, Sawada, and Moriguchi, 2011). The landslides are mainly due to the results of the interplay of the number of natural and man-made factors (Achour *et al.*, 2017).

It is important to understand the characteristics and mechanisms of individual landslides (He, Hu, Sun, Zhu, and Liu, 2019). The accurate representation of the landslide susceptible area which is prepared systemically will assist in reducing professional intervention for the decision-makers (Barella, Sobreira, and Zêzere, 2019). The Landslide Susceptibility Mapping (LSM) at the regional scale is of great importance to identify the risk, mitigation, land management, and planning in rugged terrain (Sun *et al.*, 2018). The effective landslide risk map enables decision-makers for the fund allocation for risk management (Akgun, Kıncal, and Pradhan, 2012). However, it is still challenging work to create reliable spatial prediction and assessment of landslide due to the complex nature of influencing factors and human activities (Zhao, Wang, Jiang, Liu, and Wei, 2019).

The LSM is one of the preliminary steps to avoid losses. The LSM requires different datasets. Among the various data Digital Elevation Model (DEM) is one of the most important and widely used datasets for the landslide study. Most of the DEMs are freely available while few are commercial DEM. Some the DEMs has very high spatial resolution while many are of moderate resolution. Spatial resolution is very important for determining the fundamental characteristics of ground from the remote sensing data. The spatial resolution defines the smallest scale at which the actual surface

of the earth is being extracted, identified, and mapped from the remote sensing platform (Mora, Lenzano, Toth, and Grejner, 2014). The spatial resolution determines the depth of information on the real ground surface. Most of the landslide study utilized the various DEMs for deriving the primary and secondary influencing factors. However, there is minimal research on the impact of DEMs on the accuracy of the landslide studies (Mahalingam and Olsen, 2016).

### 1.2 Problem Statement

The topography of Bhutan is characterized by a moderate to the steep slope with high mountains and narrow rivers. Bhutan is characterized by extreme tectonic activity due to the collision of the Indian and Eurasian continental plates which results in the uplift of the Himalayas (National Adaptation Programme of Actions [NAPA], 2014). The mountains are predominantly made up of uplifted sedimentary and metamorphic rocks, which are very fragile and sensitive to erosion during the monsoon season. Its fragile geology makes Bhutan highly vulnerable to landslides National (NAPA, 2014). Similarly, the subtropical or alpine weathering action on unstable rocks is common in the region. This weathering action makes the region fragile and creates tension due to tectonic movement. This has resulted in weak and highly fractured rock and highly prone to landslides (Dawson, Neves, Sarkar, and Dijkstra, 2018). The steep and rugged terrain fails to hold the weak slope. The fast flowing rivers undercutting of the riverbank increasing the risk of landslides (Keunza, Dorji, and Wangda, 2004).

Bhutan is located at the foot of the giant Himalayan mountain. The giant Himalayan mountain blocks the wind which carries the clouds. This results in condensation of the cloud and falls back as very heavy precipitation during the monsoon season in Nepal, Bhutan, and India. The monsoon rainfall is one of the main triggering factors for the landslide. However, the intensity of the rainfall differs from place to place which causes differences in the event of the landslides.

The growth of the population increased pressure on the natural resources and anthropogenic activities which intensified the risk of the landslides in Bhutan (Keunza *et al.*, 2004). The developmental activities such as the construction of roads, building houses, irrigation channels, etc., are inevitable as the population size increases (Pasang and Kubíček, 2018). Similarly, there is increased pressure on natural resources such as

the extraction of stones quarry, minerals, timbers, etc. Such activities result in cutting off the toe of the slope, extensive deforestation for agriculture. Landslide of varying degrees occurs relatively more in the southern part of Bhutan. Among the many landslides risk area, the Ossey watershed area experiences one of the worst landslides in Bhutan which causes frequent blockage of the national highway every year(Thongley and Vansarochana, 2021b). Sometimes, the landslides even claim the precious life of the people and property destruction. However, there is no research carried on the landslide at the Ossey watershed area.

Regarding the datasets used for assessing the landslides, none of the scholars checked how the spatial resolution deviates the accuracy of the landslides. Generally, it is believed that the higher resolution gives greater accuracy for the landslide mapping. This study will also focus on how spatial resolution will affect the accuracy of the LSM.

### 1.3 Objectives of the study

The following are objectives framed for the research to mitigate the landslides problem

1. To find the relation between the landslide occurrences and the influencing factors
2. To develop a landslide susceptibility map using bivariate statistical models and categorize based on the severity of the landslides
3. To compare accuracy on the Landslide Susceptibility Mapping (LSM) using different spatial resolution Digital Elevation Model (DEM) using an individual statistical model
4. To assess the accuracy of the Landslide Susceptibility Mapping (LSM) using three statistical models for individual Digital Elevation Models (DEM).

### 1.4 Research Questions

The research question for the above objectives are as follow:

1. Where is the very high, high, moderate, low, and very low landslide prone zone at Ossey watershed area?
2. How does the individual influencing factors contribute to the landslides?

3. How does the spatial resolution of DEM affect the accuracy of landslide studies?
4. Which model is the most suitable for the LSM?

**1.5 Purpose of the study**

Bhutan is a mountainous country in the Himalayan region characterized by lots of steep and rugged slopes. The orographic effect of the great Himalayan mountain results in very heavy rainfall in Bhutan. The average annual rainfall ranges from about 500mm/year in northern and as high as 5000 mm/year in the southern part of Bhutan. Due to the convergence of the Euro-Asian plates, the Himalayan is a relatively new mountain with loose sedimentary rocks. The combination of loose rocks, heavy rainfall, and the steep slopes result in the chronic landslides during the monsoon season.

Although Bhutan is one of the top landslide prone areas in the South Asian country, Bhutan doesn't have a landslide susceptibility map which will assist in the planning and development of the infrastructure. Moreover, even though some parts of Bhutan is one of the most landslide prone area, nobody has researched the landslides or none of the agency has published the landslide map. The Bhutanese government and private individuals keep on constructing buildings, roads, schools, etc without checking the stabilities of the area which results in loss of million worth properties and causes fatalities.

The study takes account of the many influencing factors. The broad factors are geomorphological factors, hydrological factors, environmental factors, and human factors. The degree of impact from individual influencing factors differs from one another. Even the different classes of individual influencing factors contribute differently. This research gives information on how the individual factors contribute to the landslide, how each class within the factors contributes to the landslide, and how the overall combination of the factors shows the landslides susceptibility. There are many methods to evaluate LSM. The degree of accuracy differs from one another in all the methods. This study uses three bivariate statistical models which include Frequency Ratio (FR), Index of Entropy(IOE), and Weight of Evidence (WOE), and three hybrid models derived from the three primary statistical models. The hybrid models are FR-

IOE, IOE-WOE, and WOE-FR. The study compares accuracy among the different models and hybrid models.

The different DEMs are used to derive the geomorphological factors for the landslides. The DEMs used for the study are STRM 90m, SRTM 30m, and ALOS PALSAR 12.5m. The study focus on comparing the accuracy of the LSM using the different accuracy parameters. The validation and comparison of the accuracy of the different statistical models and DEMs are done using the confusion matrix, Receiver Operating Characteristics (ROC) curve, cohen's kappa index, and Root Mean Square Error (RMSE). This study compares accuracy among the DEMs and the different statistical models for the landslide mapping.

**1.6 Significance of the study**

The landslide susceptibility map will guide the government organizations and private individuals for developmental activities. Although most of the area is a landslide prone area, we cannot keep the land under-utilized. The map will depict the severity of the landslides such as very low, low, moderate, high, and very high landslide susceptible areas for the large scale area. This map will help in locating the safest zone for future planning of infrastructure development.

It is not possible to conduct a practical test for the large area and rugged terrain to show landslide susceptible zone. Moreover, it will be very expensive and time-consuming. The Geographic Information System (GIS) technology help in processing the remote sensing data and other ancillary data from the relevant organization. The result from this study shows the landslide susceptibility zone with minimum cost in less time and more efficient.

Since this study compares the accuracy of statistical models namely frequency ratio, index of entropy, the weight of evidence, and combination of these statistical models it will assist future researchers in choosing the appropriate model for the landslides studies. Similarly, researchers can understand how the changes in spatial resolution deviate accuracy of the LSM.

# CHAPTER II
# LITERATURE REVIEW

## 2.1 Landslides

The landslide comprises of mass movement of all varieties of materials on the slope in the form of topples, debris flow, rockfall, etc. except the avalanche of snow and ice (Varnes, 1984). The principle types of movement are falling, sliding, flowing, or their combinations (Varnes, 1978). The landslides are classified based on types of material types, movement, causes, and factors. The classification of the types of slope failure is important because the engineers can design an appropriate remedial safety measure (Varnes, 1978). Similarly, the researchers, geologists and geographers can interpret past landslide events and predict future landslide trends. The landslides are caused by both natural factors and human activities. The natural factor includes the nature of the terrain, precipitation, geological factors, etc. and the human factor includes the improper planned developmental activities. The slope imbalance caused by human activities includes road construction, timber extraction, mining, etc in absence of a systematic approach for the identification of unstable areas (Jaafari, Najafi, Pourghasemi, Rezaeian, and Sattarian, 2014).

Every year the landslide claims thousands of lives and responsible for causing damage to million worth properties around the world (Aleotti and Chowdhury, 1999). Although most landslides are more prevalent in the mountainous region, the landslides can occur anywhere in the world with enough local relief to generate gravitational stresses exceeding its bearing capacity (Varnes and Eckel, 1958).

As per the international disaster database EM-DAT, the total death caused by the landslides between 1910-2020 was 67052, the total injured was 12060 and the total affected was 14,679,178 globally (EM-DAT, 2020). The detail of the total death, injured, and affected by the landslide in various continents between 1910-2020 is shown in Table 1 and it is maintained by international disaster database EM-DAT. From Table 1, it is noticed that Asia is the most risky continent compared to different continents due to its higher number of death, injured and affected people.

**Table 1 The total number of deaths, injured and affected by the landslide from 1910-2020**

| | Total Death | No injured | Total Affected |
|---|---|---|---|
| Asia | 25604 | 5564 | 8,821,136 |
| Africa | 3171 | 442 | 221907 |
| America | 20869 | 5484 | 5574270 |
| Europe | 16830 | 518 | 40450 |
| Oceania | 578 | 52 | 21415 |
| Global data | 67052 | 12060 | 14,679,178 |

**Source:** EM-DAT, 2020

In recent years, researchers around the world are giving more attention to landslides due to a high impact on the socio-economic as well as pressure on the developmental activities on the mountainous region (Aleotti and Chowdhury, 1999). There is a great improvement in the new technology and the computational power in understanding the causes, triggering factors, and mechanics of the landslides, with the advancement in engineering and the physical science research, (Clague and Stead, 2012). The exact mechanism of landslide initiation is very complicated to understand due to a large number of the variability of factors (Li and Wang, 2019). However, with the use of field surveys, statistical analysis, and digital image processing approach combine with several influencing factors are found to be significant to determine the stable slope mapping (Foumelis, Lekkas, and Parcharidis, 2004). The first step used by researchers for landslide prevention and mitigation is LSM (Li and Wang, 2019).

### 2.2 Landslides studies in Bhutan

Bhutan is a tiny landlocked country in the Himalayan region sandwiched between two giant countries namely India and China. Bhutan is characterized by steep and rugged terrain which is heavily affected by the landslides during monsoon season due to heavy precipitation. Although the country is one of the most landslide-prone areas, there isn't much research done on landslides in Bhutan. The past studies on landslides in Bhutan cover only a certain portion of the area, that doesn't cover the most crucial and the most landslide-prone area. The study carried out on landslide in Bhutan includes LSM using information value at Phuntsholing by (Pasang and Kubíček, 2018), landslide prone zonation using information at Tashigang-Samdrup Jongkhar highway value by Thongley and Vansarochana (2020), landslides in Bhutan by Keunza *et al.*

(2004), determination of probabilities of landslide event-a case study of Bhutan by Sarkar and Dorji (2019), application of soil nailing for the landslide mitigation in Bhutan: A case study at Sorchen Bypass by Sarkar *et al.* (2017), Bhutanese road and bridge resilience to floods and landslide-First suggestions for assessment and response by Dawson *et al.* (2018), method for landslide risk evaluation and road operation management: A case study of Bhutan by Cheki and Shibayama (2008).

Bhutan is located in one of the most severe seismic regions with seismic zone-V as per the Bureau of Indian Standard which is has a similar tectonic setting as Northern India and Nepal (Pasang and Kubíček, 2018). The active tectonic activities in the Himalayan region, Bhutan has been recognized a prone natural disaster that includes landslides (Keunza *et al.*, 2004). Due to its location in the Himalayan foothill of the great Himalayan Mountain, it is heavily affected by the orographic effect of the Himalayan mountain. The orographic effect results in a heavy downpour in monsoon season which causes several landslides now and then in different parts of the country. The road network in Bhutan encounters challenging topography, heavy rainfall, and earthquake with a wide risk of floods and landslides (Dawson *et al.*, 2018). The focus on the landslide is heightened by the development activities in the fragile geologic Himalayan region (Keunza *et al.*, 2004).

**2.3 Types of Landslides based on the movement.**

Although the term landslides is the most common and generic term, all the landslide has its distinct characteristic. It is essential to identify the types of slope movement for the remedial measures as a precautionary measure in the future. Figure 1 shows the detail elaboration on types of landslide and Table 2 is the classification of landslide based on Varnes (1978).

A **fall** (Figure 1(a)) is a mass (soil or rock) detached from its original position from a steep slope or cliff with little or no shear displacement (Varnes, 1978). A **topples** (Figure 1(b)) is a forward and rotation movement of the mass of soil or rock about its axis below the center of gravity of the displaced mass (Cruden and Varnes, 1996).

A **slide** (Figure 1(c)) is a downward displacement of the slope materials on the rupturing surface or thin zones of the intense shear strain (Highland and Bobrowsky, 2008). Initially, the slope failure occurs at the local area which later expands from its

original area (Varnes, 1978). The slides are categorized into rotational slides, translational slides, and block slides.

**Table 2 Types of landslides based on movement.**

| TYPES OF MOVEMENT | | TYPES OF MATERIAL | | |
|---|---|---|---|---|
| | | BED ROCKS | ENGINEERING SOILS | |
| | | | Predominantly coarse | Predominantly fine |
| FALLS | | Rock fall | Debris fall | Earth fall |
| TOPPLES | | Rock Topple | Debris topple | Earth topple |
| SLIDES | ROTATIONAL | Rockslide | Debris slide | Earth slide |
| | TRANSLATIONAL | | | |
| LATERAL SPREADS | | Rock Spread | Debris spread | Earth spread |
| FLOWS | | Rock Flow (Deep Creep) | Debris flow (Soil Creep) | Earth flow |
| COMPLEX Combination of two or more principle type of movement | | | | |

**Source:** USGS, 2004

A **spread** (Figure 1(d)) is a distinctive lateral extension of soil and rock mass combined accompanied by a subsidence of the fractured mass of cohesive materials into underlying materials (Cruden and Varnes, 1996). The spread may be due to the liquefaction or flow of the softer underlying materials and it is common on the gentle slope or flat terrain (Varnes, 1978). This slope failure is also caused by the rapid ground motion such as Earthquake or artificially induced motion (Highland and Bobrowsky, 2008).

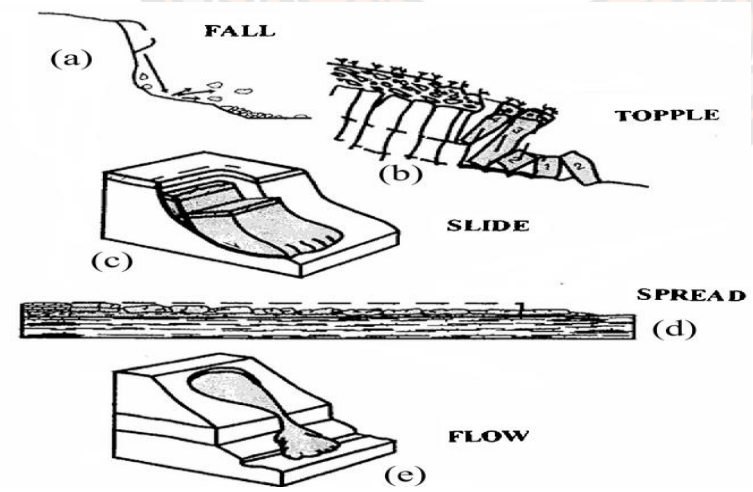


**Figure 1 The most common types of landslides**
**Source:** Cruden and VanDine, 2013

A **flow** (Figure 1(e)) is a rapid mass movement of the combination of loose soil, rock, organic matter, air, and water mobilize as a slurry that flows downslope. The common causes of flow are intense surface-water flow, heavy precipitation, or rapid snowmelt, that erodes and mobilizes loose soil or rock on steep slopes. The flow is categorized into debris flow, debris avalanche, earthflow, mudflow, and creep.

### 2.4 Causes of Landslides

The slope failures are strongly influenced by gravity, mechanical weathering, and the presence of interstitial water (Highland and Bobrowsky, 2008). The frequency and extent of the landslides depend on the variety of factors such as soil type, geology, morphology, steepness of the slope, precipitation, and built-up structure (Highland and Bobrowsky, 2008). The causes of the landslides are broadly classified into natural causes and human causes (Varnes, 1958).

In the natural causes, there is three major landslide triggering mechanism which acts independently or in combination which includes water, seismic activity, and volcanic activity(Highland and Bobrowsky, 2008). Some examples of the natural landslide causes are cutting off the slope by the rivers, discontinuities such as fractures, joints, and bedding planes, heavy precipitation, etc (Varnes, 1958).

The main human causes of landslides are due to population growth and the expansion of anthropogenic activities (Pasang and Kubíček, 2018). As the population increases, the demand for land and natural resources increases (Pasang and Kubíček, 2018). Similarly, the anthropogenic activities also increase with modernization which ultimately destabilizes the slope. The human activities undercut at the bottom of the slope and loading on the top of the slope results in exceeding the bearing strength of the soil which ultimately causes landslides. Some of the common examples of human-induced landslides are unplanned road construction, new house construction, building irrigation channel, and exploiting natural resources (Varnes, 1978).

The United States Geological Survey (USGS) has classified the landslides causes into geological causes, morphological causes, and human causes, and it is elaborated in Table 3

**Table 3 Causes of landslides**

| Geological causes | Morphological causes | Human causes |
|---|---|---|
| • Weak or sensitive materials<br>• Sheared, jointed, or fissured materials<br>• Adversely oriented discontinuity (bedding, fault, contact)<br>• Contrast in permeability or stiffness of materials | • Tectonic or volcanic uplift<br>• Glacial rebound<br>• Fluvial, wave, or glacial erosion of slope toe or lateral margins<br>• Freeze-and-thaw weathering<br>• Deposition loading slope<br>• Vegetation removal (by fire, drought)<br>• Shrink-and-swell weathering | • Excavation of slope or its toe<br>• Loading of slope or its crest<br>• Drawdown (or reservoirs)<br>• Deforestation<br>• Irrigation<br>• Mining<br>• Artificial vibration |

**Source:** USGS, 2004

## 2.5 Application of remote sensing and GIS in landslides

Remote sensing data are used for landslides identification, landslides monitoring, landslides spatial analysis, and hazard prediction (Guzzetti, Carrara, Cardinali, and Reichenbach, 1999). In recent decades, the landslide detection, mapping, monitoring, and hazard analysis becomes efficient due to rapid advancement in Earth observation through remote sensing (Tofani, Segoni, Agostini, Catani, and Casagli, 2013). Remote sensing can be considered a powerful and well-established platform for landslide mapping, monitoring, and hazard analysis (Tofani *et al.*, 2013). The integration of remote sensing data with other ancillary data such as geological maps, lithological, rainfall, and landslide inventory maps are the sources of information for the landslide assessment and GIS is a useful tool for the data analysis for the geospatial landslide risk prediction and map visualization (Metternicht, Hurni, and Gogu, 2005).

The various GIS software is an important tool for the data analysis and preparation of the LSM. It can handle large complex datasets, storage, retrieve, transformation, the efficient calculation using appropriate mathematical and statistical methods, and concise displaying of the results (Kelarestaghi and Ahmadi, 2009).

The GIS is used extensively for the preparation of a database of landslide inventory, factors, data analysis using some mathematical modeling and display the outcome. Gupta, Ghose, and Sharma (2009) stated that the combination of

mathematical modeling, remote sensing data, and GIS are presented in many research articles to evaluate the landslide hazard mapping. GIS enables analysis of landslide hazards, effective spatial management of the data, and manipulation for the analysis (Kelarestaghi and Ahmadi, 2009). The results are very easy to interpret showing a simple map that can be easily interpreted by ordinary people who don't have GIS knowledge. The advantage of the use of remote sensing data and GIS technology is that it is cost-effective and analyse difficult terrain which is not accessible (Carrara, Guzzetti, Cardinali, and Reichenbach, 1999).

Remote sensing as a data and geographic information system as a tool should go hand in hand and have a close relationship. GIS can store, manage, analyze, and display a large amount of complex data in a very short time (Kelarestaghi and Ahmadi, 2009). There are several remote sensing data with varying resolutions and numerous GIS software with the rapid advancement in science and technology (Tofani *et al.*, 2013). Some of the GIS software is open source while others are commercial software. Similarly, some of the remote sensing data are freely available online.

### 2.6 Landslide Inventory Mapping

A landslide inventory map is defined as the exact location of the existing landslides, its type, size and time of occurrence, rate of movement, and it is considered to be a fundamental part of the landslide studies (Devkota *et al.*, 2013). A landslide inventory map is an important and effective way to collect basic information of the landslides (Liu and Duan, 2018). The accuracy LSM depends on the reliability and accuracy of the landslide inventory data (Aleotti and Chowdhury, 1999). However, it is a challenging job due to the unavailability of the high resolution satellite images, real-time landslide data, lack of information on the frequency and the extent of the landslides. Some of the researchers directly download landslide information from the database of the relevant organization (Wang et., 2011). The inventory map can be even constructed from the visual interpretation of the colored ariel ortho-photograph (Bai *et al.*, 2010) while geological report which shows landslide location and sizes are also used (Zhao *et al.*, 2019). The image interpretation techniques such as color, tone, texture, etc were also used in the remote sensing data followed verification by the google earth image, and extensive field survey (Sun *et al.*, 2018). Few scholars also

used historical data of the landslides before the image interpretation and field inspection (Jaafari *et al.*, 2014).

### 2.7 Landslide and its influencing factors

It is important to choose effective landslide influencing factors. The inclusion of many redundant factors reduces accuracy of the landslide map (Thongley and Vansarochana, 2021a). There are as such no universal guidelines to choose the influencing factors on landslide occurrence. A total of fifteen factors were used for this study which includes elevation, slope, aspect, slope curvature, topographic wetness index, stream power index, drainage density, Normalized Difference Vegetation Index, Normalized Difference Soil Index, distance from the river, distance from the fault, average annual rainfall, lithology, land use land cover, and distance from the road.

The elevation is used to evaluate the changes in landform between the different geomorphologic and geologic setting (Liu and Duan, 2018). The different elevation also experiences a different amount of precipitation causing variation in landslide potentials (Zhang *et al.*, 2019). The slope gradient is shows the steepness of the slope. The various slope gradient shows the interaction of the slope gradient with the slope material's properties (Youssef, Al-Kathery, and Pradhan, 2015). The shear stress increase with the increase in the slope angle due to gravity which increases the probability of the slope failure (Mondal and Mandal, 2019). The increase in slope also increases the velocity and volume of the surface runoff. The **d**ifferent slope aspect receives different light intensity, which influences the water content of the soil, vegetation cover, soil strength, and ultimately landslide probability (Achour *et al.*, 2017). South-facing slopes are more venerable in Himalaya due to the orographic effect and more prone to a landslide (Chand, 2008). It makes the moisture and vegetation unevenly distributed and uneven evapotranspiration (Wang et al., 2011). As a result, the slope aspect has a different influence on slope stability (Sun *et al.*, 2018). The slope curvature influence the landslide probability (Zhang *et al.*, 2019). The slope curvature is in the form of an upwardly convex surface, flat surface, and upwardly concave area. The degree of concavity increases with the increase in negative value while the degree of convexity is higher in the greater positive value of slope curvature. The slope curvature is said to be flat when its value lies between -0.05 to 0.05 (Nohani *et al.*,

2019). The chance of slope failure is debatable for convex and concave curvature in many papers.

The Topographic Wetness Index (TWI) shows the flow accumulation at a point in a catchment area and the capability of water to flow downstream (Cao *et al.*, 2016). The TWI gives the information on the relationship between the local upslope contributing area and the entire slope and it affects the distribution of soil moisture and the groundwater flow (Devkota *et al.*, 2013). The Stream Power Index (SPI) measures the erosive power of water flow and contributes towards the stability of the area (Regmi *et al.*, 2014). The viscosity of the slope and the steepness of the terrain are the two important factors that govern the SPI (Saadatkhah, Kassim, and Lee, 2014). The drainage density plays an important factor in terms of stability as the saturation degrees of the materials directly affect slope stability. During the rainfall, the drainage is filled with the running water and erodes the sides which cause landslides (Kumar and Anbalagan, 2015). The saturation of the toe constituent materials of the slopes reduces the shear strength which results in the eroding action of the toe (Achour *et al.*, 2017).

The Normalized Difference Vegetation Index (NDVI) is a measure of surface reflectance which gives information on the conditions of the vegetation coverage and biomass in the study area (Jaafari *et al.*, 2014). The NDVI value ranges from -1 to 1. If the NDVI is less than zero, the ground is barren and less stable. On the other hand, if the normalized vegetation index is greater than zero, it indicates that the vegetation coverage is healthy. The forest tree roots act as a reinforcement and reduce the rate of landslide occurrence (Jaafari *et al.*, 2014). The Normalized Difference Soil Index NDSI is used to give information about the distinction about the soil with other land cover types to a certain degree. The higher value indicates the bares soil area and the lower value indicates different categories of vegetated areas (Mind'je *et al.*, 2019).

The distance from river plays significant roles in modifying the landscape by carving different rocks and soil ue to its scoring actions (Zhao *et al.*, 2019). Both sides of the rivers are usually eroded by the running river. It is observed that the slope which is closer to the river erodes more resulting in higher chances of occurrence of landslides (Sun *et al.*, 2018). Similarly, the rocks near the contact and faults are weaker due to intense shearing forces between rocks (Achour *et al.*, 2017). The probability of landslides increases we go closer to the fault. In addition, the distance from the road

also affects stability of the road.The road construction on the slope causes loss of support at its base. The loss of support at the base increases the stress of the slope and develop the cracks. This increases the frequency of the landslides near the road (Devkota *et al.*, 2013). In most of the studies, the landslides densities are higher near the road compared to other factors.

The lithology also play pivotal role in landslide due its difference in hardness, arrangement of structure, moisture retention capacity, etc. The lithology have a great influence on the physical and mechanical properties, weathering, deformation, and modes of failure of the slopes (Sun *et al.*, 2018). Many researchers accept that lithology influences the occurrence of landslides, due to its lithological variation in its characters which causes the difference in the strength and permeability of rocks and soils (Li and Wang, 2019).

Rainfall is considered as an important triggering factor for the landslide susceptibility research and it induces the erosion on the slopy area. The water from the rainfall infiltrates and increases the gravity of the soil and rock which reduces the shear strength, thus inducing landslides (Sun *et al.*, 2018).

The different land use land cover also plays in contributing role in the stability of the slope. The amount of water infiltration and retention will vary in different features such as forest, cultivated land, built-up area, etc. The land covered by forest regulates continuous water flow and water infiltrates regularly, whereas the cultivated land affects the slope stability owing to the saturation of covered soil (Devkota *et al.*, 2013).

## 2.8 Landslide Susceptibility Mapping Assessment.

The approaches for the landslide susceptibility assessment are broadly classified into qualitative and quantitative. The landslides probability is obtained by analyzing the relationship between the location of past landslide and a set of factors using qualitative or quantitative approaches(Van Westen, Van Asch, and Soeters, 2006).

### 2.8.1 Qualitative Assessment of Landslides

Qualitative approaches are subjective and heuristic in nature that works entirely based on the judgment of the person carrying out the landslide assessment (Aleotti and Chowdhury, 1999). In this method, the experts use his knowledge to assign the rank to

the classes of the factors based on the importance and calculate the weightage of the factor to produce the LSM. Some of the qualitative methods used for landslide assessment are the analytic hierarchy process (Achour *et al.*, 2017) and weighted linear combination (Ayalew, Yamagishi, and Ugawa, 2004).

### 2.8.2 Quantitative Assessment of Landslides

The quantitative method uses a numerical calculation to find the relationship between influencing factors and landslide inventory to estimate the probabilities of the future landslide occurrence(Van Westen *et al.*, 2006). The quantitative methods are categorized into deterministic and statistical approach(Aleotti and Chowdhury, 1999). Quantitative methods are widely used for landslide susceptibility studies due to higher accuracy in LSM compared to qualitative methods.

The deterministic approach is a site-specific which require field-based geotechnical data (Mandal and Mandal, 2018) and calculate the factor of safety for the landslide assessment (Aleotti and Chowdhury, 1999). Although the deterministic approach is relatively more accurate, it is feasible for the smaller areas only (Zhu and Huang, 2006). The deterministic approach is applied for site feasibility studies, especially for engineering construction.

The statistical methods are based on the correlations between the influencing factors and the distribution of past landslides (Saadatkhah *et al.*, 2014). As per the recent trend, there is a decline in heuristic (knowledge-based) methods and an increase in the data-driven methods (statistical approach). The advantage of the statistical approach is that investigator can validate the importance of each factor and decide the input influencing factor based on the weightage of the influencing factor (Aleotti and Chowdhury, 1999). The statistical approach in conjunction with GIS techniques is easy to calculate and applicable for a large area (Aleotti and Chowdhury, 1999). The statistical methods for the LSM are grouped into bivariate and multivariate statistical analysis (Pardeshi, Autade, and Pardeshi, 2013).

In the bivariate statistical method, the landslide inventory map is compared with the landslide influencing factors to get the weight of each class according to their impact of landslides (Kelarestaghi and Ahmadi, 2009). The weighted value of the classes is calculated based on landslide density in each class (Aleotti and Chowdhury, 1999).

Many investigators around the world used bivariate statistical methods such as frequency ratio (Khan *et al.*, 2019; Moazzam, Vansarochana, Boonyanuphap, and Choosumrong, 2018; Samanta, Pal, and Palsamanta, 2018), information value (Pasang and Kubíček, 2018), index of entropy Thongley and Vansarochana (2021a), statistical index (Shafapour Tehrany, Kumar, Neamah Jebur, and Shabani, 2019), and weight of evidence (Thongley and C. Vansarochana, 2020). It is proved that the bivariate statistics is more simple and precise than that of the multivariates statistics (Shahabi, Ahmad, and Khezri, 2013).

In the multivariates statistical approach, the weight of the individual influencing factors are calculated and the LSM is developed by multiplying the influencing factors with its weight. The logistic regression is widely used multivariate statistics for the LSM (Ayalew and Yamagishi, 2005).

### 2.9 Effect of spatial resolution of DEM on landslide susceptibility mapping

The DEM plays an important role in depicting the nature of the topography and deriving the influencing factors for the landslide assessment. A DEM represents the surface elevation of the ground in the form of a series of cells which is stored in the raster grid (Mahalingam and Olsen, 2016). The cell's pixel value of the DEM represents the elevation of the ground. The spatial resolution of remote sensing data is one of the most important characteristics for determining accuracy. The spatial resolution defines the smallest scale at which surface features may be extracted, identified, and mapped from remote sensing technology. Spatial resolution may refer to the ground sampling distance in an image or the grid size in a DEM (Mora *et al.*, 2014). Based on the spatial resolution, the vertical accuracy of DEMs varies from one another. When the vertical accuracies differ, it will affect the accuracy of the LSM.

### 2.10 Validation and Accuracy assessment

The landslide study will have no practical significance without validation (Li and Wang, 2019). The validation compares different models with the actual-ground situation using landslide inventory data and assess the accuracy of different models. The accuracy assessment can also be used to compare the impact of spatial resolution on the LSM developed by various spatial resolution DEMs. The most popular validation

methods used are Receiver Operating Characteristics (ROC) Curve, kappa index, and Root Mean Square Error (RMSE)

The ROC curve and the kappa index uses the same parameters for the accuracy assessment. The parameters used for the ROC curve and Kappa index are True Positive (TP), False Positive (FP), True Negative (TN), and False Negative (FN). These parameters are also used for the calculation of sensitivity, specificity, and accuracy for the comparison of the models. These parameters were derived from the landslide inventory (Actual class or ground true pixel) and the predicted class (landslide susceptibility map) and it is elaborated the Table 4.

**Table 4 Confusion matrix for observed landslide against the predicted landslide**

| | | **Observed landslide** | |
|---|---|---|---|
| | | **Landslides (1)** | **Non-landslides (0)** |
| **Predicted landslide** | **Landslides (1)** | TP | FP |
| | **Non-landslides (0)** | FN | TN |

where, TP (true positive) and TN (true negative) are the numbers of correctly classified pixels for landslide and non-landslide, respectively. On the other hand, FN (false negative) and FP (false positive) are the numbers of pixels erroneously classified for landslide and non-landslide, respectively.

The sensitivity is the proportion of landslide pixels that are correctly classified as landslide occurrences while the specificity is the proportion of the non-landslide pixels that are correctly classified as non-landslide (Bui, Tuan, Klempe, Pradhan, and Revhaug, 2016). Accuracy is the proportion of landslide and non-landslide pixels that are correctly classified (Nguyen *et al.*, 2019). The AUC of the ROC curve is used to measure accuracy and it is constructed using the sensitivity and specificity. As per Shirani, Pasandi, and Arabameri (2018), the interpretation of AUC of the ROC is given in the Table 5

**Table 5 AUC interpretation scale**

| **AUC range** | **Interpretation** |
|---|---|
| 0.9–1 | Excellent |
| 0.8-0.9 | Very good |
| 0.7-0.8 | Good |
| 0.6-0.7 | Moderate |
| 0.5-0.6 | Poor |

**Source:** Shirani et al., 2018

The Kappa index is used to check the reliability of the landslide model and the evaluation of the agreement between the value of the model and the ground reality (Bui *et al.*, 2016). When the Kappa value is -1, it indicates that the model is non-reliable while its value is equal to 1 shows that the model is perfectly reliable between model and the reality (Nguyen *et al.*, 2019). In the worst case, the kappa value is negative which indicates that the agreement is worse than the chance (Tien Bui *et al.*, 2018). As per Landis and Koch (1977), the scale of Cohen's kappa agreement is given in Table 6.

**Table 6 Scale value of Cohen's kappa agreement**

| Value | Agreement |
|---|---|
| <0 | Less than chance agreement |
| 0.01-0.20 | Slight agreement |
| 0.21-0.40 | Fair agreement |
| 0.41-0.60 | Moderate agreement |
| 0.61-0.80 | Substantial agreement |
| 0.81-0.99 | Almost perfect agreement |

**Source:** Landis and Koch, 1977

The Root Mean Square Error (RMSE) is defined as the differences between values predicted values for the landslides by the models and the observed values from the actual ground. When the RMSE value is 0, it is considered as no error which corresponds to correlation coefficient 1 and vice versa (Barnston, 1992).

# CHAPTER III

# RESEARCH METHODOLOGY

## 3.1 Study Area

### 3.1.1 Geographical location

The Ossey watershed area is situated in central Bhutan under the Sarpang district and located approximately in between 90°10’00”E and 90°50’00”E longitude and 26°50’00”N to 27°15’00”N latitude (Figure 3). The area lies on the Indian border in the south and is one of the road entry points into Bhutan from India. The Ossey watershed area covers 820.722sq.km and it ranges from 168m to 4197m above mean sea level. Generally, the area has heavy vegetation and steep natural terrain. However, the foot slopes of an area are characterized by plain with green grasses. The Gelephu city which is one of the largest city in Bhutan and it is located at the foot of the Ossey watershed area. As per the 2017 national census, about 9858 people live in Gelephu city. The Ossey watershed area is one of the most landslide prone area in Bhutan and experiences landslide every year.

**Figure 2 The landslides event at Ossey watershed area in Bhutan**

### 3.1.2 Climatic condition

The climate in the area is very hot and humid in summer with as high as 30°C. According to the National Center for Hydrology and Meteorology (NCHM) of Bhutan, the average annual rainfall ranges from 1785mm/year to 5024mm/year in the study area. The heavy monsoon rainfall trigger flood and landslide especially from May to September every year.

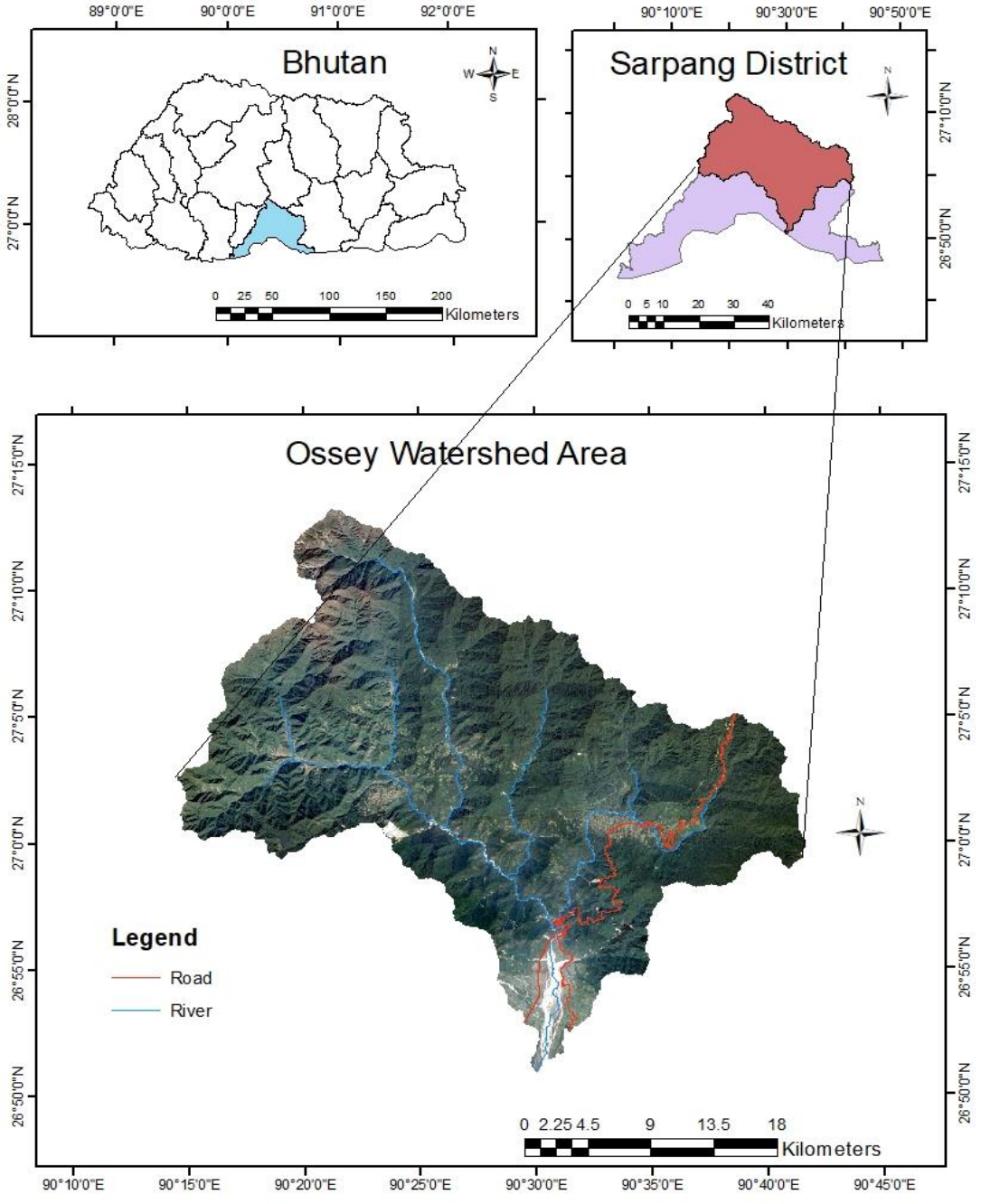


**Figure 3 Ossey watershed area in Bhutan**

### 3.1.3 Lithology

The area experiences a variety of lithological features. The area is dominated by schist and phyllite, medium to course pabble, metasedimentary rocks, conglomeratic sandstone, and massive foliated syn-Himalayan leucogranite plutons(Long et al., 2011). The detailed description of lithology is given Table 7.

**Table 7 Lithological Description of the study area**

| Geological Age | Code | Lithology |
|---|---|---|
| Miocene-Pliocene | Tsm | Tan to gray, medium- to coarse-grained sandstone and pebble- to cobble-conglomeratic sandstone |
| Paleoproterozoic | pCd | Dominated by schist and phyllite. Quartzite is thin-to medium-bedded, and medium-gray limestone interbeds. |
| Ordovician | Pzc | Tan to gray, thick-bedded, fine- to medium-grained, cliff-forming, micaceous quartzite, interbedded with biotite-muscovite-garnet schist. Interbedded with green to white, thin-bedded marble. Dominated by tan, cliff-forming marble, with lesser gray phyllite and dark-gray phyllitic quartzite. Dominantly upper greenschist facies 2.2-4.0 km-thick. |
| Neoproterozoic-Cambrian | GHlml | Dominantly amphibolite-facies, metasedimentary rocks, including quartzite, and biotite-muscovite-garnet schist and paragneiss often exhibiting kyanite, sillimanite, or staurolite, and partial melt textures |
| Cambrian-Ordovician | GHlo | Cliff-forming, massive-weathering, granite-composition orthogneiss; generally exhibits leucosomes and abundant feldspar. Paragneiss, schist, and quartzite intervals locally split out. Deformed Cambrian-Ordovician granite plutons that intruded Greater Himalayan sedimentary protoliths. |
| Miocene | Tgr | Massive to foliated, syn-Himalayan leucogranite plutons. Leucogranite intrudes the structurally-higher and structurally-lower Greater Himalayan sections, as well as Tethyan Himalayan rocks. |

**Source:** Long et al., 2011

### 3.2 Data Collection

The various types of dataset are required for the preparation of the landslide susceptibility map. Table 8 shows the brief description of satellite data and ancillary datasets were collected from the various sources.

**Table 8 Details of data source**

| Sl No | Data | Purpose | Source |
|---|---|---|---|
| 1 | STRM(30m) | Preparation of Elevation, slope, aspect, sloep curvature, Topographic Wetness Index, Stream Power Index, drainage density | National Aeronautics and Space Administration (NASA) and the National Geospatial-Intelligence Agency(NGA) |
| 2 | SRTM(90m) | | |
| 3 | ALOS PALSAR(12.5m) | | Japan Aerospace Exploration Agency (JAXA) |
| 4 | Sentinel-2(10m) | Preparation of landuse land cover map, Normalized Difference Vegetation Index, Normalized Difference Soil Index, | European Space Agency (ESA) |
| 5 | Geological map of Bhutan | Lithological Map, Fault map | Depart of Geology and Mine, Bhutan |
| 6 | Rainfall data | Rainfall Map | National Center of Metereology and Hydrology, Bhutan |
| 7 | Digital topographic map of Bhutan | Extraction of river and road map | National Land Commission of Bhutan |
| 8 | Google Earth | Identify landslide location | Google Earth Pro |

#### 3.2.1 Satellite data

The detail of various satellite data are explained in the following sections

**I. Shuttle Radar Topography Mission Digital Elevation Model (SRTM DEM)**

The Shuttle Radar Topography Mission(SRTM) is a Digital Elevation Model that covers 56°S to 60°N to generate a digital topographic database of earth. The SRTM-

30m (SRTM V3.0, 1 arc sec) is a modified version of SRTM-90m(3arc second) resolution which was released in 2000(Santillan and Makinano-Santillan, 2016). The 1arc second SRTM was released in September 2014. It consists of two antennas. The main antenna transmits and receives radar echoes while the supplementary antenna receives only radar echoes. The two different C-band and X-band interferometric radar images of the same area can be obtained from two antennas about 60m apart. The interferometric process the image and obtain interferogram which is then used to extract topographic elevation data (Yang, Meng, and Zhang, 2011). SRTM DEM data is downloaded from https://www.gislounge.com/. The tiles used for the study area are N26E90 and N27E90. The accuracy of SRTM varies with change in different geographical location (Rodriguez, Morris, and Belz, 2006). The detail of horizontal and vertical datums are shown in the Table 9.

**Table 9 Specification of SRTM**

| | |
|---|---|
| Projection | Geographic |
| Horizontal Datum | WGS84 |
| Vertical Datum | EGM96(Earth Gravitational Model 1996) |
| Vertical Units | Meters |
| Spatial Resolution | 1 arc-second for global coverage(~30meters)<br>3 arc-second for global coverage(~90meters) |

**Source:** USGS Science for a changing world

The SRTM (30m and 90m spatial resolution) were used to derive slope angle map, terrain aspect map, topographic wetness index(TWI), stream power index(SPI), Slope Curvature, and drainage density for this study.

### II. ALOS PALSAR DEM

The Advanced Land Observing Satellite (ALOS) Phased Array type L-band Synthetic Aperture Radar (PALSAR) Digital Elevation Model(DEM) is 12.5m spatial resolution which can be downloaded from Alaska Satellite Facility(ASF) Distributed Active Archive Center(DAAC). It is downloaded from https://www.asf.alaska.edu/. The ALOS PALSAR was projected using UTM, horzontal datum used was WGS84. The accuracy of the ALOS PALSAR difers from place to place.

The scene used for the study are AP_05873_FBS_F0520_RT1 and AP_05873_FBS_F0530_RT1. The ALOS PALSAR DEM is also used for the extraction of geomorphological and hydrological factors such as slope angle map,

terrain aspect map, topographic wetness index (TWI), stream power index (SPI), Slope Curvature, and drainage.

**III. Sentinel 2**

Sentinel-2 is a high resolution optical multispectral imaging satellite which consists of two polar satellites (Sentinel-2A and sentinel-2B) launched by the European Space Agency (ESA) Copernicus Programme. Sentinel-2A was launched on June 23rd 2015, while Sentinel-2B on March 07$^{th}$ 2017. The full mission of the sentinel satellite flying in the same orbit but phased at 180° with one another and revisit at a frequency of 5 days at the equator. Sentinel data products are freely available to all users and are accessible Copernicus Open Access Hub https://scihub.copernicus.eu. The sentinel-2 is projected to UTM with horizontal datum WGS84 and its available in Geographic Markup Language JPEG2000 (GMLJP2) format. The detail of sentinel 2 bands are given in the Table 10.

**Table 10 Metadata of Sentinel-2**

| Band | Central Wavelength (µm) | Resolution(m) |
|---|---|---|
| 1(Coastal) | 0.433 | 60 |
| 2(Blue) | 0.490 | 10 |
| 3(Green) | 0.560 | 10 |
| 4(Red) | 0.665 | 10 |
| 5(Vegetation Red Edge) | 0.705 | 20 |
| 6(Vegetation Red Edge) | 0.740 | 20 |
| 7(Vegetation Red Edge) | 0.783 | 20 |
| 8(NIR) | 0.842 | 10 |
| 8A(Vegetation Red Edge) | 0.865 | 20 |
| 9(Water vapour) | 0.945 | 60 |
| 10(SWIR-Cirrus) | 1.375 | 60 |
| 11(SWIR) | 1.610 | 20 |
| 12(SWIR) | 2.19 | 20 |

**Source:** Sentinel 2-User handbook

For this research, Sentinel 2 is used for identifying landslide through image interpretation technique during the landslide inventory, preparation of the Normalized Difference Vegetation Index (NDVI), Normalized Difference Soil Index (NDSI), and Land Use Land Cover (LULC) map. Three tiles are used for the study area since the area is quite large, one tile of the sentinel image didn't fit the whole study area. All the

three tiles are chosen from the same month to avoid error while preparing land use land cover map. The January month is chosen due to low cloud coverage. Table 11 shows the tiles chosen for the study area.

**Table 11 Tiles sentinels used for the study area**

| Sensor | Tiles | Acquisition Date |
|---|---|---|
| Sentinel-2 | L1C_T46RBR_A018434_20190102T043514 | 02/01/2019 |
| | L1C_T46RBQ_A009740_20190117T043639 | 17/01/2019 |
| | L1C_T46RBQ_A009926_20190130T044444 | 30/01/2019 |

### 3.2.2 Ancillary data collection

The following section elaborate on the ancillary data which are being provided by various agencies

**I. Geological map**

The geological map of Bhutan(Figure 4) is prepared by Long, McQuarrie, Tobgay, Grujic, and Hollister (2011) and it is under the custody of the Department of Geology and Mine (DGM). The geological map is prepared at a scale of 1:50000 and it is available on request from the DGM. The geological map is used to prepare the lithological and fault map for the study.

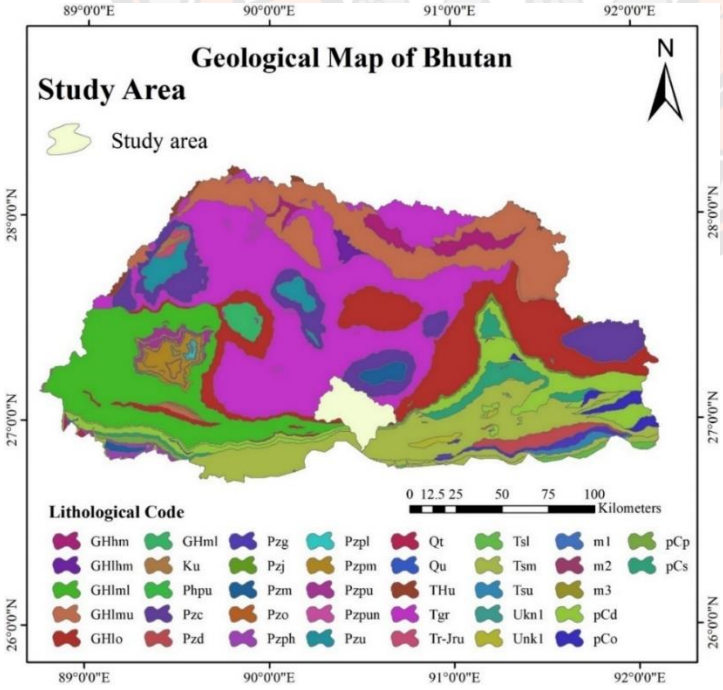


**Figure 4 Geological map of Bhutan**
**Source:** Long et al., 2011

### II. Rainfall data

The rainfall data is being monitored by the National Center for Hydrology and Meteorology (NHCM) of Bhutan. The rainfall data is used to prepare a rainfall distribution map of Bhutan and it is available on request from NHCM. For this study, 20 rainfall stations (Table 12) average annual rainfall observations from 1997-2017 are used to prepare a rainfall distribution map.

**Table 12 The average annual rainfall of Bhutan**

| Station | Coordinates | | | Average Annual Rainfall(mm) |
|---|---|---|---|---|
| | Latitude | Longitude | Height(m) | |
| Deothang | 26°51'20.88"N | 91°28'0.48" E | 800 | 3758.809 |
| Kanglung | 27°16’57.0”N | 91°31'19.99"E | 1930 | 1168.789 |
| Pemagatshel | 27°1'30'.00”N | 91°25'27.00”E | 1648 | 1765.27 |
| Bhur | 26°54'14.00"N | 90°26'2.04" E | 375 | 5154.936 |
| Dagana | 27°4’15.99” N | 89°52'28.99"E | 1460 | 1743.681 |
| Damphu | 27° 0' 0.00" N | 90° 7' 18.00"E | 1520 | 1694.826 |
| Phuntsholing | 26°51'34.99"N | 89°22'28.99"E | 220 | 3599.738 |
| Trongsa | 27°30'6.99" N | 90°30'18.00"E | 2120 | 1200.204 |
| Wangdue Phodrang | 27°29'12.00"N | 89°54'2.99" E | 1180 | 669.8546 |
| Zhemgang | 27°18'29.88"N | 90°39'19.01"E | 1905 | 1387.104 |
| Chamkhar | 27°32’25.01”N | 90°45'18.00"E | 2470 | 757.9264 |
| Gasa | 27°53'60.00"N | 89°42'59.00"E | 2760 | 1299.3345 |
| Haa | 27°23'17.16"N | 89°16'54.12"E | 2720 | 877.3564 |
| Mongar | 27°16'41.99"N | 91°14'17.99"E | 1600 | 955.2427 |
| Paro | 27°25'36.00"N | 89°25'23.00"E | 2406 | 630.46 |
| Punakha | 27°34'54.00"N | 89°51'59.00"E | 1236 | 715.8209 |
| Sibsoo | 27° 1' 0.00" N | 88°51'59.00"E | 550 | 5393.2909 |
| Simtokha | 27°26'17.99"N | 89°40'31.00"E | 2310 | 607.96909 |
| Tamangchu | 27°35’42.00”N | 91°11'48.00"E | 1750 | 812.79864 |
| Trashi Yangtse | 27°36’0.00” N | 91°30’0.00” E | 1830 | 1167.3645 |

**Source:** National Center for Hydrology and Meteorology**,** Bhutan

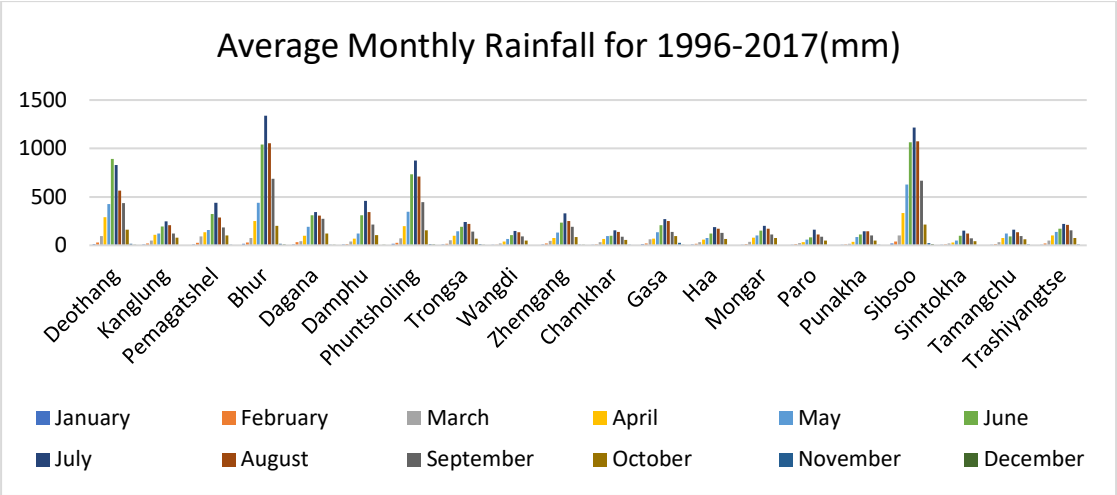


**Figure 5 Average monthly rainfall data of 20 stations from 1996-2017**

Figure 5 shows the average monthly rainfall for 20 stations in Bhutan which ranges from 1996 to 2017. It is observed from Figure 5 that Bhur, Deothang, Phuntsholing and Sibsoo rainfall stations experienced the highest rainfall over the past 21 years.

### 3.3 Research conceptual framework

To achieve the overall research objectives of the landslides susceptibility mapping, it is divided into three broad steps.

i) Data Preparation

ii) Data Analysis

iii) Validation and Accuracy Assessment

The overall conceptual framework of the work is shown in Figure 6. Firstly, the data preparation consist of landslide inventory and influencing factor preparation. Second step is the data analysis consist of LSM using the Frequency Ratio (FR), Index of Entropy (IOE), and Weight of Evidence (WOE). Then, LSM by combing FR-IOE, IOE-WOE, and WOE-FR. Finally, the validation of LSM using the confusion matrix, cohen's kappa index, ROC curve, and RMSE.

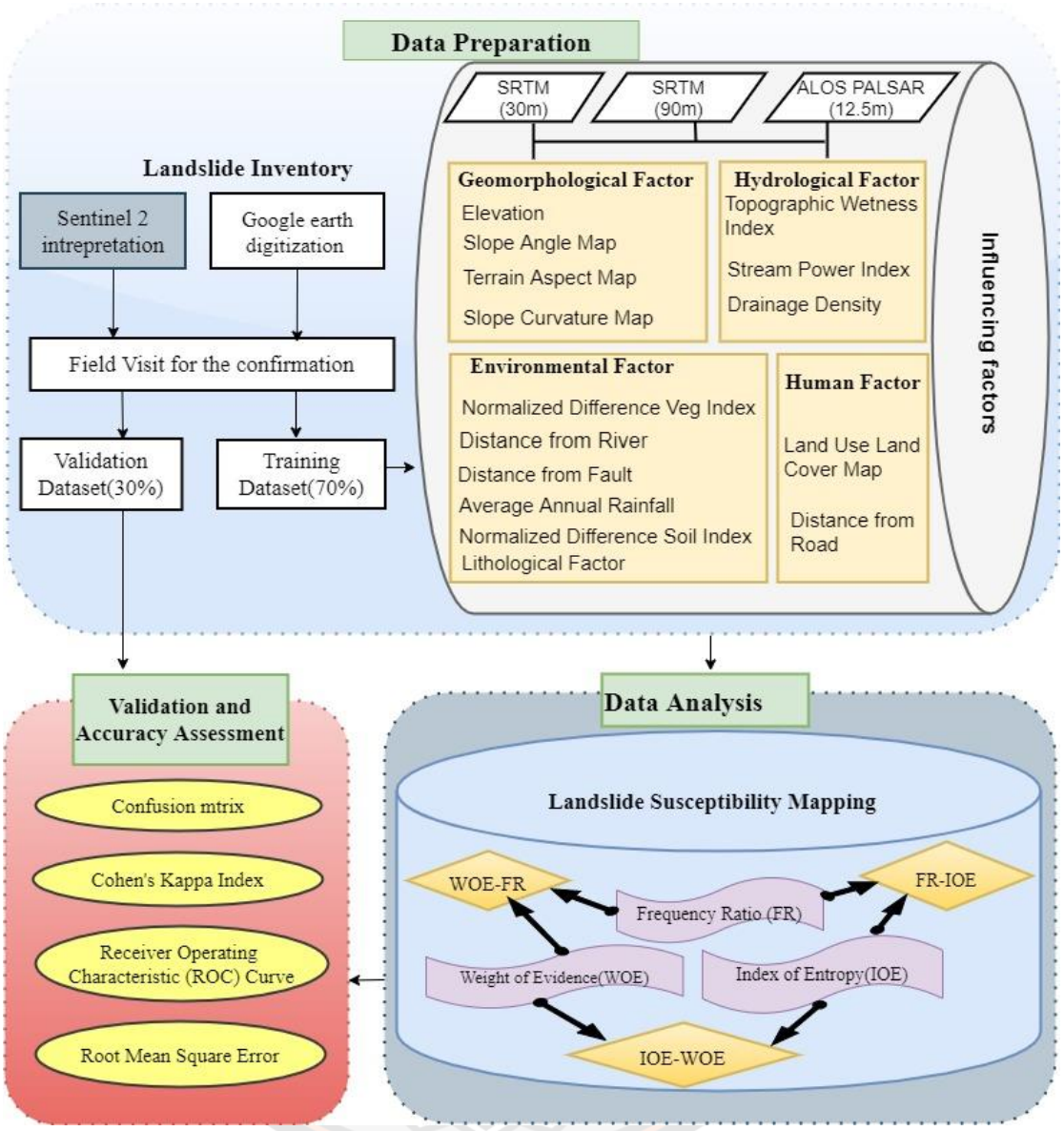


**Figure 6 Overall methodological framework**

### 3.3.1 Data Preparation

The data preparation constitute two steps. The first step consist of landslide inventory. The landslide inventory is the collection information of past and existing landslide. The second step is the influencing factor preparation which is prepared using appropriate methods from the various data as shown in Figure 7.

**I. Landslide Inventory Mapping**

The first step for the landslide assessment involvement landslide inventory mapping. The statistical approach for the LSM work on the principle past and present is key to the spatial prediction in the future under a similar condition whereby the past landslides were identified through landslide inventory (Devkota *et al.*, 2013). The accuracy of the landslide susceptibility mapping is directly dependent on the accuracy of the landslide inventory (Shirani *et al.*, 2018). Among the many techniques for the landslide inventory, this study uses sentinel-2 image interpretation, digitization of google earth, and extensive field survey.

**1) Sentinel 2 image interpretation**

Based on the recommendation of Karagianni, Lazos, and Chatzipetros (2018), the most effective band combination used for this study are Natural Color Composite (Red-Green-Blue) where the ground feature appears similar to the human eye visual system. Similarly, the color composite (SWIR1-Green-Blue) is also used to detect landslide whereby the landslide area is detected and highlighted with discerning differences in bare earth, indicating wet and dry areas in a scene.

**2) Digitization of Google Earth**

Google earth is high-resolution three-dimensional satellite imagery used for multiple purposes. The google earth is the super-imposition of the satellite images, ariel photographs, and GIS data onto a three-dimensional globe. Multiple researchers used google earth images to prepare a landslide inventory map. The google earth image is a high-resolution image and makes it easy to interpret the real ground. For this study, the google earth image from QGIS is used to locate the past landslides and then digitized with point features. The google earth locates landslides that are not identified by sentinel-2 interpretation.

**3) Extensive Field Survey**

Although remote sensing data and aerial photos are a powerful tool, their interpretation should be confirmed on the ground because many important features of the slope failure may be partially or completely obscured in dense forest (Varnes, 1984).

Similarly, the landslides identified through sentinel-2 and google earth images need field verification. Since the google earth images are made up of multiple images that are mosaic with one another, some of the images are may not be updated for a long time. When there are no updated images, there will be a missing landslide record in the digitized image or sometimes there will be excess landslides in the digitized landslides. Similarly, the composite band of the sentinel-2 image may misinterpret the landslides. The objects in the sentinel image having similar reflectance characteristics may misinterpret as landslides.

Therefore, validation of the digitized landslide inventory data is very important. The validation is normally carried by an extensive field survey using a handheld GPS. For this study, the landslide location is validated using the handheld GPS to verify the types of landslides and to validate the land use land cover simultaneously.

**II. Training dataset and validation dataset from landslide inventory**

The landslide inventory is prepared using the information from google earth, sentinel-2 image interpretation, and extensive field survey. It is digitized in point features GIS software. Although there are no fixed rules to divide the ratio of the landslides for training dataset and validation, most of the researchers used 70% of the total landslides for the training dataset and the remaining 30% for the validation (Jaafari *et al.*, 2014). The training dataset is used to train the influencing factors and derive the correlation while the validation dataset is used for checking the accuracy and validation of the prepared LSM developed by the statistical models (Pourghasemi, Mohammady, and Pradhan, 2012). The selection of the training dataset and the validation dataset is based on the random selection.

**III. Preparation of the influencing factors**

Figure 7 shows the flowchart of preparation of the influencing factors. A total of fifteen factors were used for this study. They are elevation, slope, aspect, slope curvature, topographic wetness index, stream power index, drainage density, Normalized Difference Vegetation Index (NDVI), Normalized Difference Soil Index (NDSI), proximity to the river, proximity to the fault, average annual rainfall, lithology, land use land cover (LULC), and proximity to the road. The ALOS PALSAR (12.5m),

SRTM(30m), and SRTM(90m) are used to derive elevation, slope, aspect, slope curvature, topographic wetness index, stream power index, drainage density. Similarly, sentinel-2 is used to prepare NDVI, NDSI, and LULC. The Geological map of Bhutan is used to extract lithology and fault map. The digital topographic map of Bhutan is used to extract the map of the road and river. The 21 years (1996-2017) average annual rainfall of Bhutan is used to derive a rainfall map. The factors are classified broadly into Geomorphological factors, Hydrological Factor, Environmental Factor, and Human Factors. The Geomorphological factors provide information about the earth's surface. As the geomorphological factor gives information about the earth's surface topography (Ayalew and Yamagishi, 2005). the elevation, slope, aspect, and slope curvature falls under geomorphologic factors. The topographic wetness index (TWI), stream power index (SPI), and drainage density falls under hydrologic factors. The NDVI, NDSI, proximity to the river, proximity to the fault, average annual rainfall, and lithology are categorized as environmental factors. The land use land cover and proximity to road fall under human factors. The overview of the data preparation is shown in the following diagram.

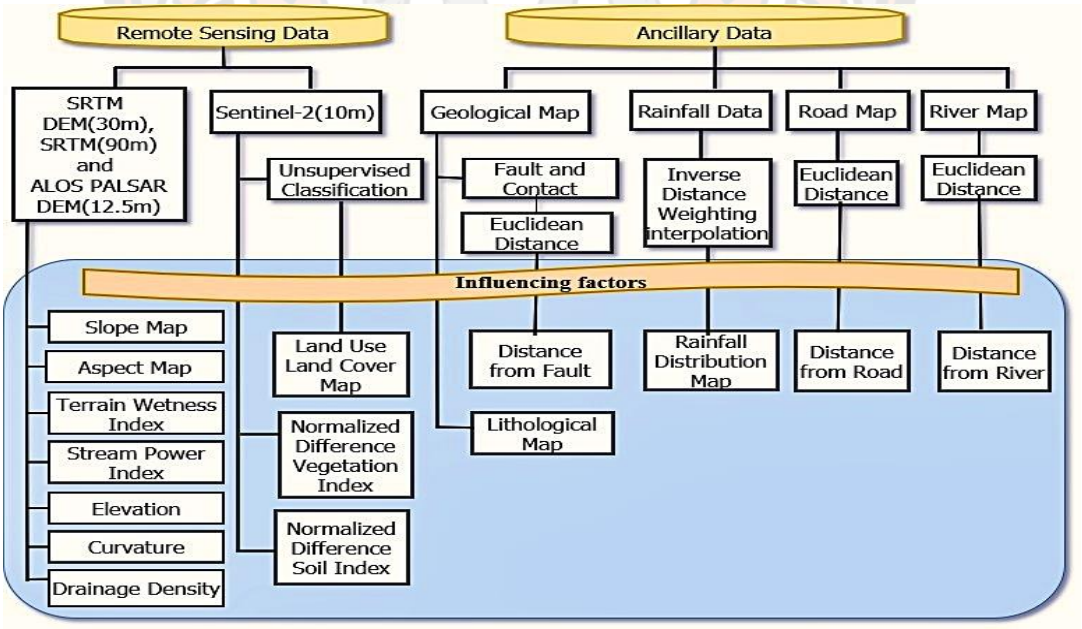


**Figure 7 Flowchart of influencing factors Preparation**

The elevation is classified into five classes as shown in Figure 8.1 for 12.5m spatial resolution, Figure 9.1 for 30m spatial resolution, and Figure 10.1 for 90m spatial resolution.

The slopes angle is classified into five classes as shown in Figure 8.2 for 12.5m spatial resolution, Figure 9.2 for 30m spatial resolution, and Figure 10.2 for 90m spatial resolution.

The aspect is reclassified into nine classes in the cardinal directions N(337.5-360 and 0-22.5), NE(22.5-67.5), E(67.5-112.5), SE(112.5-157.5), S(157.5-202.5), SW(202.5-247.5), W(247.5-292.5), NW(292.5-337.5) and flat land(-1) as shown in Figure 8.3 (12.5m spatial resolution), Figure 9.3 (30m spatial resolution), and Figure 10.3 (90m spatial resolution).

The slope curvature is classified in concave, flat, and convex as shown in Figure 8.4 for 12.5m spatial resolution, Figure 9.4 for 30m spatial resolution and Figure 10.4 for 90m spatial resolution.

The classified TWI is shown in Figure 8.5 for 12.5m spatial resolution, Figure 9.5 for 30m spatial resolution, and Figure 10.5 for 90m spatial resolution, and it is calculated using the equation given by Moore, Grayson, and Ladson (1991).

$$TWI = ln\left(\frac{\alpha}{tan\beta}\right) \qquad \text{Equation 1}$$

Where, a is the cumulative upslope area draining through a point (per unit contour length) and tan β is the slope angle at the point.

The classified SPI is shown in Figure 8.6 for 12.5m spatial resolution, Figure 9.6 for 30m spatial resolution, and Figure 10.6 for 90m spatial resolution, and it's calculated based on an equation given by Moore *et al.* (1991)

$$SPI = A_s tan\,\beta \qquad \text{Equation 2}$$

Where, *As* is the specific catchment area and β is the slope gradient in degrees.

The classified into drainage density is shown in Figure 8.7 for 12.5m spatial resolution, Figure 9.7 for 30m spatial resolution, and Figure 10.7 for 90m spatial resolution.

The NDVI is calculated using the Equation 3 as follow:

$$\text{NDVI} = \frac{\text{NIR} - \text{R}}{\text{NIR} + \text{R}} \qquad \text{Equation 3}$$

where, NIR and R are the near-infrared portions and the red portion of the electro-magnetic spectrum respectively. The NDVI is classified into five classes as shown in Figure 8.8 for 12.5m spatial resolution, Figure 9.8 for 30m spatial resolution, and Figure 10.8 for 90m spatial resolution.

The Normalized Difference Soil Index is calculated using the Equation 4.

$$\text{NDSI} = \frac{\text{SWIR2} - \text{G}}{\text{SWIR2} + \text{G}} \qquad \text{Equation 4}$$

where, SWIR and G are the near short wave infrared portion and the green portion of the electromagnetic spectrum respectively. The NDSI is classified into five classes as shown in Figure 8.9 for 12.5m spatial resolution, Figure 9.9 for 30m spatial resolution, and Figure 10.9 for 90m spatial resolution.

The GIS euclidean distance package is used for finding the distance form the river. The distance is classified into five classes as shown in Figure 8.10 for 12.5m spatial resolution, Figure 9.10 for 30m spatial resolution, and Figure 10.10 for 90m spatial resolution.

The distance from the fault is prepared using euclidean distance and classified into six zones as shown in Figure 8.11 for 12.5m spatial resolution, Figure 9.11 for 30m spatial resolution, and Figure 10.11 for 90m spatial resolution.

The Euclidean distance package from the GIS software is used for the preparation of the distance form the road. It is classified into five classes as shown in Figure 8.12 for 12.5m spatial resolution, Figure 9.12 for 30m spatial resolution, and Figure 10.12 for 90m spatial resolution.

The detail of lithology of the study area is given in the Table 7 and the Figures are shown in Figure 8.13 for 12.5m spatial resolution, Figure 9.13 for 30m spatial resolution, and Figure 10.13 for 90m spatial resolution.

To calculate the precipitation map of the study area, Inverse Distance Weighting (IDW) interpolation method was performed using rainfall data (Table 12). The IDW interpolation estimates the unknown rainfall amount is calculated by the linear weighted average of the known values from the known point that are adjacent to the unknown area (Chen and Liu, 2012). The influence on the unknown area decreases as the

distance increases from the known point. The rainfall map is classified into five classes as shown in Figure 8.14 for 12.5m spatial resolution, Figure 9.14 for 30m spatial resolution, and Figure 10.14 for 90m spatial resolution.

The land use map is prepared using sentinel-2 data using a unsupervised classification. It is classified into a agricultural land, built-up area, forest, shrubs, and water bodies. The forest covers 91.58%, agricultural land covers 3.28%, shrubs covers 2.49%, water bodies cover 1.56% and build-up area covers 1.09%. The accuracy of the land use and land cover is done using the error matrix (Table 13). For the error matrix, 200 random points were created and cross validated the LULC with the google earth. The overall accuracy of land use land cover is 79.5% as per the error matrix.

**Table 13 Accuracy assessment of the land use land cover**

| | | **Unsupervised classification** | | | | | |
|---|---|---|---|---|---|---|---|
| **Google Earth** | | **Agriculture** | **Built-up area** | **Forest** | **Shrubs** | **Water Bodies** | |
| | **Agriculture** | 19 | 2 | 6 | 4 | 0 | 31 |
| | **Built-Up Area** | 2 | 4 | 1 | 0 | 0 | 7 |
| | **Forest** | 2 | 0 | 120 | 8 | 1 | 131 |
| | **Shrubs** | 2 | 0 | 10 | 8 | 1 | 21 |
| | **Water Bodies** | 0 | 0 | 1 | 1 | 8 | 10 |
| | | 25 | 6 | 138 | 21 | 10 | 159 |

Overall accuracy=159/200x100=79.5%

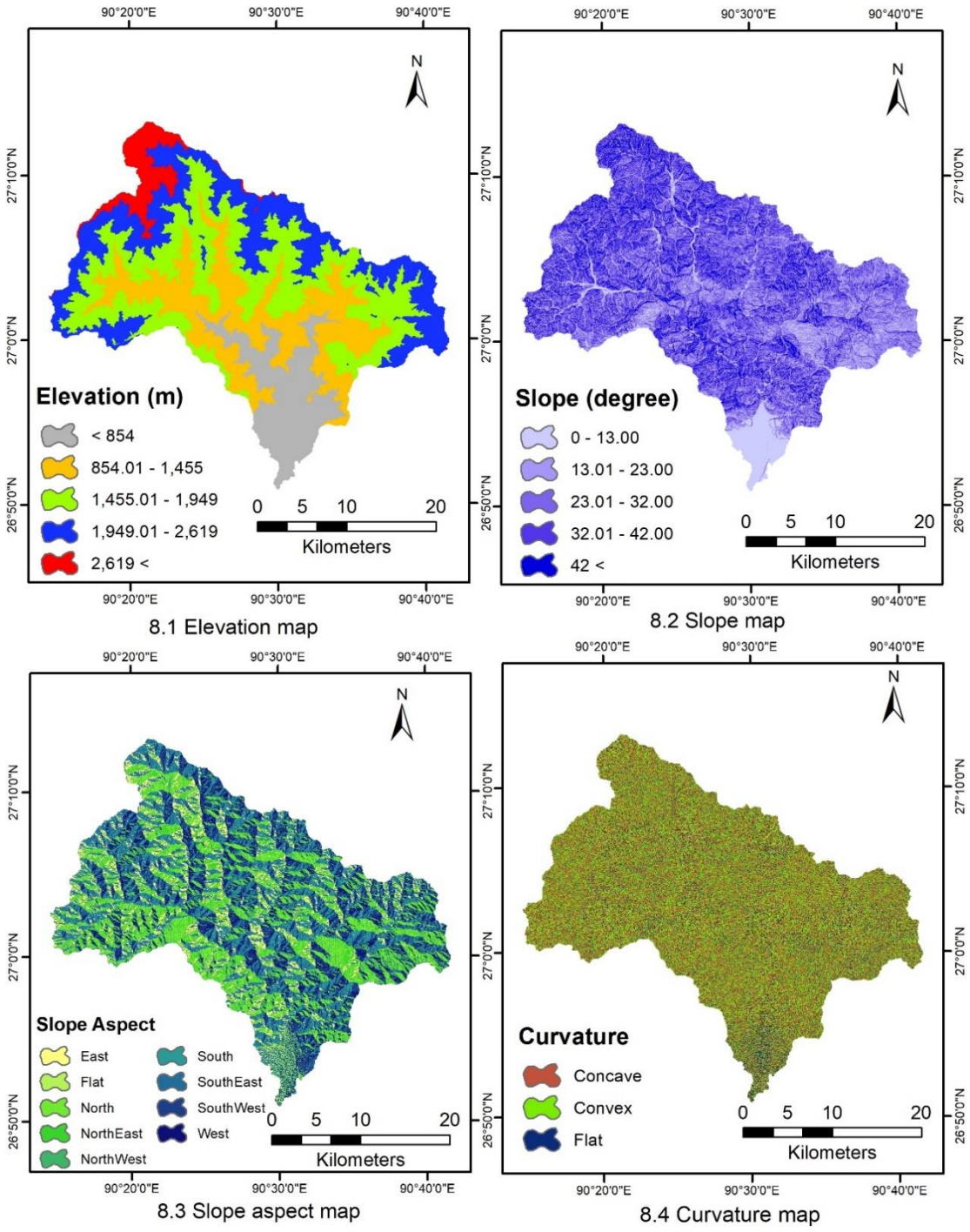


**Figure 8 Factors using spatial resolution 12.5m (8.1) Elevation, (8.2) Slope, (8.3) Slope Aspect, (8.4) Curvature, (8.5) TWI, (8.6) SPI, (8.7) Drainage density, (8.8) NDVI, (8.9) NDSI, (8.10) Dist. from river, (8.11)Dist. from fault, (8.12)Dist. From road, (8.13) Lithology, (8.14) Rainfall map, (8.15) LULC**

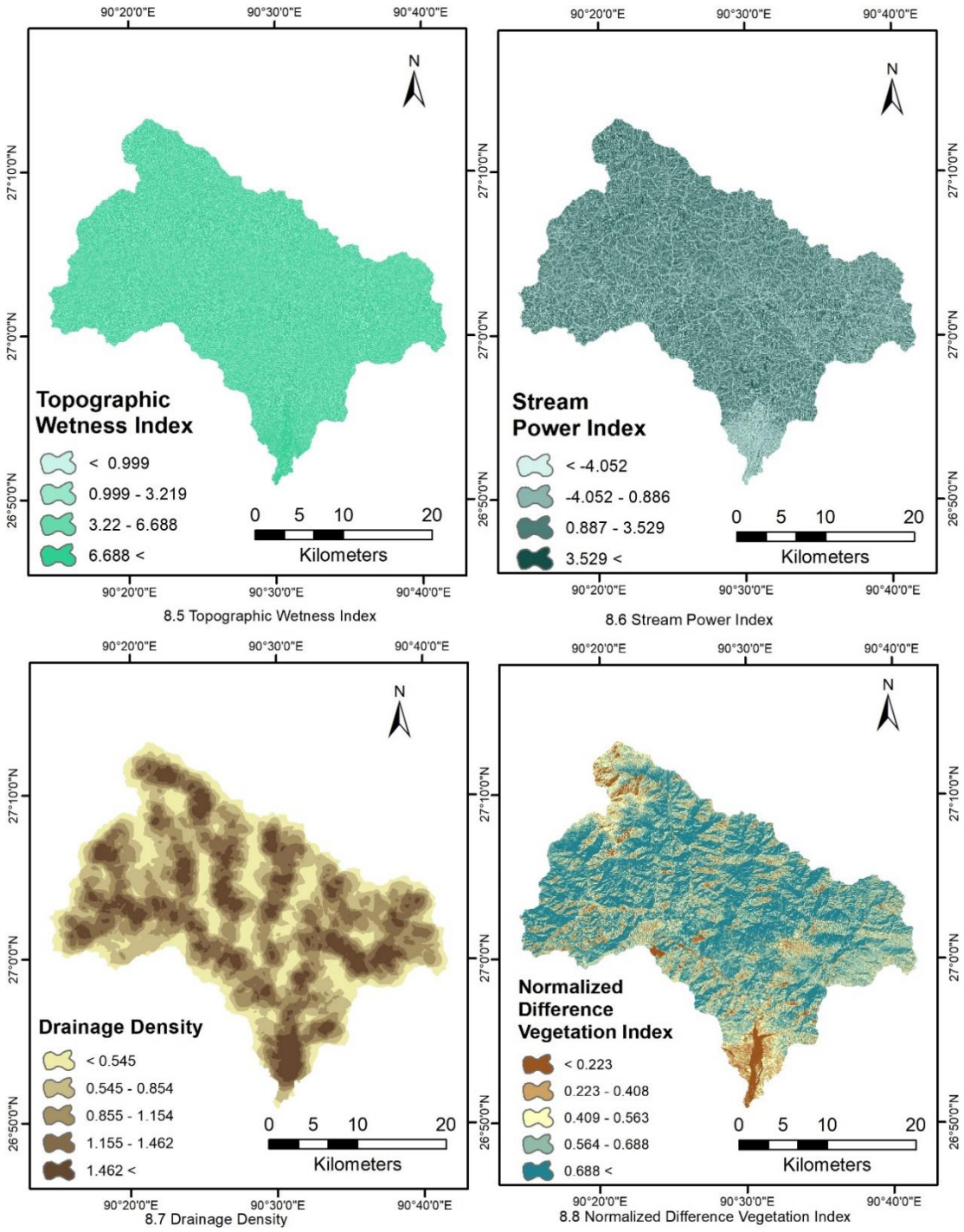


**Figure 8 Factors using spatial resolution 12.5m (8.1) Elevation, (8.2) Slope, (8.3) Slope Aspect, (8.4) Curvature, (8.5) TWI, (8.6) SPI, (8.7) Drainage density, (8.8) NDVI, (8.9) NDSI, (8.10) Dist. from river, (8.11)Dist. from fault, (8.12)Dist. From road, (8.13) Lithology, (8.14) Rainfall map, (8.15) LULC**

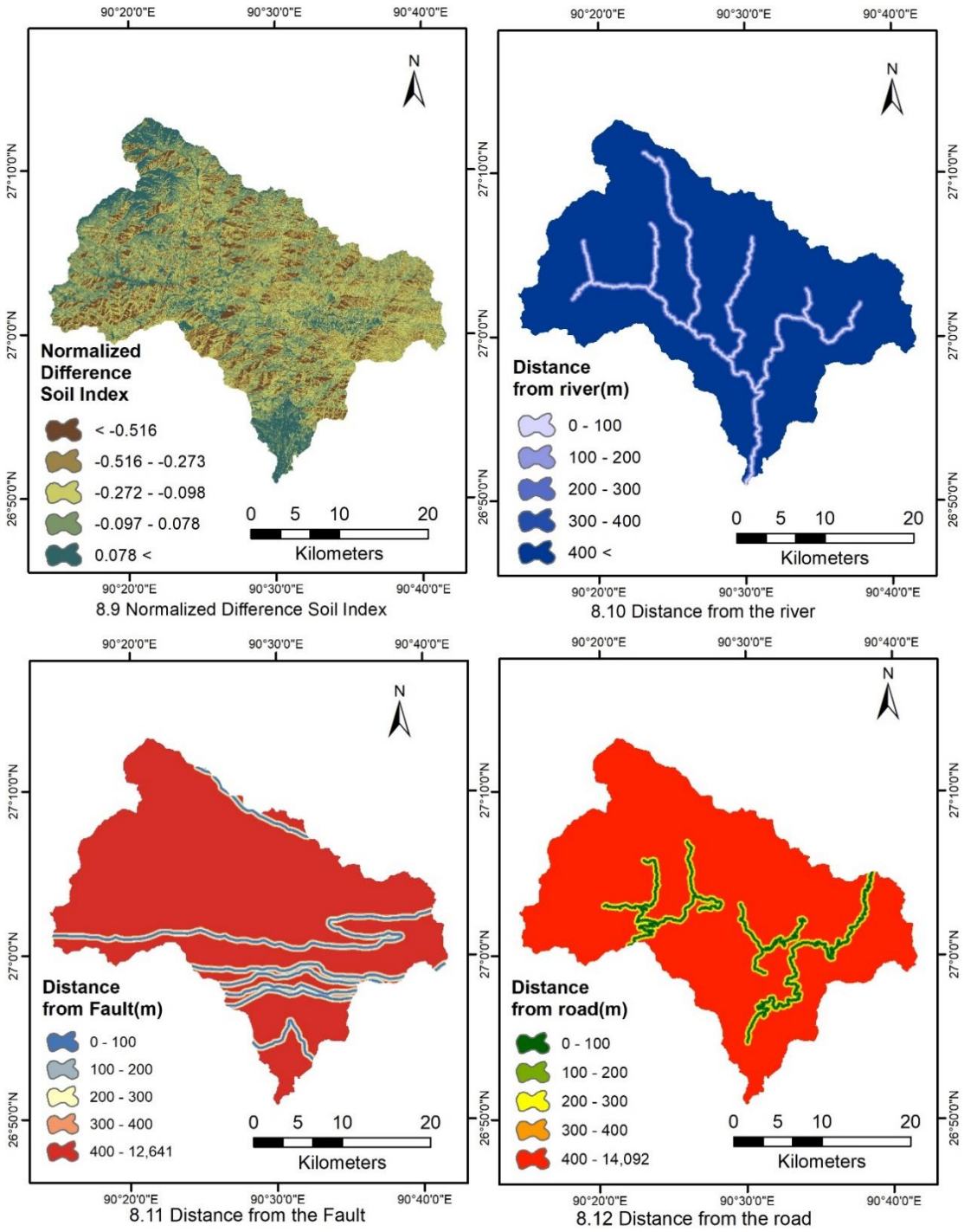


**Figure 8 Factors using spatial resolution 12.5m (8.1) Elevation, (8.2) Slope, (8.3) Slope Aspect, (8.4) Curvature, (8.5) TWI, (8.6) SPI, (8.7) Drainage density, (8.8) NDVI, (8.9) NDSI, (8.10) Dist. from river, (8.11)Dist. from fault, (8.12)Dist. From road, (8.13) Lithology, (8.14) Rainfall map, (8.15) LULC**

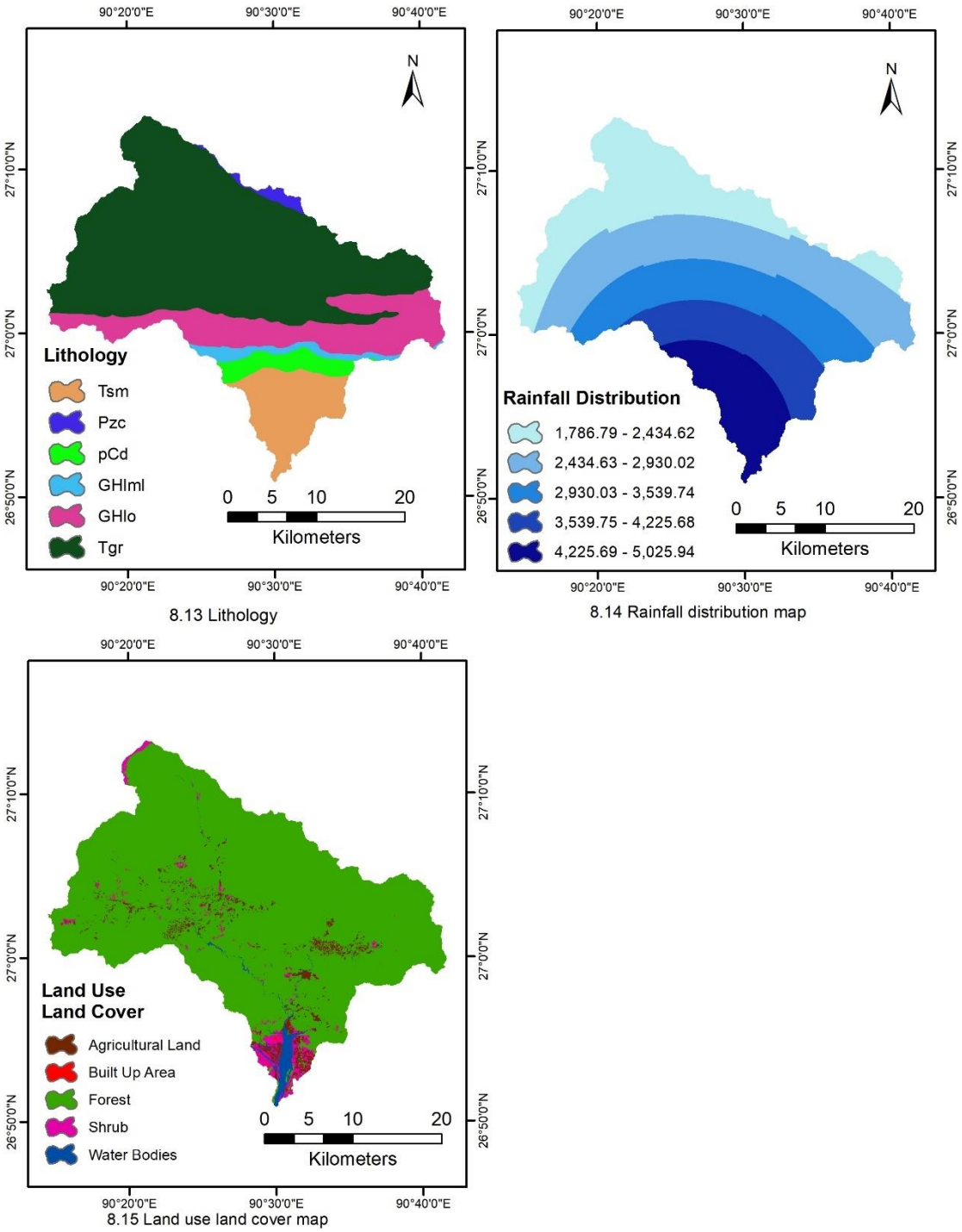


**Figure 8 Factors using spatial resolution 12.5m (8.1) Elevation, (8.2) Slope, (8.3) Slope Aspect, (8.4) Curvature, (8.5) TWI, (8.6) SPI, (8.7) Drainage density, (8.8) NDVI, (8.9) NDSI, (8.10) Dist. from river, (8.11)Dist. from fault, (8.12)Dist. From road, (8.13) Lithology, (8.14) Rainfall map, (8.15) LULC**

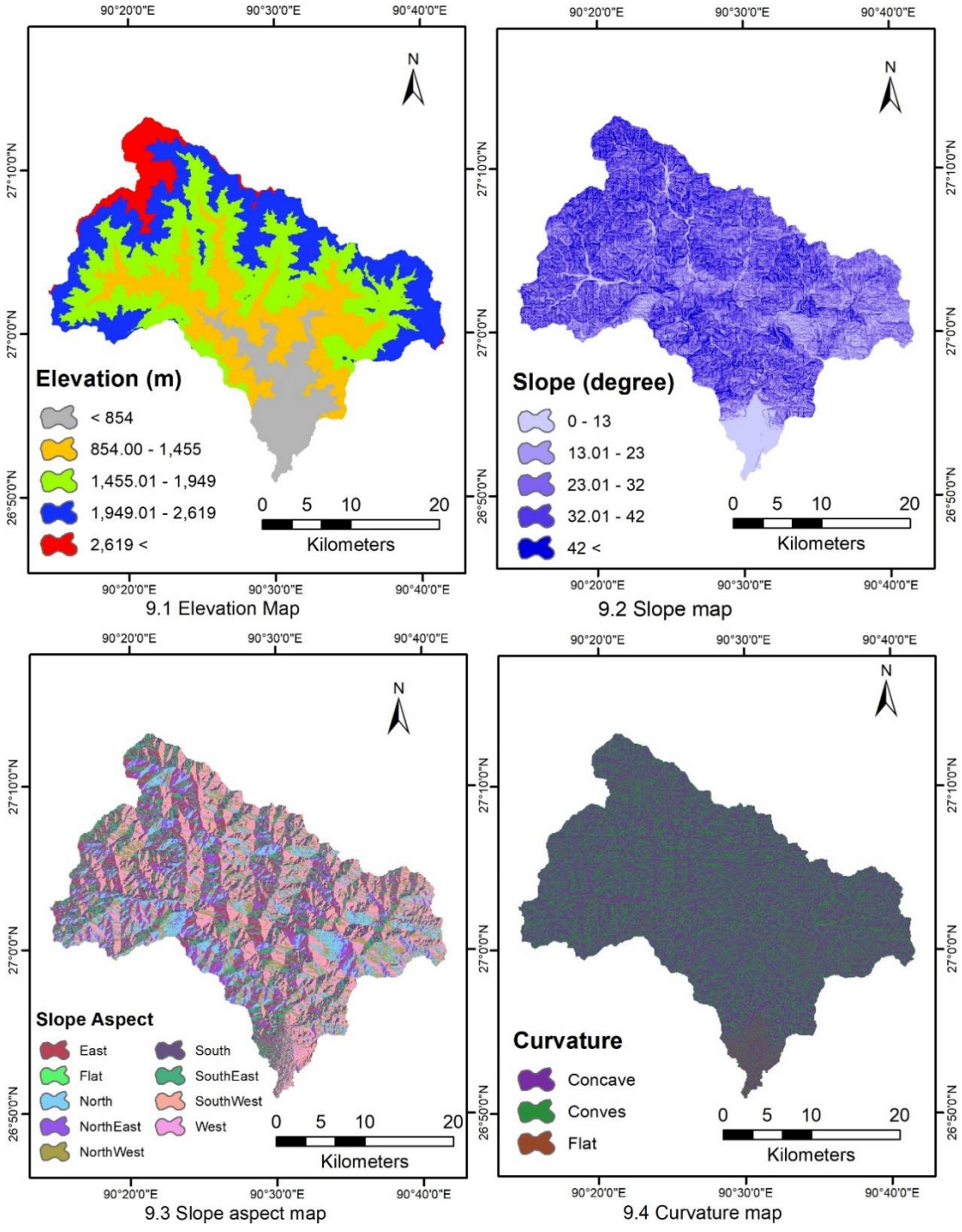


**Figure 9 Factors using spatial resolution 30m (9.1) Elevation, (9.2) Slope, (9.3) Slope Aspect, (9.4) Curvature, (9.5) TWI, (9.6) SPI, (9.7) Drainage density, (9.8) NDVI, (9.9) NDSI, (9.10) Dist. from river, (9.11)Dist. from fault, (9.12)Dist. From road, (9.13) Lithology, (9.14) Rainfall map, (9.15) LULC**

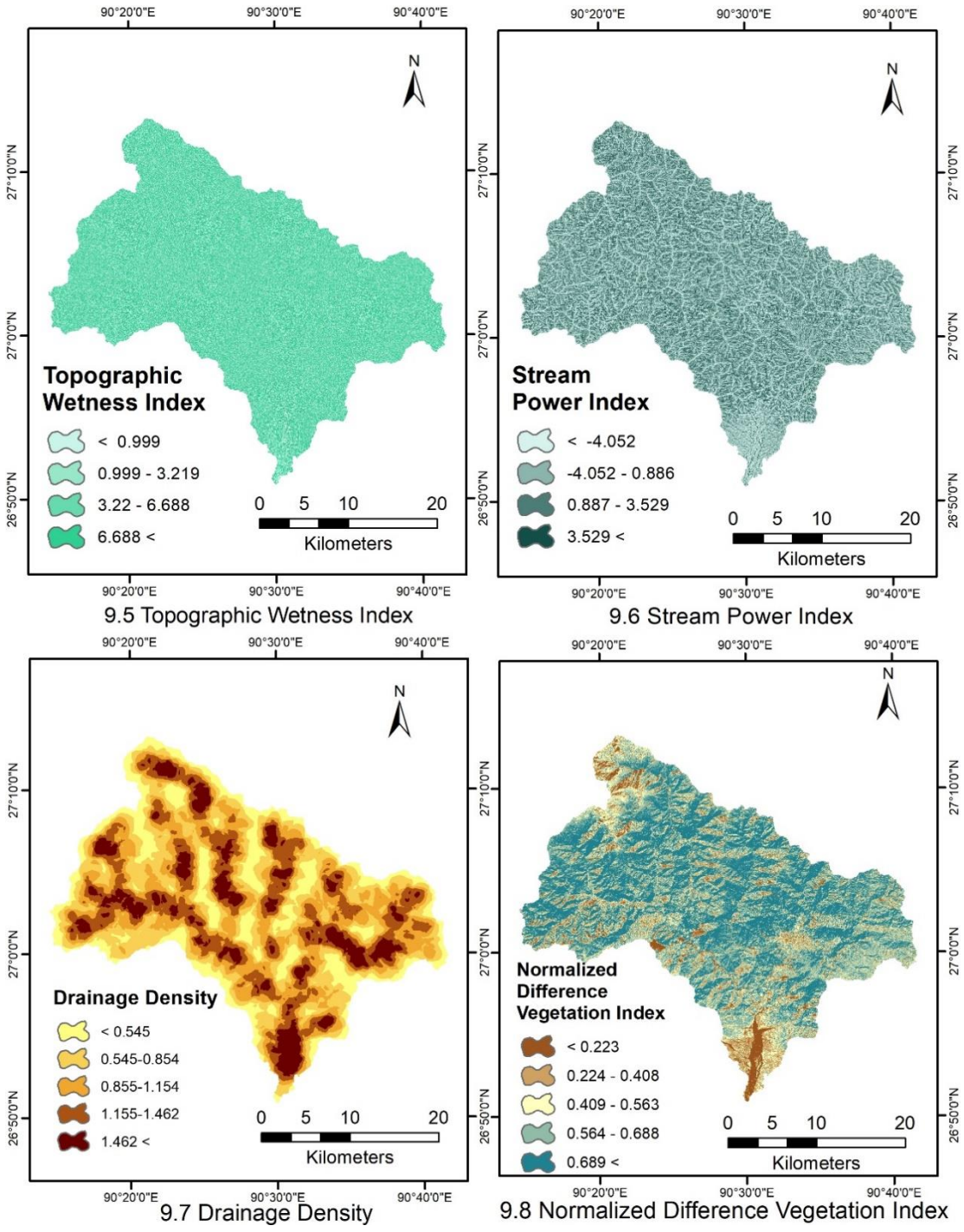


**Figure 9 Factors using spatial resolution 30m (9.1) Elevation, (9.2) Slope, (9.3) Slope Aspect, (9.4) Curvature, (9.5) TWI, (9.6) SPI, (9.7) Drainage density, (9.8) NDVI, (9.9) NDSI, (9.10) Dist. from river, (9.11) Dist. from fault, (9.12)Dist. From road, (9.13) Lithology, (9.14) Rainfall map, (9.15) LULC**

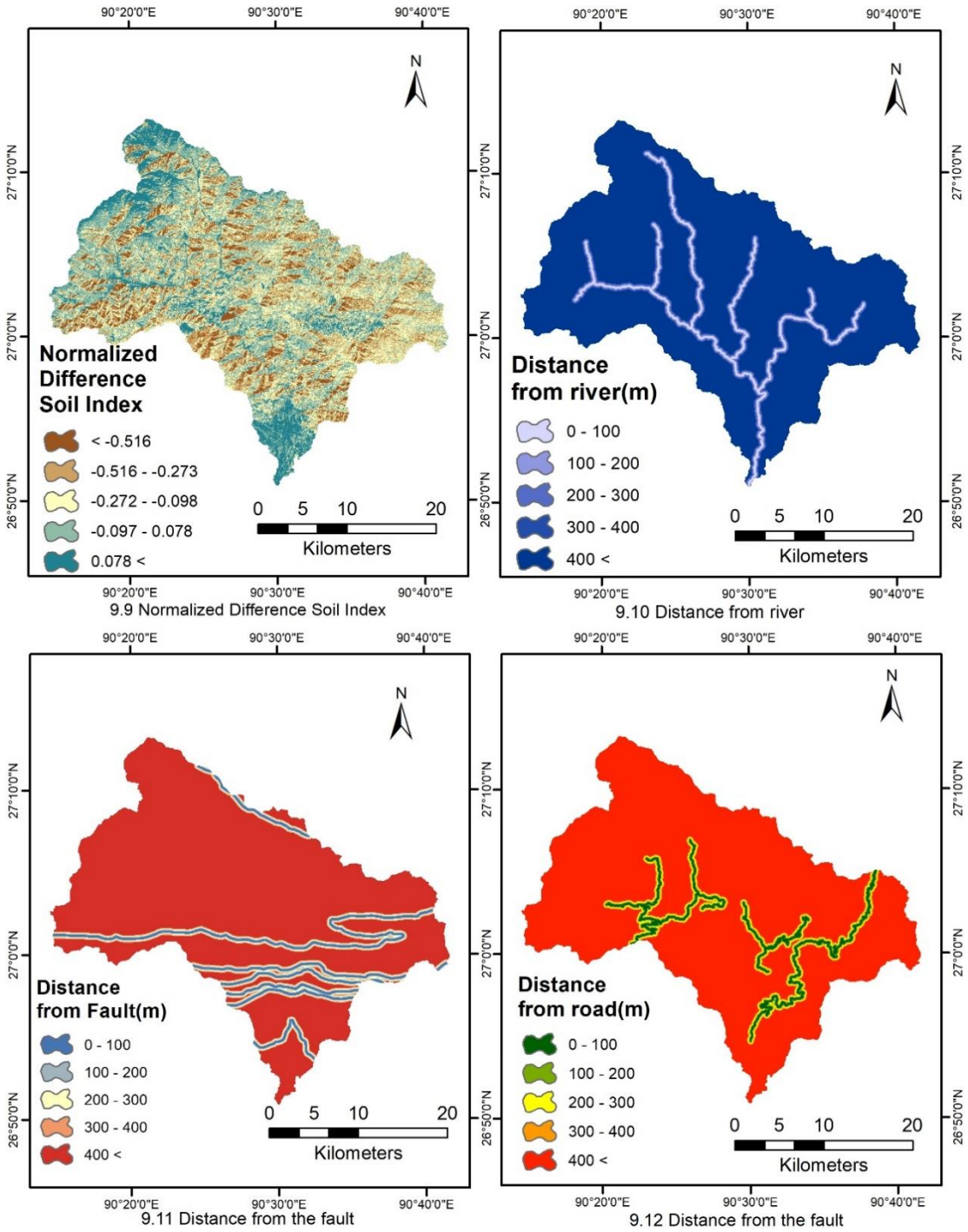


**Figure 9 Factors using spatial resolution 30m (9.1) Elevation, (9.2) Slope, (9.3) Slope Aspect, (9.4) Curvature, (9.5) TWI, (9.6) SPI, (9.7) Drainage density, (9.8) NDVI, (9.9) NDSI, (9.10) Dist. from river, (9.11) Dist. from fault, (9.12)Dist. From road, (9.13) Lithology, (9.14) Rainfall map, (9.15) LULC**

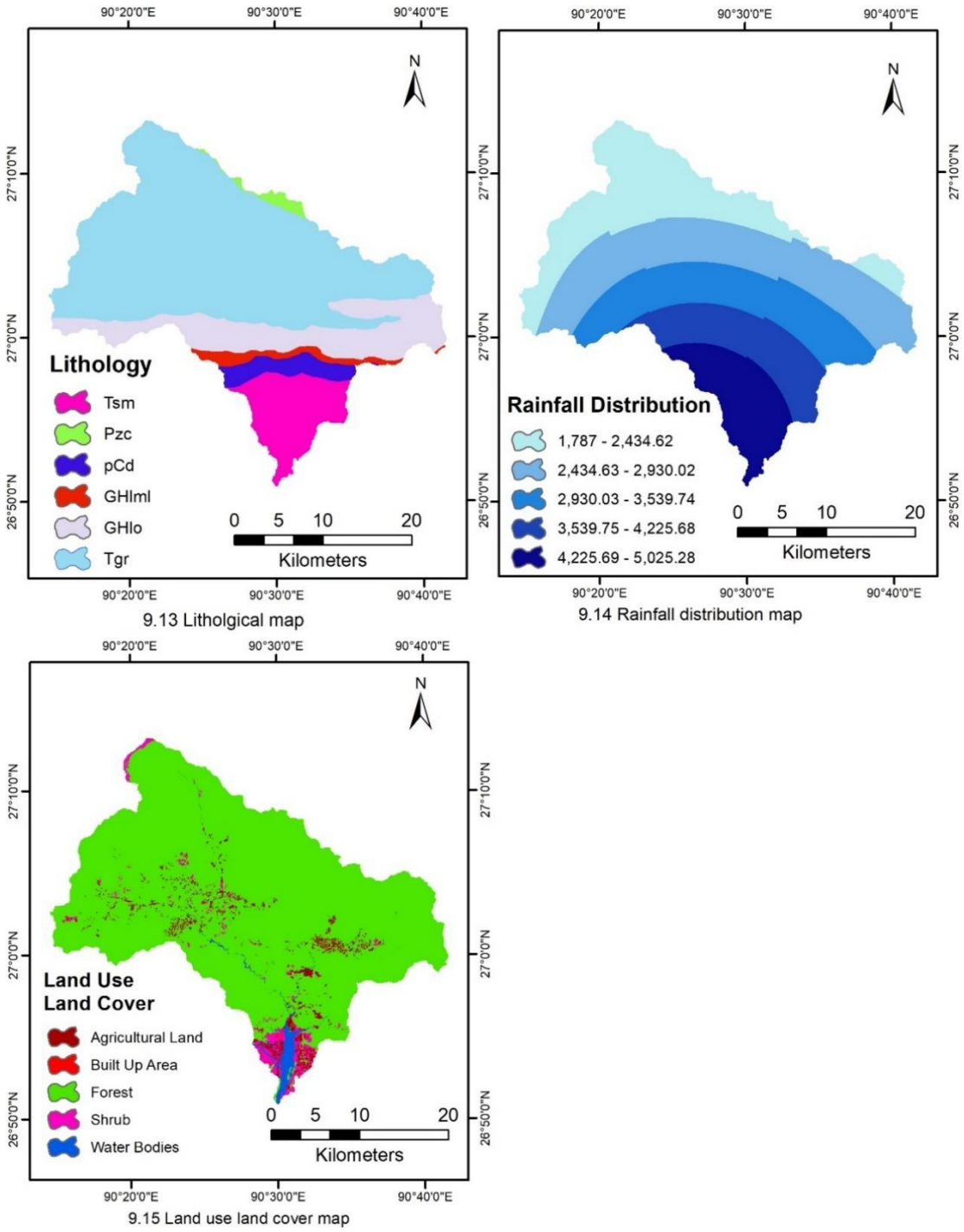


**Figure 9 Factors using spatial resolution 30m (9.1) Elevation, (9.2) Slope, (9.3) Slope Aspect, (9.4) Curvature, (9.5) TWI, (9.6) SPI, (9.7) Drainage density, (9.8) NDVI, (9.9) NDSI, (9.10) Dist. from river, (9.11) Dist. from fault, (9.12)Dist. From road, (9.13) Lithology, (9.14) Rainfall map, (9.15) LULC**

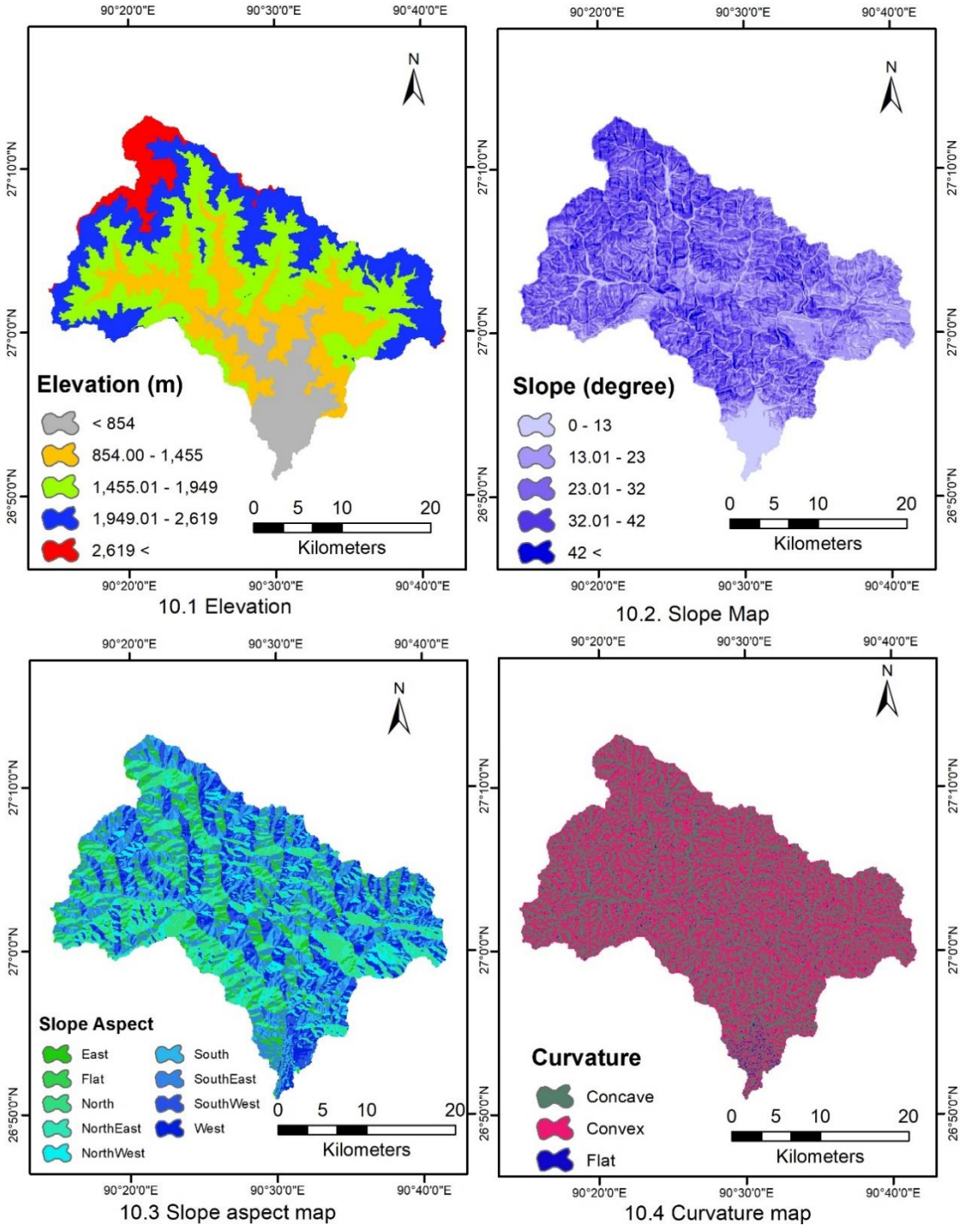


**Figure 10 Factors using spatial resolution 90m (10.1) Elevation, (10.2) Slope, (10.3)Slope Aspect, (10.4)Curvature, (10.5)TWI, (10.6)SPI, (10.7)Drainage density, (10.8)NDVI, (10.9)NDSI, (10.10)Dist. from river, (10.11)Dist. from fault, (10.12)Dist. From road, (10.13) Lithology, (10.14) Rainfall map, (10.15) LULC**

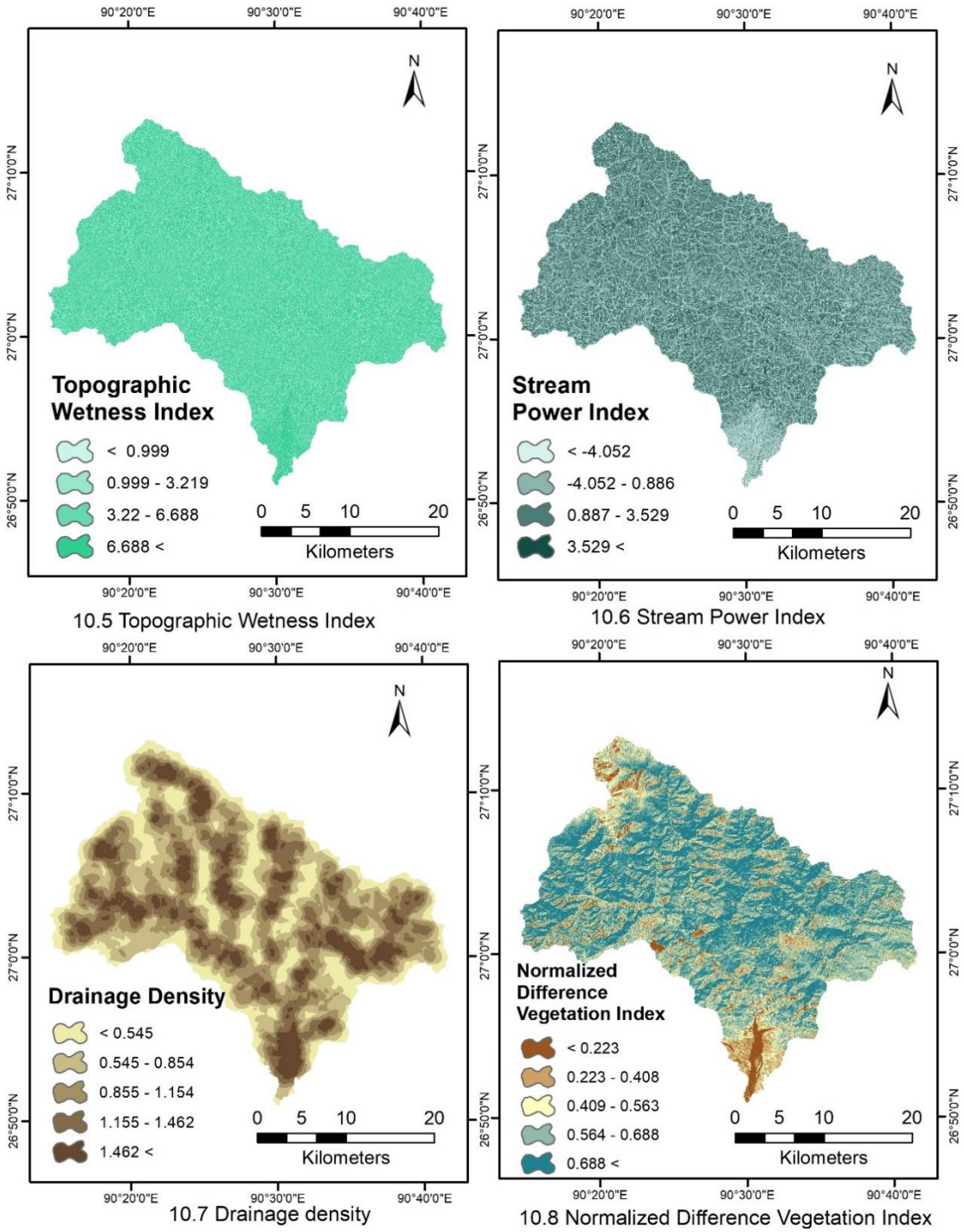


**Figure 10 Factors using spatial resolution 90m (10.1) Elevation, (10.2) Slope, (10.3)Slope Aspect, (10.4)Curvature, (10.5)TWI, (10.6)SPI, (10.7)Drainage density, (10.8)NDVI, (10.9)NDSI, (10.10)Dist. from river, (10.11)Dist. from fault, (10.12)Dist. From road, (10.13) Lithology, (10.14) Rainfall map, (10.15) LULC**

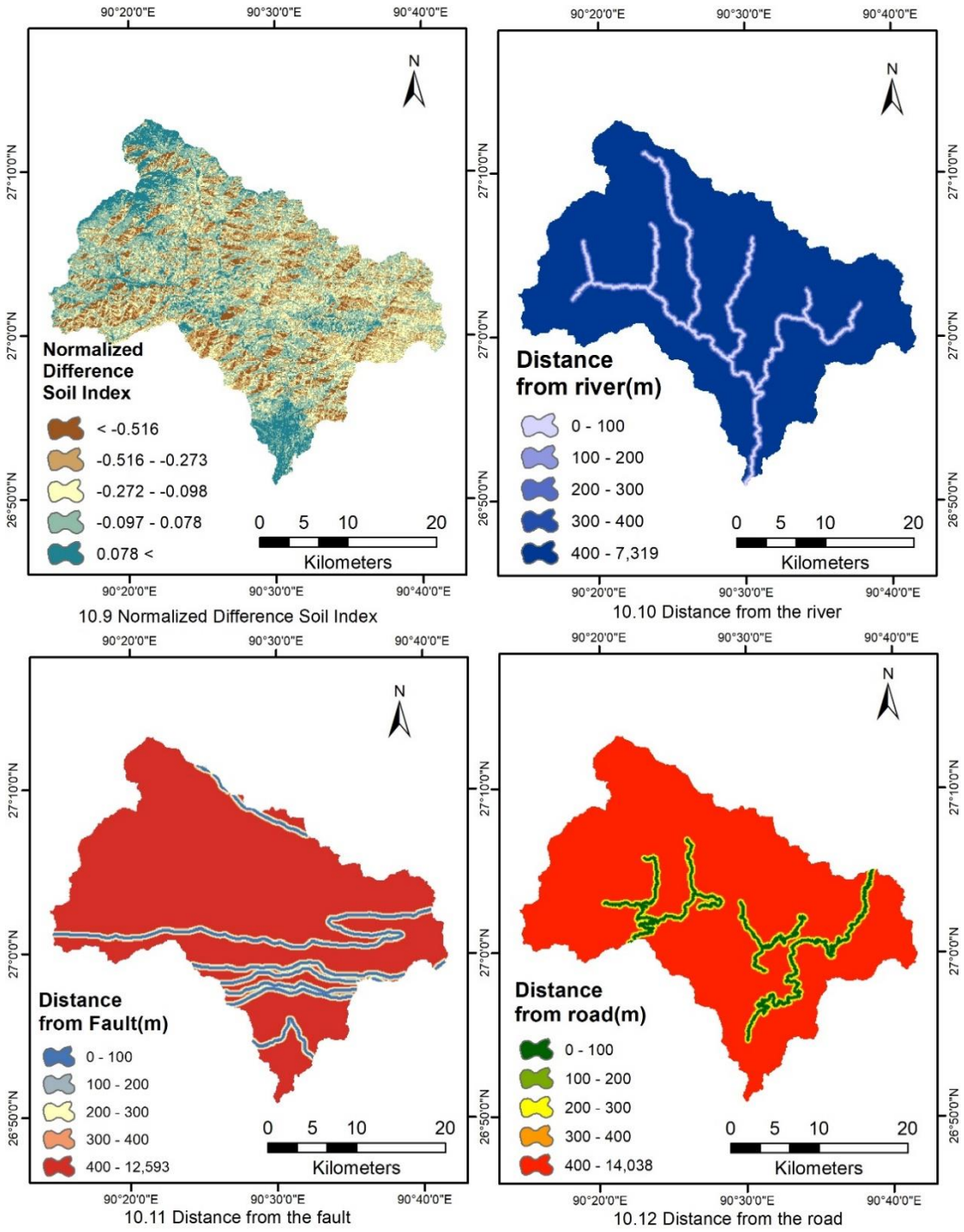


**Figure 10 Factors using spatial resolution 90m (10.1) Elevation, (10.2) Slope, (10.3)Slope Aspect, (10.4)Curvature, (10.5)TWI, (10.6)SPI, (10.7)Drainage density, (10.8)NDVI, (10.9)NDSI, (10.10)Dist. from river, (10.11)Dist. from fault, (10.12)Dist. From road, (10.13) Lithology, (10.14) Rainfall map, (10.15) LULC**

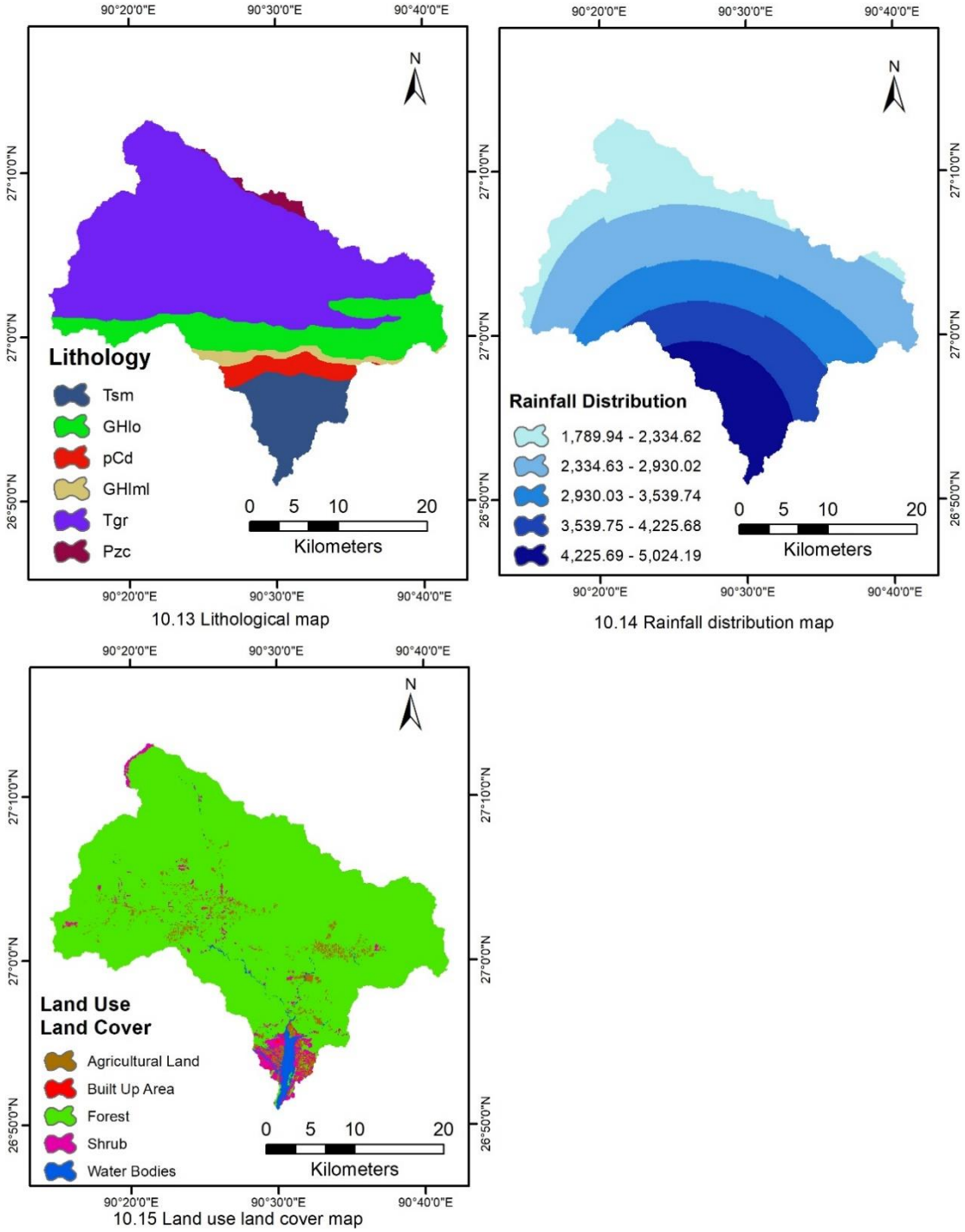


**Figure 10 Factors using spatial resolution 90m (10.1) Elevation, (10.2) Slope, (10.3) Slope Aspect, (10.4) Curvature, (10.5)TWI, (10.6)SPI, (10.7)Drainage density, (10.8)NDVI, (10.9)NDSI, (10.10)Dist. from river, (10.11)Dist. from fault, (10.12)Dist. From road, (10.13) Lithology, (10.14) Rainfall map, (10.15) LULC**

### 3.3.2 Landslides Susceptibility Assessment

There are several models for the assessment of the landslide susceptibility mapping. There is no specific rule for choosing the landslide mapping models. The models are chosen based on the individual experience, terrain nature, availability of triggering parameters, and landslide types. This study uses quantitative statistical approaches for the landslide assessment. These approaches are the frequency ratio (FR), index of entropy (IOE), and weight of evidence (WOE). Three different spatial (12.5m, 30m and 90m) were used to form in all the three different models. The LSM developed using FR, IOE, and WOE are combined to form new hybrid model. The combinations were FR and IOE to form FR-IOE, IOE and WOE to form IOE-WOE, and finally, WOE and FR combined to form WOE-FR. The statistical approaches work on the principle past and present to the future landslides prediction under a similar condition to that of the past landslides (Aleotti and Chowdhury, 1999).

**I. Frequency Ratio (FR)**

The frequency ratio (FR) technique is proved to be effective and widely used for LSM. When the frequency ratio value is large, the relationship between the landslide and the influencing factor is stronger (Jaafari *et al.*, 2014). In frequency ratio, it is assumed that all the factors carry equal weight. However, the factor's classes have different frequency ratio value. According to Khan *et al.* (2019), FR is calculated using the Equation 5

$$FR = \frac{\frac{Npix(i)}{Npix(ii)}}{\frac{Npix(iii)}{Npix(iv)}} \qquad \text{Equation 5}$$

Where, Npix(i) = The number of pixels containing landslide in a class

Npix(ii) = Total number of landslide pixels of in the factor

Npix(iii) = Total number of pixel in the class

Npix(iv) = Total number of pixels in the study area

Once the FR is calculated, the FR value is used for the reclassification of the factors. All the reclassified map of the factors are added (Equation 6) to form the Landslide Susceptibility Mapping (Khan *et al.*, 2019).

$$LSM_{FR} = \sum_{i=1}^{n} FR \qquad \text{Equation 6}$$

Where, FR is the frequency ratio, i is the influencing factor and n is the number of influencing factors.

**II. Index of entropy (IOE)**

The entropy signifies the extent of the imbalance, disorder, and instability of the system (Liu and Duan, 2018). Concerning the landslides, entropy refers to the impact of the factors on the landslides occurrence (Pourghasemi *et al.*, 2012). The entropy calculates the weight of the factors (Tien Bui *et al.*, 2018). The advantage of the index of entropy over frequency ratio is that it calculates the influencing weight of the factors on the landslide susceptibility (Aleotti and Chowdhury, 1999). The Equation 7 to Equation 12 is used to calculate the weight of the influencing factors.

$$P_{ij} = \frac{b}{a} \qquad \text{Equation 7}$$

$$(P_{ij}) = \frac{P_{ij}}{\sum_{i=1}^{sj} P_{ij}} \qquad \text{Equation 8}$$

$$H_j = -\sum_{i=1}^{sj}(Pij)\log_2(P_{ij}), \qquad j=1, 2,\ldots, n \qquad \text{Equation 9}$$

$$H_{jmax} = log_2 Sj \qquad \text{Equation 10}$$

$$I_j = \frac{H_{jmax} - H_j}{H_{jmax}}, \qquad I=(0, 1), \quad j=1, 2,.., n \qquad \text{Equation 11}$$

$$W_j = I_j P_{ij} \qquad \text{Equation 12}$$

where, b is the percentage of landslide occurrence pixels in a class to the total landslide occurrence pixels, a is the percentage of pixels in a class to the total pixels, ($P_{ij}$) is the probability density, $H_j$ and $H_{jmax}$ is the entropy values, Sj is the number of classes, $I_j$ is the information coefficient value, and $W_j$ is the factor weight value as a whole.

For the LSM, the factors are reclassified using the value of probability density ($P_{ij}$). Then the reclassified factors were multiplied with the weight ($W_j$) of the individual factors and finaly add (Equation 13) all the weighted secondarily reclassified factors produces LSM (Constantin, Bednarik, Jurchescu, and Vlaicu, 2011).

$$LSM_{IOE} = \sum C\ x\ W_j$$ Equation 13

where, $LSM_{IOE}$ is the landslide susceptibility mapping, C is the value of the class after secondary reclassification based on the probability density ($P_{ij}$), and $W_j$ is the resultant weight of a causal factor (Constantin *et al.*, 2011).

**III Weight of Evidence (WOE)**

The Weight of Evidence (WOE) is a data-driven quantitative statistical method based on Bayesian statistics(Bonham-Carter, Agterberg, and Wright, 1988). Initially, the weight of evidence is developed for the mineral potential study. However, several authors have applied for prediction of landslides, flood, groundwater potential, and other prediction model using GIS (Dahal, Hasegawa, Nonomura, Yamanaka, Dhakal, *et al.*, 2008). For landslide susceptibility assessment, the landslide probability is determined using the weight of the factors (evidence). In this method, a series of mathematical calculations are required and the detail of mathematical procedures are explained by Van Westen (2002). Two types of data required for the WoE were landslide inventory and landslide factors(Roy, Saha, Arabameri, Blaschke, and Bui, 2019). The weight describes the probability of landslide occurrence in the case of the presence as well as the absence of the evidence (Kayastha, Dhital, and Smedt, 2012). In this method, the positive and negative weight ($W^+$ and $W^-$) are assigned to each pixel of the factor classes and calculated using Equation 14 and Equation 15. $W^+$ expresses the chances of occurrence of a landslide in the case of the evidence being present and its magnitude indicate of the positive association between landslide event and the factor class (Neuhäuser, Damm, and Terhorst, 2012). On the other hand, $W^-$ describes the chances of landslide in case of absence of the evidence and its magnitude indicates a negative association between the landslide event and the factor class (Neuhäuser *et al.*, 2012)

$$W^+ = log_e \frac{P\{B|S\}}{P\{B|\bar{S}\}}$$ Equation 14

$$W^- = log_e \frac{P\{\bar{B}|S\}}{P\{\bar{B}|\bar{S}\}}$$ Equation 15

Where, P is the probability, B is the presence of potential landslide factor, while $\bar{B}$ is the absence of a potential landslide factor. S is the presence of landslide and $\bar{S}$ is the absence of landslide.

The difference between W+ and W− is known as weight contrast C, which indicates the spatial association between classes of the factor and landslides events(Dahal, Hasegawa, Nonomura, Yamanaka, Masuda, *et al.*, 2008). The C>0, if the spatial association is positive while C<0, if the spatial association is negative and C = 0 if the spatial association is lacking (Carranza, 2004).

$$C = W^{+} - W^{-} \quad \text{Equation 16}$$

Where, C is the weight contrast of $W^{+}$ and $W^{-}$.

The standard deviation S(C) of the contrast C is calculated suing Equation 17.

$$S(C) = \sqrt{S^2(W^{+}) + S^2(W^{-})} \quad \text{Equation 17}$$

Where, S2(W+) and S2(W−) are the variances of positive weight $W^{+}$ and negative weight $W^{-}$ respectively. The variance of the weight is calculated using Equation 18 and Equation 19.

$$S^2(W^{+}) = \frac{1}{N(B \cap S)} + \frac{1}{N(B \cap \bar{S})} \quad \text{Equation 18}$$

$$S^2(W^{-}) = \frac{1}{N(\bar{B} \cap S)} + \frac{1}{N(\bar{B} \cap \bar{S})} \quad \text{Equation 19}$$

Where, B is the presence of potential landslide factor, $\bar{B}$ is the absence of potential landslide factor, S is the presence of landslide and $\bar{S}$ is the absence of landslide.

When there is a small number of training points in the small area, the degree of uncertainty of the weight could be high which reduces the degree of certainty of the contrast C (Neuhäuser *et al.*, 2012). In this case, the studentized contrast (Cs) is used to measure the confidence of the factors in contributing to the landslides (Kayastha, Dhital, and De Smedt, 2012). It is defined as the ratio of the contrast C to the standard deviation and its calculated using the Equation 20 (Pradhan, Oh, and Buchroithner, 2010).

$$C_s = \frac{C}{S(C)}$$ Equation 20

Where, the C is the contrast, and S(C) is the standard deviation.

To develop LSM, all the classes of the factors are reclassified using the contrast value (C). Then, add all the reclassified factors. Equation 21 is used for the development of the LSM.

$$LSM_{WOE} = \sum_{i=1}^{n} C_{ij}$$ Equation 21

where LSM is a landslide susceptibility map, and $C_{ij}$ is the contrast for class i of conditioning factor j, n is the number of factors.

It is assumed that the contrast is normally distributed. If the studentized contrast (*Cs*) is more than 1.96, it is 95% confident that there is a positive overall association between the landslide event and the evidence. On the other hand, if the studentized contrast is less than -1.96, the confidence level is 95% disfavoring the landslides occurrence. When the studentized contrast lies in between -1.96 and 1.96, there is no significant relationship between the evidence and the landslides(Kayastha, Dhital, and De Smedt, 2012).

**IV Hybrid landslide susceptibility mapping**

The hybrid landslide susceptibility mapping consist of preparation of LSM by combination of Frequency Ratio-Index of Entropy (FR-IOE), Index of Entropy-Weight of Evidence (IOE-WOE), and Weight of Evidence-Frequency Ratio (WOE-FR).

### 3.3.3 Accuracy Assessment

For the validation, 30% of the landslide inventory is used for the validation of the landslide susceptibility map. The validation dataset which is observed from the ground is made in the binary number. The landslide is assigned with 1 and an equal number of non-landslide with 0. Then the binary data set has to convert into a raster file which is of equal cell size with that of factors.

**I. Confusion Matrix**

The confusion matrix is used for the calculation of the statical indices for the landslides. The confusion matrix uses the observed landslides with the predicted landslides which will help in the calculation of True Positive (TP), False Negative (FN), False Positive (FP), and True Negative (TN). The TP, FP, FN, and TN are used to calculate true positive rate (Equation 22), false positive rate (Equation 23), and accuracy (Equation 24).

$$\text{TPR or Sensitivity} = \frac{\text{TP}}{\text{TP} + \text{FN}} \quad \text{Equation 22}$$

$$\text{FPR or } (1 - \text{Specificity}) = \frac{\text{FP}}{\text{FP} + \text{TN}} \quad \text{Equation 23}$$

$$\text{Accuracy} = \frac{\text{TP} + \text{TN}}{\text{TP} + \text{FN} + \text{FP} + \text{FN}} \quad \text{Equation 24}$$

**II. Cohen's Kappa Index**

The kappa index is calculated based on the Equation 25 to Equation 27

$$\text{Kappa} = \frac{\text{P}_{\text{obs}} - \text{P}_{\text{exp}}}{1 - \text{P}_{\text{exp}}} \quad \text{Equation 25}$$

$$P_{obs} = \frac{\text{TP} + \text{TN}}{\text{n}} \quad \text{Equation 26}$$

$$P_{exp} = \frac{(\text{TP} + \text{FN})(\text{TP} + \text{FP}) + (\text{FP} + \text{TN})(\text{FN} + \text{TN})}{\text{n}^2} \quad \text{Equation 27}$$

Where, n represent the total pixel of the training dataset, TP represent True Positive, FN represent False Negative, FP represent False Positive and TN represent True Negative are calculated in from the confusion matrix, $P_{obs}$ is the observed agreements; $P_{exp}$ is the expected agreements.

**III. The Receiver Operating Characteristic (ROC) curve**

The ROC curve is constructed using sensitivity and specificity. The *x*-axis and y-axis of the ROC curve are 1-specificity and sensitivity, respectively(Zhang *et al.*, 2019). The Area Under Curve(AUC) is calculated using the Equation 28. The AUC value ranges from 0.5 (inaccurate model) to 1 for the ideal model with higher performance (Tien Bui *et al.*, 2018).

$$AUC = \frac{\sum TP + \sum TN}{P + N}$$ Equation 28

where TP is the number of landslides that are correctly classified, TN is the number of incorrectly classified landslides, P is the total number of landslides and N is the total number of non-landslides.

### IV. Root Mean Square Error (RMSE)

The Root Mean Square Error (RMSE) is used to calculate relative error between the models (Nguyen *et al.*, 2019). When the RMSE value is 0, it is considered as no error which corresponds to correlation coefficient 1 and vice versa (Barnston, 1992).

The RMSE is calculated using the Equation 29.

$$RMSE = \sqrt{\frac{1}{n}\sum_{i=1}^{n}(X_{pred} - X_{obs})^2}$$ Equation 29

where n is the total number of samples in the validation dataset; $X_{pred}$ is the predicted values from the LSM and $X_{obs}$ is the observed data from the real ground.

# CHAPTER IV
# RESULT AND DISCUSSION

## 4.1 Landslide Inventory

The landslides inventory was done using the interpretation of the sentinel-2 image, google earth image, and verified through field investigation using handheld GPS. Although the landslide inventory comprises of data collection of date of landslide event and it's frequency of occurrence, it is not mandatory to have these data since the spatial location of the past landslides is enough to analyze the LSM (Nohani *et al.*, 2019). Similarly, due to the unavailability of the exact date of landslide event and frequency of the landslides at Ossey watershed area, this study could not collect the date and frequency of the landslides.

A total of 164 landslides locations were identified at the Ossey watershed area during the landslide inventory (Appendix A). The research uses Varnes (1978) landslide classification method to classify the landslide present at the study site. The types of landslides present at the study area include 116 (70.73%) translational slides, 38 (23.17%) debris flow, 6 (3.66%) debris avalanche, 2 (1.22%) earth flow, 1 (0.61%) rockfall, and 1 (0.61%) creep. The detail of the individual landslides was given in Appendix A. The most prominent landslide present at the study site was the translational slide and the debris flow.

A total of 115 (70%) of the landslides were used for training the data which will be used in FR, IOE, and WOE. The remaining 49 (30%) landslide locations were used for validation of the model. The selection of the training and validation dataset was based on random selection. The training datasets were digitized into point features that are converted into a raster format of 12.5m, 30m, and 90m spatial resolution to make compatible with the influencing factors. Similarly, the validation dataset was also made into a raster format of 12.5m, 30m, and 90m spatial resolution to validate the LSM which is 12.5m, 30m, and 90m spatial resolution.

## 4.2 Evaluation of landslide influencing factors using bivariate statistical models

The spatial resolution used for this study is 12.5m, 30m, and 90m which is the same as the source resolution of the source DEM. The Frequency Ratio (FR), Index of

Entropy (IOE), and Weight of Evidence (WOE) analysis were used for all three spatial resolution. The study area consists of 5,252,600 pixels for the 12.5m spatial resolution, 911,947 pixels for the 30m spatial resolution, and 101,183 pixels for the 90m spatial resolution.

### 4.2.1 Relationship in the Frequency Ratio

The FR value shows the weight of the individual factor classes. The higher FR value indicates a stronger correlation between the factor's class and landslides (Nohani *et al.*, 2019). Table 14 shows the average FR value of three different spatial resolutions (12.5m, 30m, and 90m) of the individual classes of the fifteen factors calculated using Equation 5. The detail of FR calculations was given in the Appendix B for spatial resolution 12.5m, 30m and 90m. It was observed that all the different spatial resolutions acted in a similar trend using the FR. The average FR calculation for the three different spatial resolution factors (12.5m, 30m, and 90m) were shown in Table 14. The higher value of frequency shows a higher probability of landslides.

From Table 14, it is noticed that the frequency ratio (FR) value generally decreases with an increase in elevation for all three spatial resolutions. This shows that the probability of the landslides decreases as the elevation increases. This may be due to weak lithology and high precipitation in the lower elevation and vice versa. During the field visit, it is confirmed that the lower elevation area corresponds to the steeper slopes. This similar pattern of the result was observed by (Jaafari *et al.*, 2014). While comparing with the spatial resolution with the FR value, it was observed that the FR value is slightly higher in all the classes for the finer spatial resolution.

Regarding the slope gradient, the FR value increases with an increase slope gradient. This reveals that the landslide probability increases as the slope becomes steeper. The result follows a similar trend with the number of other literatures that shows a similar result and the field investigation also witnesses that the steeper slopes experience more landslides. Regarding the variation of FR value with changes in spatial resolution, it is noticed that FR value increases systematically. However, it is observed that as the spatial resolution becomes courser, the FR value increases with a big jump compared to the finer spatial resolution.

**Table 14 Relationship between the landslide and influencing factors using frequency ratio model**

| Factor | Class | % of pixel in class | % of landslide in class | Frequency Ratio |
|---|---|---|---|---|
| Elevation (m) | < 854.00 | 12.83 | 34.49 | 2.69 |
| | 854.00 - 1455 | 23.42 | 30.43 | 1.30 |
| | 1455.01 - 1949 | 32.15 | 18.55 | 0.58 |
| | 1949.01 - 2619 | 25.91 | 12.17 | 0.47 |
| | 2619 < | 5.69 | 4.35 | 0.77 |
| Slope (Degree) | 0 - 13.00 | 10.39 | 7.54 | 0.72 |
| | 13.01 - 23.00 | 22.69 | 17.97 | 0.77 |
| | 23.01 - 32.00 | 31.76 | 27.25 | 0.86 |
| | 32.01 - 42.00 | 26.97 | 27.83 | 1.04 |
| | 42 < | 8.20 | 19.42 | 2.60 |
| Aspect | Flat | 0.32 | 0.00 | 0.00 |
| | North | 12.23 | 4.93 | 0.40 |
| | NorthEast | 10.88 | 6.67 | 0.61 |
| | East | 12.13 | 13.04 | 1.07 |
| | SouthEast | 14.37 | 27.54 | 1.92 |
| | South | 13.09 | 17.68 | 1.35 |
| | SouthWest | 14.14 | 13.33 | 0.94 |
| | West | 12.08 | 7.25 | 0.60 |
| | NorthWest | 10.78 | 9.57 | 0.89 |
| Curvature | Concave | 46.43 | 55.07 | 1.18 |
| | Flat | 6.85 | 5.80 | 0.54 |
| | Convex | 46.72 | 39.13 | 0.85 |
| TWI | < 0.999 | 23.29 | 24.64 | 1.06 |
| | 0.999 - 3.219 | 21.29 | 22.32 | 1.02 |
| | 3.220 - 6.688 | 4.88 | 3.77 | 0.79 |
| | 6.688 < | 50.54 | 49.28 | 0.97 |
| SPI | < -4.052 | 24.80 | 17.97 | 0.74 |
| | -4.052 - 0.886 | 36.90 | 34.78 | 0.94 |
| | 0.887 - 3.529 | 31.71 | 39.13 | 1.28 |
| | 3.529 < | 6.58 | 8.12 | 1.22 |
| Drainage Density | < 0.545 | 18.33 | 5.51 | 0.30 |
| | 0.545 - 0.854 | 25.33 | 31.88 | 1.26 |
| | 0.855 - 1.153 | 24.19 | 37.97 | 1.57 |
| | 1.154 - 1.462 | 21.17 | 18.55 | 0.87 |
| | 1.462 < | 10.99 | 6.09 | 0.55 |
| NDVI | <223 | 4.20 | 20.58 | 4.90 |
| | 0.223 - 0.407 | 10.93 | 19.71 | 1.80 |
| | 0.408 - 0.562 | 16.64 | 15.94 | 0.96 |
| | 0.563 - 0.688 | 28.52 | 22.32 | 0.79 |
| | 0.688 < | 39.71 | 21.45 | 0.54 |
| NDSI | < -0.516 | 9.24 | 7.25 | 0.78 |
| | -0.516 - -0.273 | 18.04 | 9.28 | 0.51 |
| | -0.274 - -0.097 | 28.03 | 14.78 | 0.53 |
| | -0.098 - 0.078 | 31.45 | 35.94 | 1.14 |
| | 0.078 < | 13.24 | 32.75 | 2.47 |
| Distance from river (m) | 0-100 | 3.71 | 6.09 | 1.64 |
| | 100-200 | 2.85 | 1.16 | 0.40 |

| | | | | |
|---|---|---|---|---|
| | 200-300 | 3.23 | 3.48 | 1.08 |
| | 300-400 | 2.85 | 3.48 | 1.22 |
| | 400< | 87.36 | 85.80 | 0.98 |
| Distance from fault (m) | 0-100 | 4.67 | 1.74 | 0.35 |
| | 100-200 | 3.64 | 4.06 | 1.12 |
| | 200-300 | 3.99 | 5.22 | 1.31 |
| | 300-400 | 3.20 | 4.06 | 1.28 |
| | 400< | 84.49 | 84.93 | 1.01 |
| Distance from Road (m) | 0-100 | 3.48 | 4.35 | 1.26 |
| | 100-200 | 2.36 | 2.03 | 0.87 |
| | 200-300 | 2.56 | 5.51 | 2.15 |
| | 300-400 | 2.17 | 1.45 | 0.67 |
| | 400< | 89.44 | 86.67 | 0.97 |
| Lithology | Tsm | 10.58 | 27.23 | 2.57 |
| | Pzc | 6.67 | 7.25 | 0.92 |
| | pCd | 3.79 | 10.43 | 2.75 |
| | GHlml | 2.52 | 4.35 | 1.73 |
| | GHlo | 33.27 | 25.51 | 0.94 |
| | Tgr | 43.17 | 24.64 | 0.66 |
| Rainfall (mm) | 1786.79 - 2434.61 | 25.57 | 16.52 | 0.65 |
| | 2434.62 - 2930.01 | 28.56 | 12.46 | 0.44 |
| | 2930.02 - 3539.74 | 20.30 | 14.20 | 0.70 |
| | 3539.75 - 4225.67 | 13.53 | 34.20 | 2.53 |
| | 4225.68 - 5025.93 | 12.02 | 22.61 | 1.88 |
| LULC | Agricultural Land | 3.26 | 1.74 | 0.53 |
| | Built Up Area | 0.09 | 0.00 | 0.00 |
| | Forest | 92.61 | 94.78 | 1.02 |
| | Shrub | 2.47 | 3.19 | 1.29 |
| | Water Bodies | 1.57 | 0.29 | 0.18 |

In the case of slope aspect, it is noticed that the south (1.35), south-east (1.92), and east (1.07) facing slopes corresponds to a higher value of FR in all the three resolution. This shows that the south, south-east, and east-facing slopes experience more landslides. The result is perfectly matching with the landslide frequency that Bhutan encounters. The south and east-facing slopes experience relatively more precipitation and experience relatively a greater number of landslides. This may be due to the orographic effect of the giant Himalayan mountain. The winds that come from the Indian Ocean are blocked by the Himalayan mountain, condense it, and finally precipitate on the south and east-facing slopes. This ultimately causes a greater number of landslides. In the slope aspect, all three resolutions follow a similar trend with the FR value.

Regarding the slope curvature, the FR of the concave slope (1.18) is more than 1 indicating higher chances of the landslide, followed by convex (0.85) and flat area

(0.54). The previous study by Jaafari *et al.* (2014) also shows similar results. These concave curvature terrains retain more moisture and reduce the stability causing more landslides. However, the landslide probability is still debatable for the curvature in most of the literature.

The topographic wetness index (TWI) indicates the amount of water accumulation at any point in an area (Sun *et al.*, 2018). It was observed that the lowest TWI class (<0.999) corresponds to the highest FR value in all three spatial resolutions. The FR decreases with an increase in TWI and the finding is agreed with the result of Regmi *et al.* (2014).

The Stream power index (SPI) measures the erosive capacity of the flowing water in the study area (Sun *et al.*, 2018). The FR generally increases with an increase in the SPI value for all three different spatial resolutions. This shows that the erosive power of the flowing water augments the landslide probability. A similar result was obtained by Jaafari *et al.* (2014).

The relationship between the drainage density and the frequency ratio doesn't follow the regular trend for this study. This may be due to fragile and rugged terrain in certain drainage density in a specific area. The highest FR value corresponds to the drainage density class 0.546-0.854 and 0.855 - 1.153. Regarding the behavior of the different spatial resolution, all the three spatial resolution behave similar characteristic concerning frequency ratio.

The NDVI value -1 to 0 represents water, 0 to 0.2 represent barren land, rock, and built-up area, and 0.2 to 1 represents the vegetated area (Alex, Ramesh, and Sridevi, 2017). As the NDVI value increases, the strength of vegetation also increases. In this study, the FR value decreases with an increase in the NDVI in all three different spatial resolutions, and a similar result was obtained by (Nohani *et al.*, 2019). The greater NDVI value reveals healthy vegetation coverage which reinforces and stabilize the soil. This result reveals that the landslides are more common in the less vegetated area.

Normalized Difference Soil Index is used to give information about the distinction between the soil with other land cover types to a certain degree. The higher value indicates the bares soil area and the lower value indicates different categories of vegetated area (Mind'je *et al.*, 2019). From the result, it is indicated that the higher FR

increases with an increase in NDVI. This shows the bare soil is exposed to direct surface water and rainfall. This exposed surface is relatively more prone to landslides.

From the result, the landslide was more common within a distance of 400m from the river with a higher value of FR in all three spatial resolutions. The field investigation also confirmed that the landslides are common within a certain distance. In the research of Nohani *et al.* (2019), a total of 45% of the total landslides were encountered within 400m of the river. All three spatial resolution behaved similar characters in this study concerning distance to the river.

Faults are the discontinuities of the geological setting that usually decrease the rock strength (Devkota *et al.*, 2013). For this study, the FR value is higher within 400m, and it decreases while the distance goes beyond the 400m. This indicates the landslides are more common within 400m of the fault line. A similar trend was also reported by Jaafari *et al.* (2014). All three different spatial resolution act in a similar pattern.

It is observed that the FR decreases with an increase in the distance from the road. The distance within 300m from the road is more prone to the landslides because the FR value is more within 300m. This is due to the anthropogenic activities of the road construction which destabilizes the area.

Regarding the Lithology, the detail description of the lithology is given in Table 7. From Table 14, it was noticed that the order of highest FR to lowest FR are pCd, Tsm, GHlml, GHlo, Pzc, and Tgr. This shows that the most landslide-prone area corresponds to pCd, followed by Tsm, GHlml, GHlo, Pzc, and Tgr. All the different spatial resolutions acted in a similar pattern.

The FR increases with an increase in rainfall intensity in all three different spatial resolutions. This shows that the landslide probability increases with an increase in the rainfall intensity and agree with the fact that the landslides are also triggered by rainfall (Jaafari *et al.*, 2014).

In the case of the land use land cover, the FR of shrub and Forest corresponds to the highest FR value. This may be due to unsuitable lands for human habitation which is very steep, rugged, and fragile landslides in the shrubs and forest. The built-up area has zero FR value. This is due to the number of landslide preventive measures in the costly built-up area.

### 4.2.2 Relationship in the Index of Entropy

The entropy shows the degree of imbalance, disorder, unstable behavior, and uncertainty in the system (Shirani *et al.*, 2018). With regards to the landslides, entropy refers to the degree of influence or instability caused by the influencing factors on the landslides occurrence (Pourghasemi *et al.*, 2012). The entropy value is used to calculate the weight of the individual influencing factors (Tien Bui *et al.*, 2018). The Equation 7 to Equation 12 is used for the calculation of the weight of the landslides influencing factors.

The spatial relationship between the landslide event and the three different resolution (12.5m, 30m, and 90m) factors using the Index of Entropy was shown in the Appendix C. It was noticed that all three spatial resolutions show a similar trend of pattern in all the influencing factors for the Index of Entropy. The entropy value is used to calculate the weight ($W_{ij}$) of the individual factors (Tien Bui *et al.*, 2018). The $W_{ij}$ of Table 14 shows the average weight of the influencing factor of three spatial resolution (12,5m, 30m, and 90m) for the Index of Entropy. The higher value of $W_{ij}$ indicates the higher magnitude of influence of the influencing factors on the landslide occurrences (Mondal and Mandal, 2019). Among the fifteen factors, the most dominant five factors were NDVI (0.394), followed by the land use land cover (0.176), rainfall (0.163), Normalized Difference Soil Index (0.134), elevation (0.158), and lithology (0.125).

Every class of the individual factors contributes differently to the landslides event. The probability density ($P_{ij}$) is calculated using the Equation 8 and it is used to compare how the individual classes of each landslide influencing factors contribute to the landslide events.

From the result of ($P_{ij}$) of Table 15, it is noticed that the lowest elevation is highly susceptible to the landslides with the highest probability density of 0.47. As the elevation increases, the ($P_{ij}$) decreases. This indicates that the landslide probability decreases with an increase in altitude. This may be due to the coincidence of the lowest elevation with the heavy rainfall and steep rugged terrain. A similar result was also obtained by Mondal and Mandal (2019) whose study area is also located in the part of the Himalayan region with similar geotechnical setting and meteorological characteristics.

**Table 15 Relationship between the factor's class and landslide event using the Index of Entropy**

| Factor | Class | % of pixel class | % of landslide | $P_{ij}$ | $(P_{ij})$ | $H_j$ | $H_{jmax}$ | $I_j$ | $W_{ij}$ |
|---|---|---|---|---|---|---|---|---|---|
| Elevation (m) | < 854.00 | 12.83 | 34.49 | 2.69 | 0.47 | 2.006 | 2.322 | 0.136 | 0.158 |
| | 854.00 - 1455 | 23.42 | 30.43 | 1.30 | 0.22 | | | | |
| | 1455.01 - 1949 | 32.15 | 18.55 | 0.58 | 0.10 | | | | |
| | 1949.01 - 2619 | 25.91 | 12.17 | 0.47 | 0.08 | | | | |
| | 2619 < | 5.69 | 4.35 | 0.77 | 0.13 | | | | |
| Slope (Degree) | 0 - 13.00 | 10.39 | 7.54 | 0.72 | 0.12 | 2.106 | 2.322 | 0.093 | 0.114 |
| | 13.01 - 23.00 | 22.69 | 17.97 | 0.77 | 0.13 | | | | |
| | 23.01 - 32.00 | 31.76 | 27.25 | 0.86 | 0.15 | | | | |
| | 32.01 - 42.00 | 26.97 | 27.83 | 1.04 | 0.17 | | | | |
| | 42 < | 8.20 | 19.42 | 2.60 | 0.43 | | | | |
| Aspect | Flat | 0.32 | 0.00 | 0.00 | 0.00 | 2.840 | 3.170 | 0.104 | 0.090 |
| | North | 12.23 | 4.93 | 0.40 | 0.05 | | | | |
| | NorthEast | 10.88 | 6.67 | 0.61 | 0.08 | | | | |
| | East | 12.13 | 13.04 | 1.07 | 0.14 | | | | |
| | SouthEast | 14.37 | 27.54 | 1.92 | 0.24 | | | | |
| | South | 13.09 | 17.68 | 1.35 | 0.17 | | | | |
| | SouthWest | 14.14 | 13.33 | 0.94 | 0.12 | | | | |
| | West | 12.08 | 7.25 | 0.60 | 0.08 | | | | |
| | NorthWest | 10.78 | 9.57 | 0.89 | 0.12 | | | | |
| Curvature | Concave | 46.43 | 55.07 | 1.18 | 0.48 | 1.351 | 1.585 | 0.148 | 0.103 |
| | Flat | 6.85 | 5.80 | 0.54 | 0.19 | | | | |
| | Convex | 46.72 | 39.13 | 0.85 | 0.33 | | | | |
| TWI | < 0.999 | 23.29 | 24.64 | 1.06 | 0.28 | 1.983 | 2.000 | 0.009 | 0.008 |
| | 0.999 - 3.219 | 21.29 | 22.32 | 1.02 | 0.26 | | | | |
| | 3.220 - 6.688 | 4.88 | 3.77 | 0.79 | 0.20 | | | | |
| | 6.688 < | 50.54 | 49.28 | 0.97 | 0.26 | | | | |
| SPI | < -4.052 | 24.80 | 17.97 | 0.74 | 0.18 | 1.940 | 2.000 | 0.030 | 0.032 |
| | -4.052 - 0.886 | 36.90 | 34.78 | 0.94 | 0.23 | | | | |
| | 0.887 - 3.529 | 31.71 | 39.13 | 1.28 | 0.31 | | | | |
| | 3.529 < | 6.58 | 8.12 | 1.22 | 0.29 | | | | |
| Drainage Density | < 0.545 | 18.33 | 5.51 | 0.30 | 0.06 | 2.127 | 2.322 | 0.084 | 0.076 |
| | 0.545 - 0.854 | 25.33 | 31.88 | 1.26 | 0.28 | | | | |
| | 0.855 - 1.153 | 24.19 | 37.97 | 1.57 | 0.35 | | | | |
| | 1.154 - 1.462 | 21.17 | 18.55 | 0.87 | 0.19 | | | | |
| | 1.462 < | 10.99 | 6.09 | 0.55 | 0.12 | | | | |
| NDVI | <223 | 4.20 | 20.58 | 4.90 | 0.54 | 1.835 | 2.322 | 0.210 | 0.394 |
| | 0.223 - 0.407 | 10.93 | 19.71 | 1.80 | 0.21 | | | | |
| | 0.408 - 0.562 | 16.64 | 15.94 | 0.96 | 0.11 | | | | |
| | 0.563 - 0.688 | 28.52 | 22.32 | 0.79 | 0.09 | | | | |
| | 0.688 < | 39.71 | 21.45 | 0.54 | 0.06 | | | | |
| NDSI | < -0.516 | 9.24 | 7.25 | 0.78 | 0.15 | 2.036 | 2.322 | 0.123 | 0.134 |
| | -0.516 - -0.273 | 18.04 | 9.28 | 0.51 | 0.10 | | | | |
| | -0.274 - -0.097 | 28.03 | 14.78 | 0.53 | 0.10 | | | | |
| | -0.098 - 0.078 | 31.45 | 35.94 | 1.14 | 0.21 | | | | |
| | 0.078 < | 13.24 | 32.75 | 2.47 | 0.46 | | | | |
| Distance from river (m) | 0-100 | 3.71 | 6.09 | 1.64 | 0.31 | 2.203 | 2.322 | 0.051 | 0.055 |
| | 100-200 | 2.85 | 1.16 | 0.40 | 0.07 | | | | |
| | 200-300 | 3.23 | 3.48 | 1.08 | 0.20 | | | | |
| | 300-400 | 2.85 | 3.48 | 1.22 | 0.23 | | | | |
| | 400< | 87.36 | 85.80 | 0.98 | 0.18 | | | | |
| Distance from fault | 0-100 | 4.67 | 1.74 | 0.35 | 0.07 | 2.181 | 2.322 | 0.061 | 0.060 |
| | 100-200 | 3.64 | 4.06 | 1.12 | 0.22 | | | | |

| | | | | | | | | | |
|---|---|---|---|---|---|---|---|---|---|
| (m) | 200-300 | 3.99 | 5.22 | 1.31 | 0.26 | | | | |
| | 300-400 | 3.20 | 4.06 | 1.28 | 0.25 | | | | |
| | 400< | 84.49 | 84.93 | 1.01 | 0.20 | | | | |
| Distance from road (m) | 0-100 | 3.48 | 4.35 | 1.26 | 0.21 | 2.182 | 2.322 | 0.060 | 0.071 |
| | 100-200 | 2.36 | 2.03 | 0.87 | 0.15 | | | | |
| | 200-300 | 2.56 | 5.51 | 2.15 | 0.36 | | | | |
| | 300-400 | 2.17 | 1.45 | 0.67 | 0.11 | | | | |
| | 400< | 89.44 | 86.67 | 0.97 | 0.16 | | | | |
| Lithology | Tsm | 10.58 | 27.23 | 2.57 | 0.27 | 2.383 | 2.585 | 0.079 | 0.125 |
| | Pzc | 6.67 | 7.25 | 0.93 | 0.10 | | | | |
| | pCd | 3.79 | 10.43 | 2.75 | 0.29 | | | | |
| | GHlml | 2.52 | 4.35 | 1.73 | 0.18 | | | | |
| | GHlo | 33.27 | 25.51 | 0.94 | 0.10 | | | | |
| | Tgr | 43.17 | 24.64 | 0.66 | 0.07 | | | | |
| Rainfall (mm) | 1786.79 - 2434.61 | 25.57 | 16.52 | 0.65 | 0.10 | 2.015 | 2.322 | 0.132 | 0.163 |
| | 2434.62 - 2930.01 | 28.56 | 12.46 | 0.44 | 0.07 | | | | |
| | 2930.02 - 3539.74 | 20.30 | 14.20 | 0.70 | 0.11 | | | | |
| | 3539.75 - 4225.67 | 13.53 | 34.20 | 2.53 | 0.41 | | | | |
| | 4225.68 - 5025.93 | 12.02 | 22.61 | 1.88 | 0.30 | | | | |
| LULC | Agricultural Land | 3.26 | 1.74 | 0.53 | 0.18 | 1.622 | 2.322 | 0.301 | 0.176 |
| | Built Up Area | 0.09 | 0.00 | 0.00 | 0.00 | | | | |
| | Forest | 92.61 | 94.78 | 1.02 | 0.35 | | | | |
| | Shrub | 2.47 | 3.19 | 1.29 | 0.42 | | | | |
| | Water Bodies | 1.57 | 0.29 | 0.18 | 0.05 | | | | |

Regarding the slope gradient, it is noticed that the ($P_{ij}$) value increases with increases in the slope gradient. The field verification also confirmed that the steeper slopes exhibit more landslides. The result is agreed with the results of Devkota *et al.* (2013).

In the case of aspect, the slope facing south, southeast, and southwest experiences more landslide with higher ($P_{ij}$). The rest of the slope directions are less susceptible to the landslides. Devkota *et al.* (2013) studied landslide in Nepal which is also a part of the Himalayan region and he observed a similar result. This may be due blockage of wind that comes from the south (Indian Ocean) by the giant Himalayan mountain. The condense wind finally drops as precipitation which triggers relatively more landslides on the south-facing slope.

Regarding the slope curvature, the ($P_{ij}$) is debatable with respect to the different spatial resolution. In this study, the concave slope curvature (0.48) corresponds with higher (Pij) indicating more susceptible to landslide, followed by convex slope curvature (0.33) and flat area (0.19). This result is evident that concave terrain holds more water which decreases the soil strength and augments soil erosion. This result is agreed with the result of Devkota *et al.* (2013).

In the case of Topographic Wetness Index (TWI), the landslide pattern of ($P_{ij}$) doesn't follow a systematic trend concerning TWI value. However, it is noticed that the behavior of the different spatial resolutions acted similar to one another.

The landslide is also influenced significantly by the stream power index. It was noticed that the ($P_{ij}$) increases with the increases in SPI value for all three different spatial resolutions. This indicates that the erosive power of the stream increases the landslide event. A similar result was observed by (Wang, Li, Chen, and Bai, 2015).

Although the drainage density doesn't follow the regular increment trend with ($P_{ij}$), it is noticed that there is a slight increase of ($P_{ij}$) with drainage density. This indicates the chances of the landslide are slightly higher with an increase in the drainage density.

For this study, the Normalized Difference Vegetation Index (NDVI) is the top influential factor. The ($P_{ij}$) decreases with an increase in NDVI value for all different spatial resolutions. This indicates that the landslide occurrence decreases with the increase in vegetation strength and vice versa. The vegetation roots reinforce the slope surface and minimize the landslides. The result is agreed with the theoretical concept of reinforcement of soil by the vegetation roots and a similar result was obtained by Mondal and Mandal (2019).

Normalized Difference Soil Index indicate the distinction between the soil with other land cover types using its value. The higher value indicates the bares soil area and the lower value indicates different categories of vegetated area (Mind'je *et al.*, 2019). From Table 15, it noticed that the barren area is more susceptible to the landslides.

Regarding the distance from the river, it was noticed that the landslides are more prominent within a distance of 400m from the river with a higher value of ($P_{ij}$) for all the three different spatial resolutions. The field verification also confirmed that the landslides are more common within 400m from the river.

For the susceptibility of the landslide with respect to the distance from the fault, it is noticed that the ($P_{ij}$) is higher in between the distance of 100m to 400. This shows that the landslide is less common beyond 400m from the fault. All three different spatial resolutions acted in a similar manner for the distance from the fault.

In the case of a road, the distance from the road doesn't follow the systematic trend with the value of ($P_{ij}$) value. However, it was noticed that the landslides are more common within 300 m from the road.

Pertaining to the lithology, the landslide is more common for the class pCd (0.29), followed by Tsm (27), and GHlml (0.18) with decreasing order of ($P_{ij}$). The least landslide-prone lithology are GHlo (0.10), Pzc (0.10), and Tgr (0.07).

Regarding the rainfall, the ($P_{ij}$) also increases with the increase in rainfall amount. This shows that the more landslides events take place in the area having a high amount of rainfall. A similar result was obtained by Jaafari *et al.* (2014).

In the case of land use land cover, the landslide probability is still debatable for different classes. For this study, the most landslide-prone class is a shrub (0.42) and forest (0.35), followed by agricultural land (0.18). As per this study, the build-up area and the water bodies corresponds to negligible landslides. Technically, the water bodies don't have the soil attached to it and there will be no landslides. Similarly, the build-up area consists of costly infrastructure which is protected by the landslide protection walls such as retaining walls resulting is no landslides.

### 4.2.3 Relationship in the Weight of Evidence

The detail calculation of weight $W^+$ and $W^-$, contrast C, variance $S^2(W^+)$ and $S^2(W^-)$, standard deviation S(C), and studentized contrast Cs for the conditioning factors using the spatial resolution 12.5m, 30m and 90m are given in the Appendix D.

The Equation 14 to Equation 20 are used to calculate the weight, contrast, variance, standard deviation, and studentized contrast. The average parameters of the Weight of Evidence are given in Table 16.

It is observed that the studentized contrast decreases with an increase in elevation. The highest studentized contrast (6.489) corresponds to the lowest class (144.00 - 854.01) of the elevation for all the different spatial resolutions. The most significant elevation is lower than 854m above the mean sea level with studentized contrast more than 1.96 indicating a confidence level of 95% in favor of positive association between the landslide and the class of the elevation for all the classes of the different spatial resolution. A similar result was observed by Wang et al. (2016).

**Table 16 Relation between the landslide event and the factor's class using the Weight of Evidence**

| Factor | Class | % of class | % of Landslide | $W^+$ | $W^-$ | C | $S^2(W^+)$ | $S^2(W^-)$ | S(C ) | Cs |
|---|---|---|---|---|---|---|---|---|---|---|
| Elevation (m) | < 854.00 | 12.83 | 34.49 | 0.987 | -0.287 | 1.274 | 0.025 | 0.013 | 0.197 | 6.489 |
| | 854.00 - 1455 | 23.42 | 30.43 | 0.260 | -0.096 | 0.357 | 0.029 | 0.013 | 0.203 | 1.769 |
| | 1455.01 - 1949 | 32.15 | 18.55 | -0.550 | 0.183 | -0.733 | 0.047 | 0.011 | 0.240 | -3.053 |
| | 1949.01 - 2619 | 25.91 | 12.17 | -0.756 | 0.170 | -0.926 | 0.072 | 0.010 | 0.285 | -3.245 |
| | 2619 < | 5.69 | 4.35 | -0.268 | 0.014 | -0.282 | 0.200 | 0.009 | 0.457 | -0.617 |
| Slope (Degree) | 0 - 13.00 | 10.39 | 7.54 | -0.349 | 0.031 | -0.380 | 0.123 | 0.009 | 0.361 | -0.992 |
| | 13.01 - 23.00 | 22.69 | 17.97 | -0.276 | 0.058 | -0.334 | 0.054 | 0.011 | 0.252 | -1.233 |
| | 23.01 - 32.00 | 31.76 | 27.25 | -0.153 | 0.064 | -0.218 | 0.032 | 0.012 | 0.210 | -1.031 |
| | 32.01 - 42.00 | 26.97 | 27.83 | 0.035 | -0.011 | 0.046 | 0.031 | 0.012 | 0.208 | 0.220 |
| | 42 < | 8.20 | 19.42 | 0.933 | -0.133 | 1.066 | 0.054 | 0.011 | 0.251 | 4.312 |
| Aspect | Flat | 0.32 | 0.00 | 0.000 | 0.003 | 0.000 | 0.000 | 0.009 | 0.062 | -0.001 |
| | North | 12.23 | 4.93 | -0.912 | 0.080 | -0.992 | 0.178 | 0.009 | 0.432 | -2.291 |
| | NorthEast | 10.88 | 6.67 | -0.525 | 0.046 | -0.571 | 0.141 | 0.009 | 0.384 | -1.422 |
| | East | 12.13 | 13.04 | 0.072 | -0.011 | 0.083 | 0.067 | 0.010 | 0.277 | 0.302 |
| | SouthEast | 14.37 | 27.54 | 0.649 | -0.167 | 0.816 | 0.031 | 0.012 | 0.209 | 3.914 |
| | South | 13.09 | 17.68 | 0.293 | -0.055 | 0.347 | 0.050 | 0.010 | 0.246 | 1.447 |
| | SouthWest | 14.14 | 13.33 | -0.067 | 0.009 | -0.076 | 0.067 | 0.010 | 0.276 | -0.244 |
| | West | 12.08 | 7.25 | -0.521 | 0.054 | -0.575 | 0.123 | 0.009 | 0.363 | -1.566 |
| | NorthWest | 10.78 | 9.57 | -0.122 | 0.013 | -0.135 | 0.091 | 0.010 | 0.318 | -0.416 |
| Curvature | Concave | 46.43 | 55.07 | 0.155 | -0.198 | 0.352 | 0.016 | 0.020 | 0.192 | 1.830 |
| | Flat | 6.85 | 5.80 | -0.153 | 0.011 | -0.164 | 0.131 | 0.009 | 0.314 | -0.347 |
| | Convex | 46.72 | 39.13 | -0.180 | 0.133 | -0.312 | 0.023 | 0.015 | 0.192 | -1.609 |
| TWI | < 0.999 | 23.29 | 24.64 | 0.053 | -0.020 | 0.072 | 0.047 | 0.012 | 0.238 | 0.335 |
| | 0.999 - 3.219 | 21.29 | 22.32 | 0.010 | -0.015 | 0.025 | 0.051 | 0.012 | 0.243 | 0.208 |
| | 3.220 - 6.688 | 4.88 | 3.77 | -0.261 | 0.012 | -0.273 | 0.448 | 0.009 | 0.617 | -0.480 |
| | 6.688 < | 50.54 | 49.28 | -0.027 | 0.023 | -0.051 | 0.018 | 0.017 | 0.187 | -0.271 |
| SPI | < -4.052 | 24.80 | 17.97 | -0.312 | 0.090 | -0.402 | 0.052 | 0.010 | 0.248 | -1.650 |
| | -4.052 - 0.886 | 36.90 | 34.78 | -0.066 | 0.032 | -0.098 | 0.026 | 0.013 | 0.198 | -0.480 |
| | 0.887 - 3.529 | 31.71 | 39.13 | 0.237 | -0.115 | 0.352 | 0.023 | 0.015 | 0.195 | 1.799 |
| | 3.529 < | 6.58 | 8.12 | 0.144 | -0.017 | 0.161 | 0.127 | 0.009 | 0.363 | 0.637 |
| Drainage Density | < 0.545 | 18.33 | 5.51 | -1.205 | 0.146 | -1.351 | 0.159 | 0.009 | 0.409 | -3.296 |
| | 0.545 - 0.854 | 25.33 | 31.88 | 0.230 | -0.092 | 0.322 | 0.027 | 0.013 | 0.200 | 1.610 |
| | 0.855 - 1.153 | 24.19 | 37.97 | 0.451 | -0.201 | 0.652 | 0.023 | 0.014 | 0.192 | 3.391 |
| | 1.154 - 1.462 | 21.17 | 18.55 | -0.132 | 0.033 | -0.165 | 0.047 | 0.011 | 0.240 | -0.686 |
| | 1.462 < | 10.99 | 6.09 | -0.591 | 0.054 | -0.644 | 0.143 | 0.009 | 0.390 | -1.652 |
| NDVI | <223 | 4.20 | 20.58 | 1.555 | -0.190 | 1.745 | 0.045 | 0.011 | 0.236 | 7.599 |
| | 0.223 - 0.407 | 10.93 | 19.71 | 0.575 | -0.105 | 0.680 | 0.046 | 0.011 | 0.236 | 2.939 |
| | 0.408 - 0.562 | 16.64 | 15.94 | -0.045 | 0.008 | -0.053 | 0.055 | 0.010 | 0.255 | -0.201 |
| | 0.563 - 0.688 | 28.52 | 22.32 | -0.245 | 0.083 | -0.328 | 0.039 | 0.011 | 0.224 | -1.466 |
| | 0.688 < | 39.71 | 21.45 | -0.644 | 0.262 | -0.906 | 0.043 | 0.011 | 0.231 | -3.831 |
| NDSI | < -0.516 | 9.24 | 7.25 | -0.244 | 0.022 | -0.266 | 0.120 | 0.009 | 0.360 | -0.735 |
| | -0.516 - -0.273 | 18.04 | 9.28 | -0.669 | 0.102 | -0.771 | 0.094 | 0.010 | 0.322 | -2.383 |
| | -0.274 - -0.097 | 28.03 | 14.78 | -0.664 | 0.168 | -0.832 | 0.062 | 0.010 | 0.267 | -3.054 |
| | -0.098 - 0.078 | 31.45 | 35.94 | 0.132 | -0.068 | 0.200 | 0.024 | 0.014 | 0.195 | 1.034 |
| | 0.078 < | 13.24 | 32.75 | 0.905 | -0.255 | 1.160 | 0.027 | 0.013 | 0.199 | 5.839 |
| Distance from river (m) | 0-100 | 3.71 | 6.09 | 0.493 | -0.025 | 0.519 | 0.145 | 0.009 | 0.392 | 1.331 |
| | 100-200 | 2.85 | 1.16 | -0.950 | 0.017 | -0.967 | 0.833 | 0.009 | 0.907 | -1.043 |
| | 200-300 | 3.23 | 3.48 | 0.075 | -0.003 | 0.078 | 0.250 | 0.009 | 0.509 | 0.154 |
| | 300-400 | 2.85 | 3.48 | 0.199 | -0.006 | 0.206 | 0.250 | 0.009 | 0.509 | 0.404 |
| | 400< | 87.36 | 85.80 | -0.018 | 0.116 | -0.134 | 0.010 | 0.062 | 0.267 | -0.504 |
| Distance from fault (m) | 0-100 | 4.67 | 1.74 | -1.212 | 0.030 | -1.242 | 0.750 | 0.009 | 0.839 | -1.390 |
| | 100-200 | 3.64 | 4.06 | 0.107 | -0.004 | 0.111 | 0.217 | 0.009 | 0.474 | 0.240 |
| | 200-300 | 3.99 | 5.22 | 0.259 | -0.013 | 0.272 | 0.170 | 0.009 | 0.422 | 0.668 |
| | 300-400 | 3.20 | 4.06 | 0.197 | -0.009 | 0.206 | 0.233 | 0.009 | 0.487 | 0.521 |
| | 400< | 84.49 | 84.93 | 0.005 | -0.030 | 0.036 | 0.010 | 0.058 | 0.261 | 0.129 |
| Distance from road (m) | 0-100 | 3.48 | 4.35 | 0.227 | -0.009 | 0.236 | 0.200 | 0.009 | 0.457 | 0.517 |
| | 100-200 | 2.36 | 2.03 | -0.161 | 0.004 | -0.164 | 0.444 | 0.009 | 0.670 | -0.225 |
| | 200-300 | 2.56 | 5.51 | 0.765 | -0.031 | 0.796 | 0.159 | 0.009 | 0.409 | 1.949 |
| | 300-400 | 2.17 | 1.45 | -0.449 | 0.007 | -0.457 | 0.667 | 0.009 | 0.810 | -0.516 |
| | 400< | 89.44 | 86.67 | -0.031 | 0.233 | -0.264 | 0.010 | 0.066 | 0.274 | -0.964 |
| Lithology | Tsm | 10.58 | 27.23 | 0.945 | -0.206 | 1.151 | 0.031 | 0.012 | 0.208 | 5.530 |
| | Pzc | 6.67 | 7.25 | -0.091 | -0.007 | -0.084 | 0.681 | 0.010 | 0.747 | 0.067 |
| | pCd | 3.79 | 10.43 | 1.012 | -0.072 | 1.083 | 0.083 | 0.010 | 0.305 | 3.551 |
| | GHlml | 2.52 | 4.35 | 0.546 | -0.019 | 0.565 | 0.200 | 0.009 | 0.457 | 1.236 |
| | GHlo | 33.27 | 25.51 | -0.111 | 0.173 | -0.284 | 0.037 | 0.012 | 0.220 | -1.548 |
| | Tgr | 43.17 | 24.64 | -0.430 | 0.383 | -0.814 | 0.349 | 0.012 | 0.464 | -3.974 |
| Rainfall | 1786.79 - 2434.61 | 25.57 | 16.52 | -0.437 | 0.115 | -0.552 | 0.053 | 0.010 | 0.251 | -2.197 |

| | | | | | | | | | | |
|---|---|---|---|---|---|---|---|---|---|---|
| (mm) | 2434.62 - 2930.01 | 28.56 | 12.46 | -0.830 | 0.203 | -1.033 | 0.070 | 0.010 | 0.282 | -3.657 |
| | 2930.02 - 3539.74 | 20.30 | 14.20 | -0.358 | 0.074 | -0.431 | 0.062 | 0.010 | 0.267 | -1.614 |
| | 3539.75 - 4225.67 | 13.53 | 34.20 | 0.927 | -0.273 | 1.200 | 0.026 | 0.013 | 0.197 | 6.106 |
| | 4225.68 - 5025.93 | 12.02 | 22.61 | 0.632 | -0.128 | 0.760 | 0.038 | 0.011 | 0.223 | 3.408 |
| LULC | Agricultural Land | 3.26 | 1.74 | -0.628 | 0.016 | -0.644 | 0.500 | 0.009 | 0.713 | -0.902 |
| | Built Up Area | 0.09 | 0.00 | 0.000 | 0.001 | -0.001 | 0.000 | 0.009 | 0.093 | -0.010 |
| | Forest | 92.61 | 94.78 | 0.023 | -0.374 | 0.397 | 0.009 | 0.175 | 0.427 | 0.878 |
| | Shrub | 2.47 | 3.19 | 0.225 | -0.007 | 0.233 | 0.289 | 0.009 | 0.542 | 0.493 |
| | Water Bodies | 1.57 | 0.29 | -0.198 | 0.013 | -0.211 | 0.333 | 0.009 | 0.397 | -0.312 |

The studentized contrast increases with the increase in slope gradient indicating the landslides are more prominent in the steep slope. A similar result was observed by Wang et al. (2016) and Roy *et al.* (2019). The most significant slope angle is more than 42° with studentized contrast more than 1.96 indicating a confidence level of 95% in favor of a positive association between the landslide and the class of the slope gradient.

In the case of the slope aspect, the contrast value is higher for south (1.447), southeast (3.914), and east (1.447) facing slopes. This may be due to the effect of the giant Himalayan mountain. Since the Ossay watershed is situated in the Himalayan region, the prevailing monsoon wind direction from the south is blocked by the giant Himalayan mountains. This wind finally gets condense which results in heavy precipitation on the south-facing slopes. The most landslide-prone area is south-east ($C_s$>1.96) with a 95% confidence level. Kayastha, Dhital, and De Smedt (2012) and Roy *et al.* (2019) also found that the south-facing slope is more susceptible to landslides.

In the case of the slope curvature, the studentized contrast is highest for concave curvature (1.830). The concave curvature holds the water and the adjoining soil becomes loose which ultimately destabilizes an area resulting in relatively higher landslides than convex and flat area.

In the Topographic Wetness Index (TWI), it is observed that there is no regular trend flow in between the TWI and the studentized contrast. However, it is noticed that there is a slight decrease in studentized contrast with the increase in the TWI.

Regarding the stream power index (SPI), the studentized contrast increases with an increase in SPI value. This signifies that the landslides are more prominent in the higher SPI value. A similar result was obtained by Roy *et al.* (2019) and Wang et al.(2016).

There is a slight increase of studentized contrast with an increase in the drainage density. The lowest studentized contrast corresponds to the lowest drainage density and

all the three different spatial resolution acted with similar behavior on the drainage density.

The two lowest NDVI classes (<0.223) and (0.223 - 0.407) correspond to the highest studentized contrast with more than 1.96 indicating a higher correlation with a confidence level of 95%. On the other hand, the highest NDVI class (0.689 - 0.902) corresponds to the lowest studentized contrast with less than -1.96 disfavoring the landslides by a 95% confidence level. It was noticed that when the NDVI is more, studentized contrast is less and vice versa. This result is agreed with the result of Roy *et al.* (2019). This means that the probability of landslide occurrence is less in a healthy vegetated area or an area having a high NDVI value.

Normalized Difference Soil Index (NDSI) indicate the distinction between the soil with other land cover types using its value. The higher value indicates the bares soil area and the lower value indicates different categories of vegetated area (Mind'je *et al.*, 2019). From Table 16, it is observed that the highest NDSI class (0.078 - 0.745) corresponds to the highest studentized contrast (5.839). This reveals that the bare soils are exposed to the direct runoff resulting in more prone to the landslides during the monsoon season.

Regarding the distance from the river, it is observed that the studentized contrast within the 100m is maximum. As the distance goes away from the river, the studentized contrast decreases. This shows that the landslide probability decreases as we go away from the river.

In the case of the distance from the fault, the relationship between the studentized contrast and the distance from the fault does not have a systematic trend. However, it is noticed that the studentized contrast is more in between the distance of 100m to 400m from the fault. This shows that the landslide is more common between distance of 100-400m from the fault. The different spatial resolution has behaved in a similar characteristic in this factor.

The landslide is more common within the distance of 300m from the road. However, the impact of the road is quite insignificant on the landslide. As the distance increase from 300m, the studentized contrast is decreasing for all three different spatial resolutions.

The lithological class Tsm (siwalik group) and pCd (daling shumar group) have more studentized contrast ($C_s$>1.96). This shows Tsm and pCd contributes significantly to the landslide with the confidence level of 95%. The remaining lithology does not have a great impact on the landslides.

Rainfall is considered as one of the main triggering factors for the landslides. The result shows that the landslide increases with an increase in rainfall amount. The studentized contrast is more than 1.96 for the rainfall intensity of more than 3539.74mm indicating a confidence level of 95% positive association. This clearly indicates landslides are highly correlated to the higher rainfall intensity.

In the case of land use, all the classes are having studentized contrast in between -1.96 to 1.96 indicating there is less significance on the landslide by the different land use classes at Ossay watershed area.

### 4.3 Landslide Susceptibility mapping using statistical models

The LSM was prepared using the FR, IOE, and WOE for individual 12.5m, 30m, and 90m spatial resolution. Then, the hybrid LSM was also prepared by combining these using these models for 12.5m, 30m, and 90m spatial resolution. These hybrid LSM were FR-IOE, IOE-WOE, and WOE-FR. The LSM generated using different models need a classification for better visual interpretation (Jaafari *et al.*, 2014). There are several classification packages in GIS software. The appropriate classification method is chosen based on the distribution of the landslide susceptibility value (Ayalew and Yamagishi, 2005). The selection of classification methods depends on the data value distribution of LSM (Jaafari *et al.*, 2014). The natural break classification identifies distinct breakpoints of the distribution of the pattern and divides into classes whose boundaries are of relatively big jumps in the values (Osaragi, 2002). Therefore, considering the data value distribution and visualization, natural break classification was used for this study for all the LSM. All the final LSM is classified into five classes using the natural break classification for the comparison purpose. The classes of LSM were very low, low, moderate, high and very high susceptibility zone.

Regarding the LSM using FR, the factors were reclassified using the FR value from Appendix B for 12.5m, 30m, and 90m resolution. All the reclassified factors were

summed up using the Equation 6 to form LSM for 12.5m (Figure 11(a)), 30m (Figure 11 (b)), and 90m (Figure 11(c)). From the Table 17, it is noticed that the area coverage is smallest (2.54%, 20.86sq.km) for the finest spatial resolution (12.5m) and the area coverage is largest (6.17%, 50.59 sq.km) for the coarse spatial resolution (90m) for the very high landslide susceptibility zone. On the other hand, it is noticed that the area coverage is large (35.03%, 287.50 sq.km) for the finest spatial resolution (12.5m) and the area coverage is smaller (30.23%, 247.80 sq.km) for the coarse spatial resolution (90m) for the very low landslide susceptibility zone. It is observed that the area increases as we go from a very high susceptibility zone to a very low susceptibility zone for all three different spatial resolutions. However, for 30m and 90m spatial resolution, the area decreases slightly in very low susceptibility zone while comparing the low susceptibility zone.

**Table 17 Area coverage in different LSM zone using different models**

| Models | LSM zone | 12.5m spatial resolution | | 30m spatial resolution | | 90m spatial resolution | |
|---|---|---|---|---|---|---|---|
| | | Area($km^2$) | Percentage | Area($km^2$) | Percentage | Area($km^2$) | Percentage |
| Frequency Ratio | Very Low | 287.5 | 35.03 | 252.04 | 30.75 | 247.8 | 30.23 |
| | Low | 268.29 | 32.69 | 253.18 | 30.88 | 269.8 | 32.92 |
| | Moderate | 130.3 | 15.88 | 155.94 | 19.02 | 148.55 | 18.12 |
| | High | 113.77 | 13.86 | 108.61 | 13.25 | 102.85 | 12.55 |
| | Very High | 20.86 | 2.54 | 49.99 | 6.09 | 50.59 | 6.17 |
| | | | | | | | |
| Index of Entropy | Very Low | 457.4 | 55.73 | 274.43 | 33.44 | 264.45 | 32.27 |
| | Low | 216.86 | 26.42 | 220.51 | 26.87 | 229.07 | 27.95 |
| | Moderate | 112.07 | 13.66 | 178.47 | 21.74 | 168.99 | 20.62 |
| | High | 17.63 | 2.15 | 110.29 | 13.44 | 96.44 | 11.77 |
| | Very High | 16.75 | 2.04 | 37.06 | 4.51 | 60.64 | 7.4 |
| | | | | | | | |
| Weight of Evidence | Very Low | 171.44 | 20.89 | 164.52 | 20.04 | 163.05 | 19.87 |
| | Low | 279.67 | 34.08 | 253.82 | 30.93 | 262.62 | 32 |
| | Moderate | 185.62 | 22.62 | 201.98 | 24.61 | 195.87 | 23.87 |
| | High | 109.95 | 13.4 | 120.43 | 14.67 | 113.46 | 13.83 |
| | Very High | 74.04 | 9.02 | 80.00 | 9.75 | 85.58 | 10.43 |

In the case of IOE, all the factors were secondarily reclassified using the value of landslide probability density (Pij) from the Appendix C for the spatial resolution 12.5m, 30m, and 90m. The LSM is developed by adding all the weighted secondarily reclassified influencing factors using the Equation 13. The LSM developed using the 12.5m, 30m, and 90 were shown in Figure 12(a), Figure 12(b) and Figure 12(c), respectively. From the Table 17, it is noticed that the area coverage is smallest (16.75 sq.km) for the finest spatial resolution (12.5m) and largest (60.64sq.km) for the coarse spatial resolution (90m) for the very high landslide susceptibility zone. On the other

hand, it is noticed that the area coverage is large (457.40 sq.km) for the finest spatial resolution (12.5m) and smallest (264.45 sq.km) for the coarse spatial resolution (90m) for the very low landslide susceptibility zone. Unlike LSM using the FR, the area increases as we go from a very high susceptibility zone to a very low susceptibility zone for all three different spatial resolution.

For WOE, all the classes of the factors are reclassified using the contrast value (C) from Appendix D for spatial resolution 12.5m, 30m, and 90m. Then, add all the reclassified factors using Equation 21 to form the LSM. The LSM developed using WOE for 12.5m (Figure 13(a)), 30m (Figure 13(b)), and 90m (Figure 13(c). Similar to Frequency Ratio and Index of Entropy, it is noticed that the area coverage is smallest (9.02%, 74.04 sq.km) for the finest spatial resolution (12.5m) and largest (10.43%, 85.58sq.km) for the coarse spatial resolution (90m) for the very high landslide susceptibility zone (Table 17). On the other hand, it is noticed that the area coverage is large (20.87%, 171.44sq.km) for the finest spatial resolution (12.5m) and smallest (19.87%, 163.05sq.km) for the coarse spatial resolution (90m) for the very low landslide susceptibility zone. The area increases as the landslide susceptibility zone go from a very high susceptibility zone to a low susceptibility zone. However, unlike FR and IOE, the WOE area decreased when it reaches a very low susceptibility zone for all spatial resolutions.

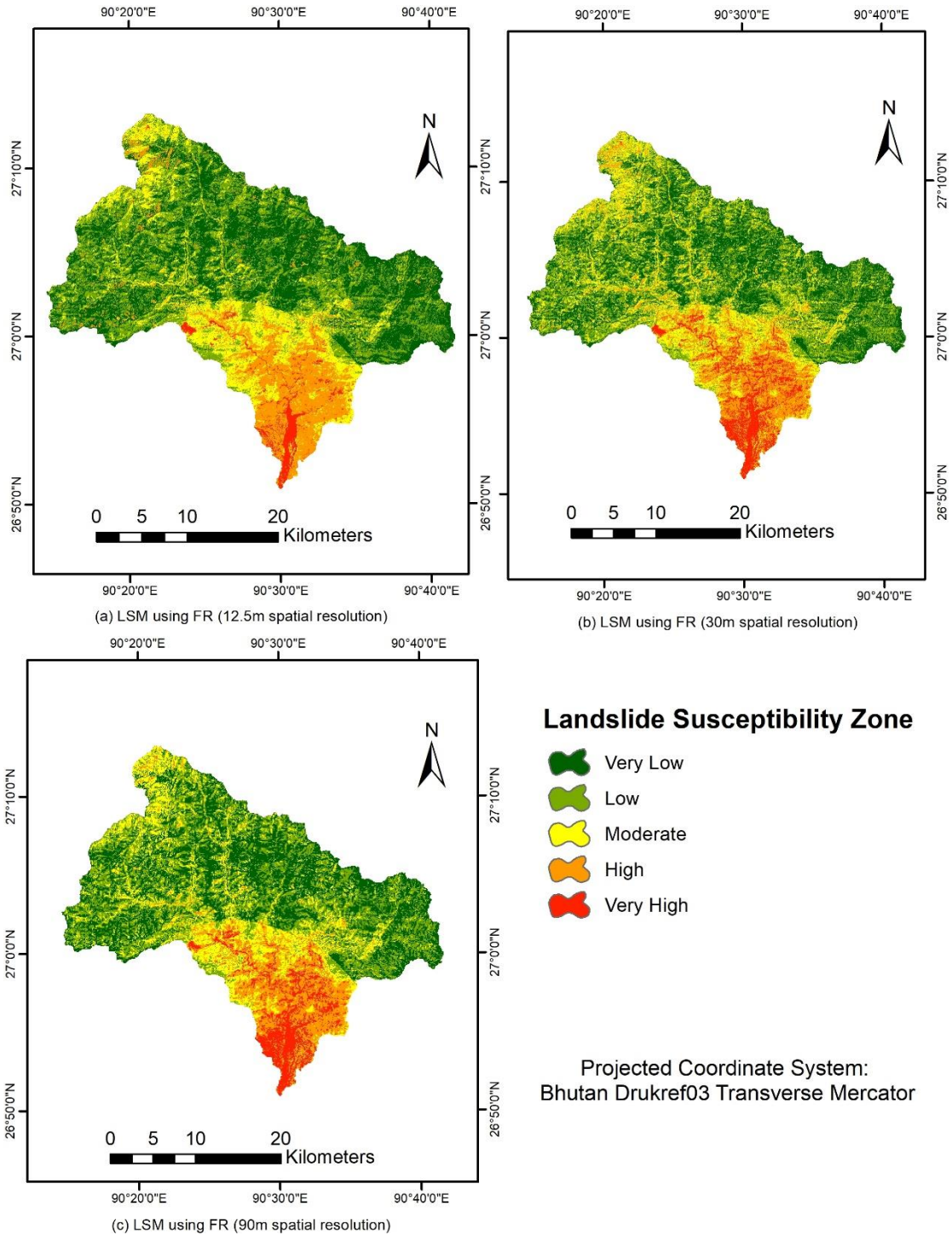


**Figure 11 Landslide susceptibility mapping using Frequency Ratio (a) 12.5m spatial resolution, (b) 30m spatial resolution, (c) 90m spatial resolution**

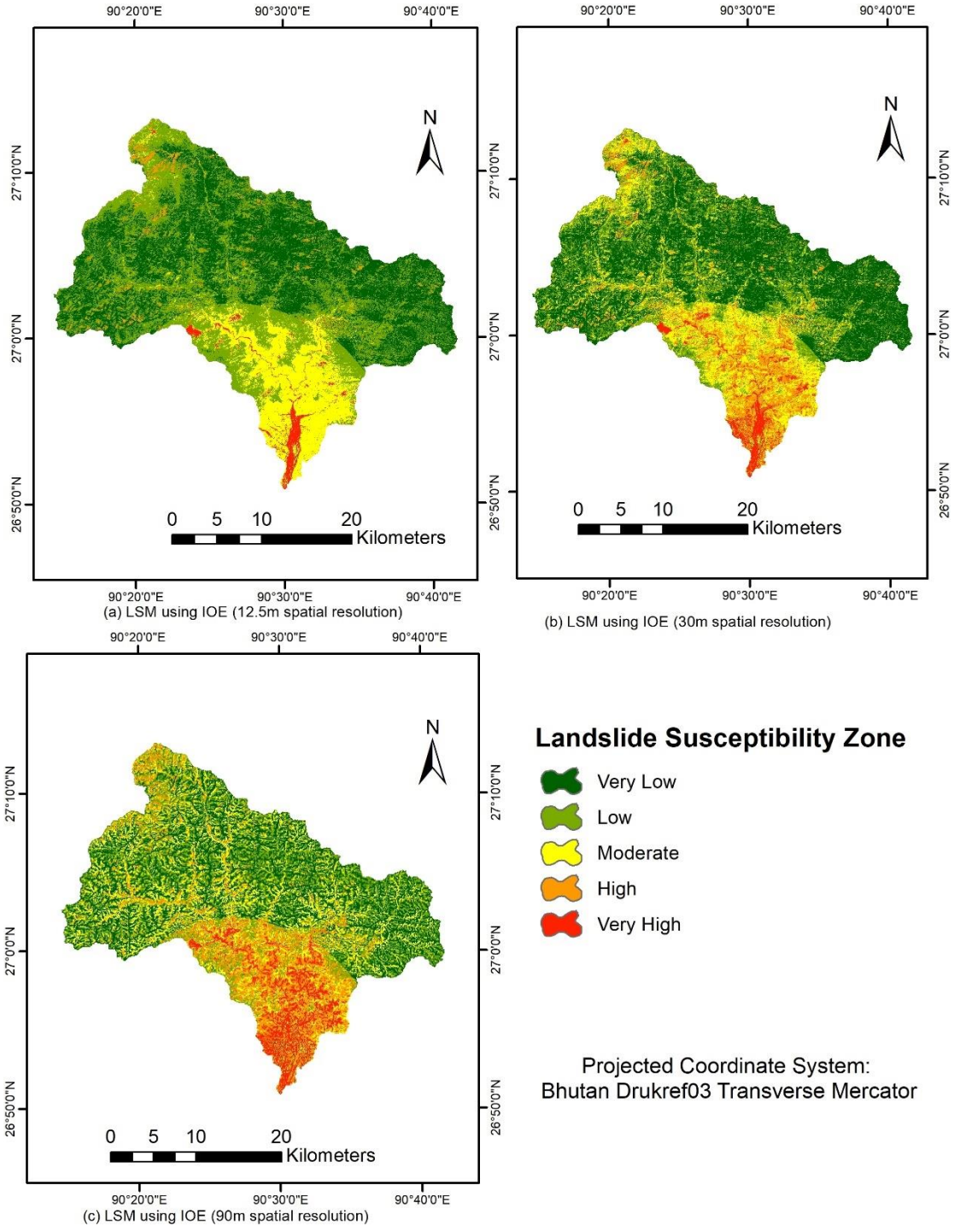


**Figure 12 Landslide susceptibility mapping using Index of Entropy (a) 12.5m spatial resolution, (b) 30m spatial resolution, (c) 90m spatial resolution**

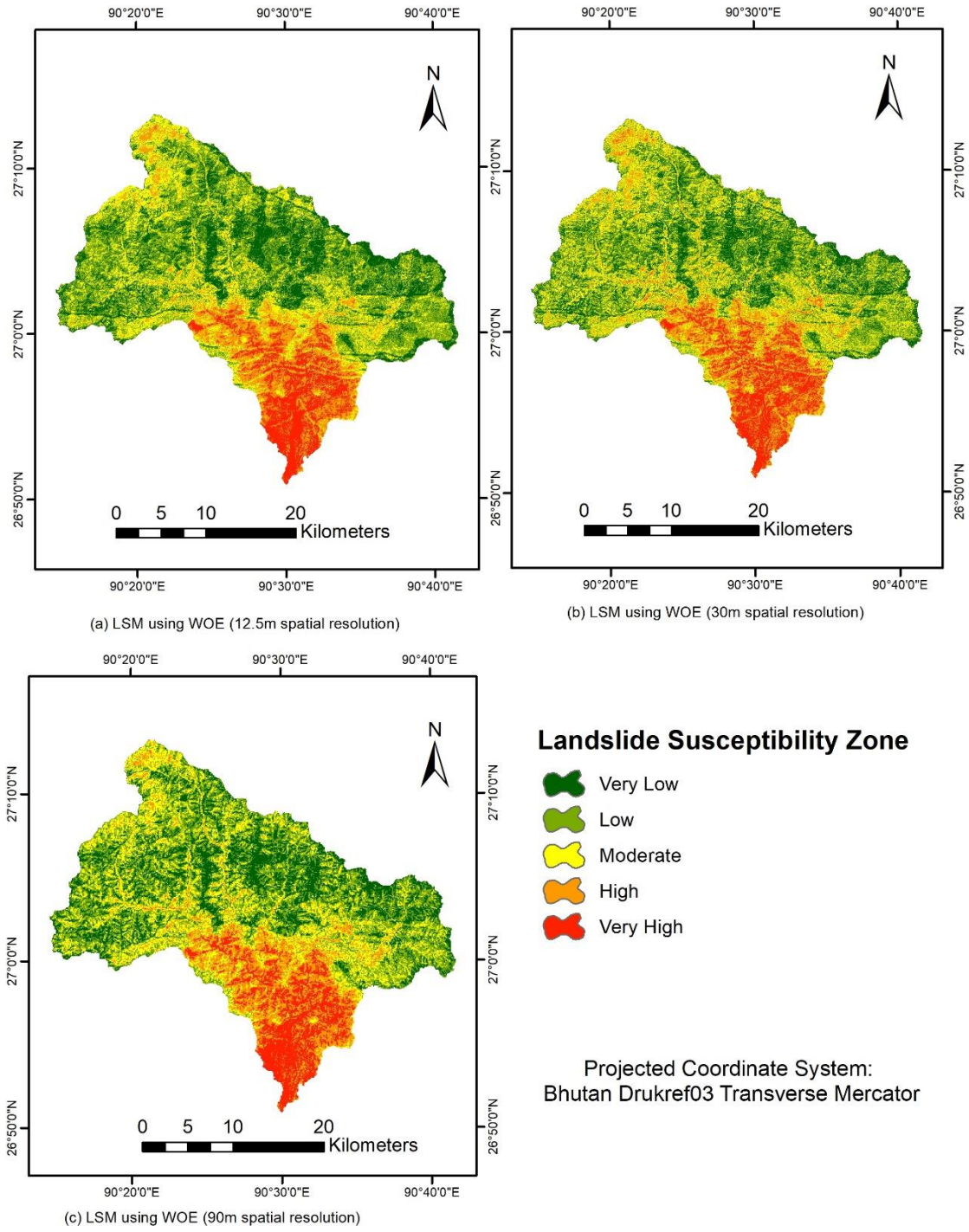


**Figure 13 Landslide susceptibility mapping using Weight of Evidence (a) 12.5m spatial resolution, (b) 30m spatial resolution, (c) 90m spatial resolution**

### 4.4 Hybrid landslide susceptibility mapping

A total of three hybrid landslide susceptibility mapping were developed for 12.5m, 30m, and 90m spatial resolution. The hybrid LSM was formed by combining Frequency Ratio and Index of Entropy (FR-IOE LSM), Index of Entropy and Weight of Evidence (IOE-WOE LSM), and Weight of Evidence and Frequency Ratio (WOE-FR LSM). All the hybrid LSM were classified into five classes using the natural break for uniformity and comparison purposes with primary models and other hybrid models. The classes of hybrid LSM were very low, low, moderate, high, and very high susceptibility zone.

The classified hybrid LSM developed using 12.5m spatial resolution was shown in Figure 14(a) (FR-IOE LSM), Figure 14(b)(IOE-WOE LSM), and Figure 14(c) (WOE-FR LSM). The classified hybrid LSM developed using 30m spatial resolution was shown in Figure 15(a) (FR-IOE LSM), Figure 15(b)(IOE-WOE LSM), and Figure 15(c) (WOE-FR LSM). The classified hybrid LSM developed using 90m spatial resolution were shown in Figure 16(a) (FR-IOE LSM), Figure 16(b)(IOE-WOE LSM), and Figure 16(c) (WOE-FR LSM).

**Table 18 Area coverage in different spatial resolution LSM using hybrid models**

| Spatial Resolution | Zones | FR-IOE | | IOE-WoE | | WOE-FR | |
|---|---|---|---|---|---|---|---|
| | | Percentage | Area($km^2$) | Percentage | Area($km^2$) | Percentage | Area($km^2$) |
| **12.5m** | **Very Low** | 33.74 | 276.91 | 21.04 | 172.68 | 21.93 | 179.98 |
| | **Low** | 34.28 | 281.31 | 35.07 | 287.79 | 34.52 | 283.28 |
| | **Moderate** | 15.86 | 130.14 | 22.23 | 182.42 | 21.71 | 178.16 |
| | **High** | 13.66 | 112.15 | 13.32 | 109.36 | 13.42 | 110.13 |
| | **Very High** | 2.46 | 20.21 | 8.34 | 68.47 | 8.43 | 69.18 |
| | | | | | | | |
| **30m** | **Very Low** | 29.69 | 243.69 | 18.09 | 148.49 | 18.52 | 151.97 |
| | **Low** | 31.94 | 262.12 | 31.06 | 254.93 | 31.03 | 254.67 |
| | **Moderate** | 19.88 | 163.16 | 26.21 | 215.09 | 25.57 | 209.85 |
| | **High** | 12.94 | 106.19 | 15.46 | 126.88 | 15.33 | 125.8 |
| | **Very High** | 5.55 | 45.59 | 9.18 | 75.36 | 9.56 | 78.46 |
| | | | | | | | |
| **90m** | **Very Low** | 29.53 | 242.05 | 20.66 | 169.3 | 20.86 | 170.93 |
| | **Low** | 34.78 | 285.07 | 32.86 | 269.28 | 32.27 | 264.47 |
| | **Moderate** | 17.8 | 145.92 | 23.59 | 193.35 | 23.53 | 192.87 |
| | **High** | 12.33 | 101.09 | 13.55 | 111.04 | 13.82 | 113.25 |
| | **Very High** | 5.55 | 45.45 | 9.35 | 76.62 | 9.53 | 78.07 |

From the Table 18, it is noticed that the IOE-WOE and WOE-FR have identical characteristics during the classification using the natural break classification for all three spatial resolution. However, FR-IOE behaves slightly different from the IOE-WOE and WOE-FR. The area coverage is smallest for the FR-IOE and largest for the

other two hybrid LSM in a very high landslide susceptibility zone for all three spatial resolution. On contrary, it is noticed that the area coverage is largest for the FR-IOE and smaller for the other two models in the very low landslide susceptibility zone for all three spatial resolution. It is observed that the area increases until the high landslide susceptibility zone and then decreases after crossing the high landslide susceptibility zone for all three hybrid LSM.

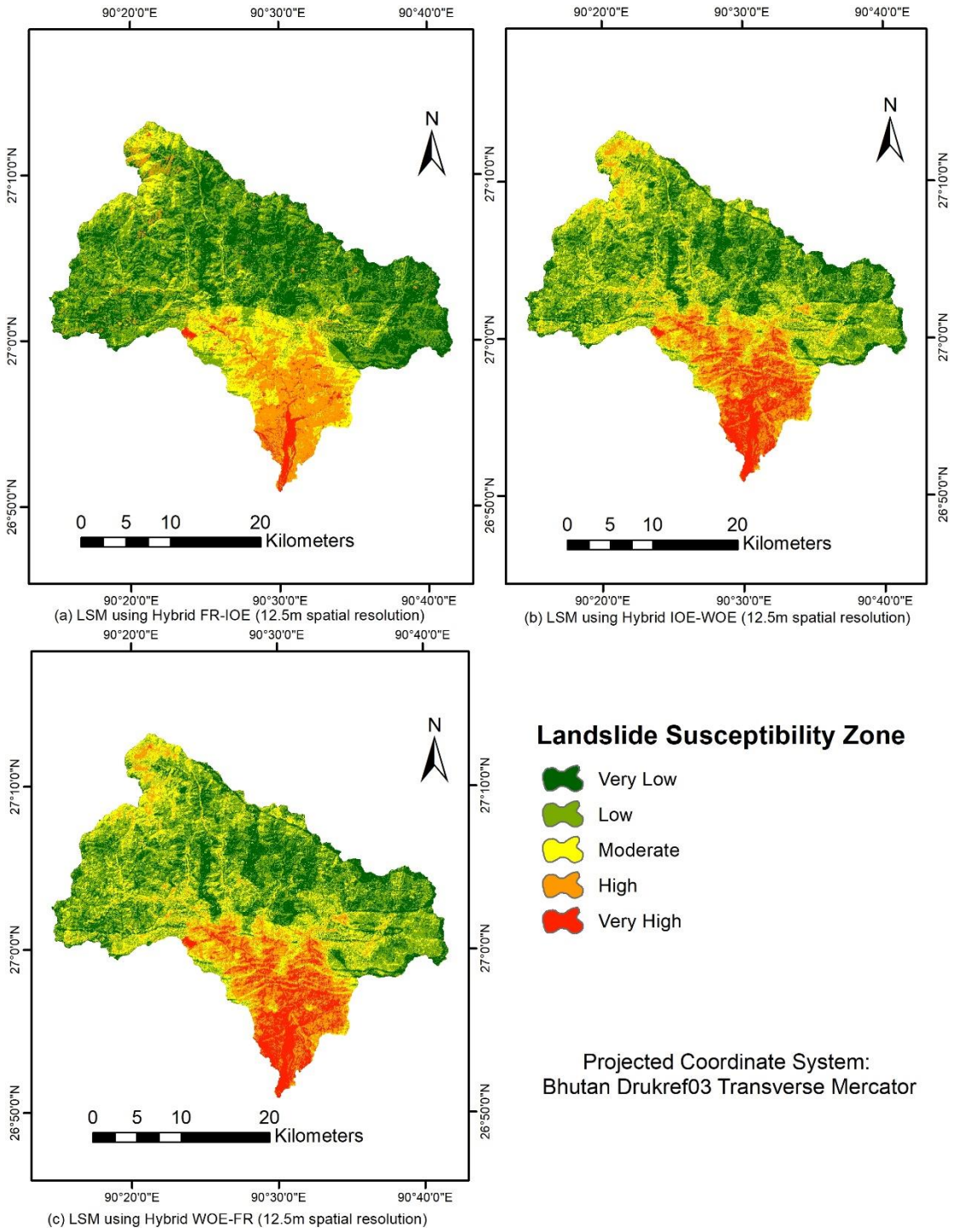


**Figure 14 Hybrid landslide susceptibility using 12.5m spatial resolution (a) FR-IOE, (b) IOE-WOE, (c) WOE-FR**

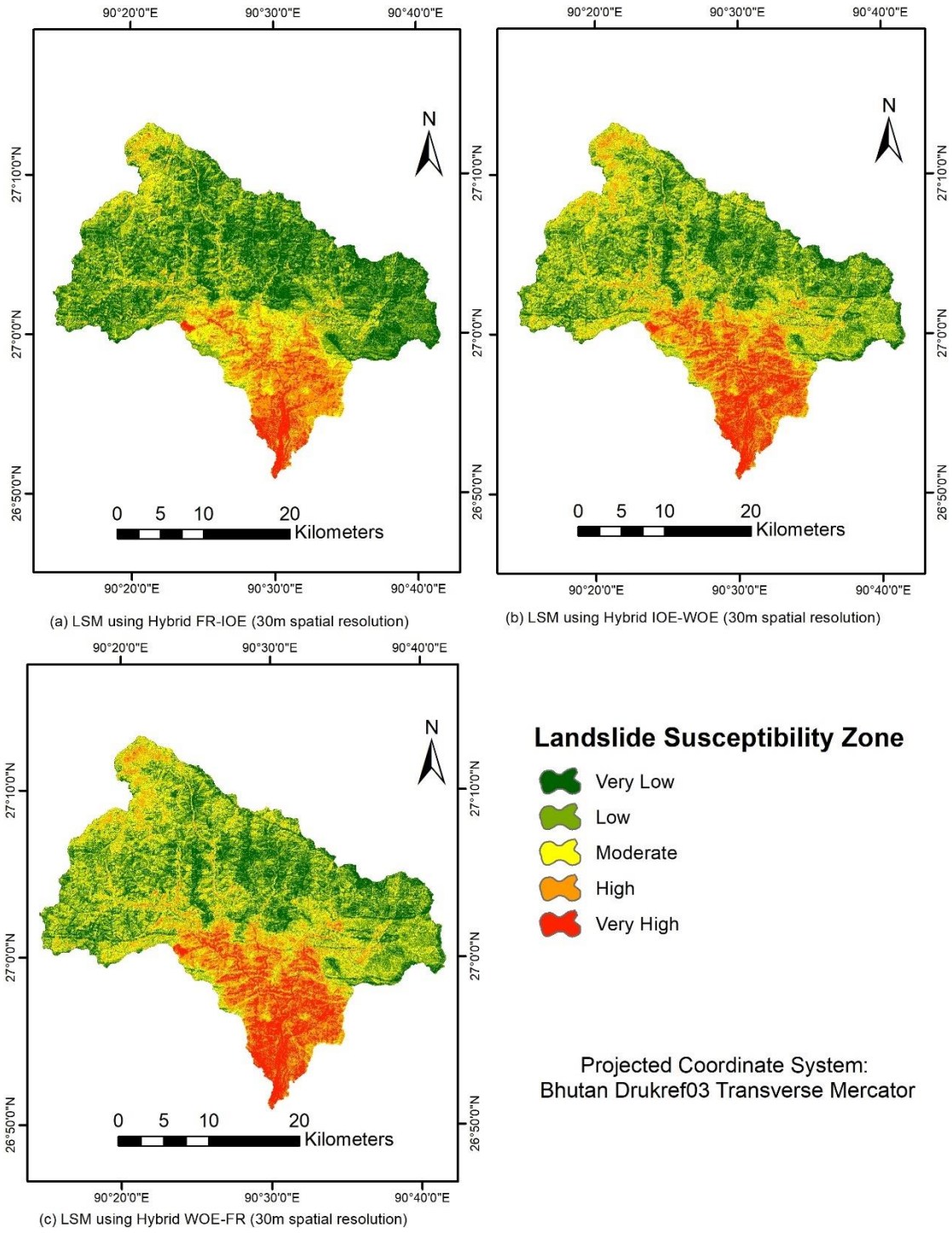


**Figure 15 Hybrid landslide susceptibility using 30m spatial resolution (a) FR-IOE, (b) IOE-WOE, (c) WOE-FR**

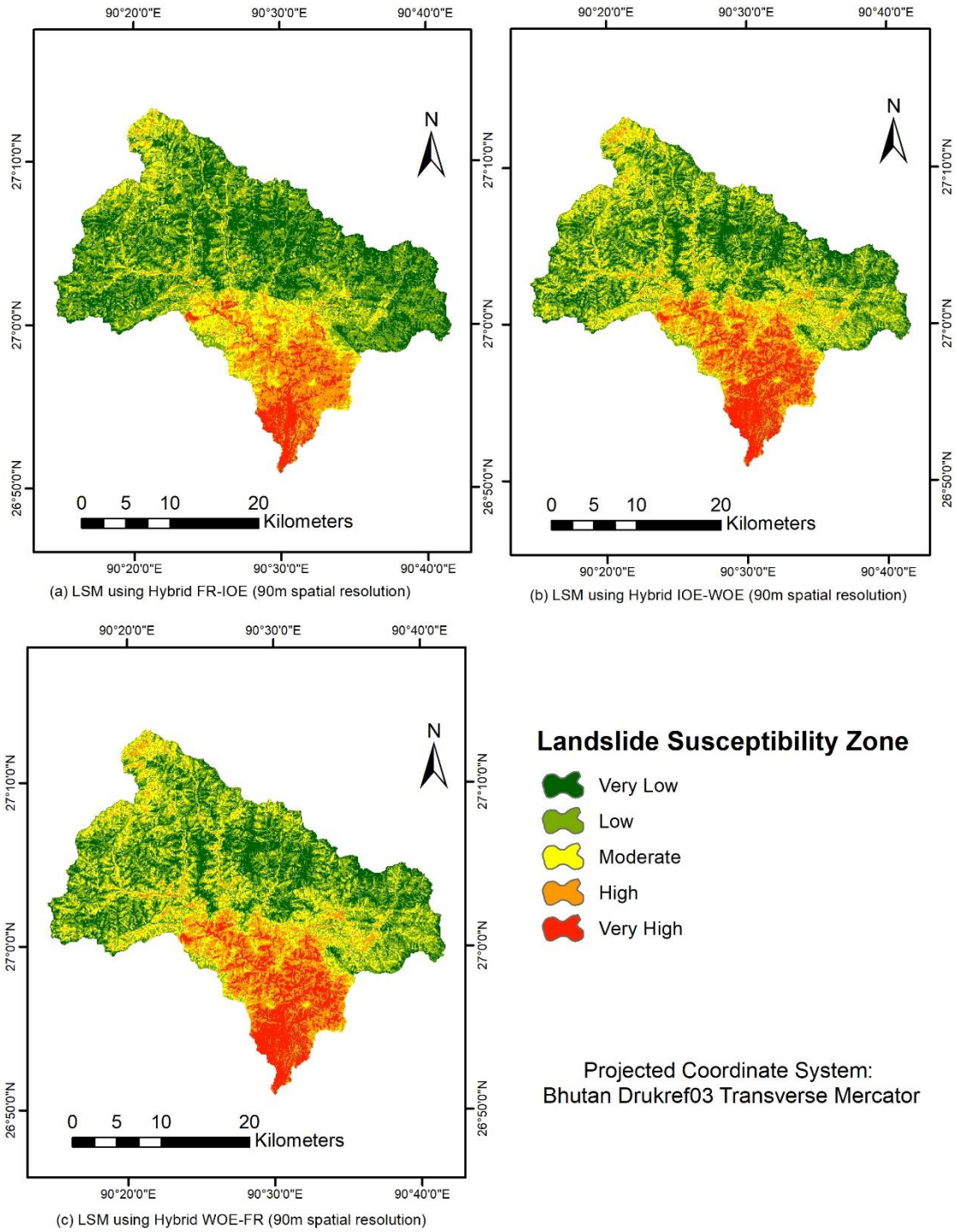


**Figure 16 Hybrid landslide susceptibility using 90m spatial resolution (a) FR-IOE, (b) IOE-WOE, (c) WOE-FR**

### 4.5 Validation of Landslide Susceptibility Mapping using statistical methods.

It is important to evaluate the efficiency of the model and the accuracy of the LSM (Kaur *et al.*, 2019). The commonly used method for validation is comparing the

observed data (landslide inventory data) with the predicted data (Shirani *et al.*, 2018). For this study, 30% (49 landslide points) of the landslide data from the inventory were used for the validation dataset. The equal number of non-landslide points is also identified for the validation datasets. Assign the value 1 for landslide points and 0 for non-landslide points for validation datasets.

This study uses a confusion matrix which calculates Sensitivity (Equation 22), 1-Specificity (Equation 23), Accuracy (Equation 24), kappa index (Equation 25), and area under the curve (Equation 28), and Root Mean Square Error (Equation 29) for the validation of landslide susceptibility map.

### 4.5.1 Validation of LSM produced by 12.5m spatial resolution.

#### I. Confusion Matrix

The confusion matrix compares the landslide status of the real ground with the predicted landslide status from the models. The confusion matrix decides statistical parameters such as true positive (TP), true negative (TN), false positive (FP), false negative (FN) and the concept of confusion matrix is shown in the Table 4. These parameters are used for calculating the sensitivity, specificity, accuracy, kappa index, and AUC. The summary of the statistical indices are given in Table 19.

**Table 19 Validation for 12.5m spatial resolution LSM**

| | FR | IOE | WOE | FR-IOE | IOE-WOE | WOE-FR |
|---|---|---|---|---|---|---|
| **TP** | 39 | 34 | 38 | 39 | 38 | 39 |
| **TN** | 38 | 40 | 38 | 38 | 38 | 39 |
| **FP** | 11 | 9 | 11 | 11 | 11 | 10 |
| **FN** | 10 | 15 | 11 | 10 | 11 | 10 |
| **Sensitivity** | 0.7959 | 0.6939 | 0.7755 | 0.7959 | 0.7755 | 0.7959 |
| **Specificity** | 0.7755 | 0.8163 | 0.7755 | 0.7755 | 0.7755 | 0.7959 |
| **Accuracy** | 0.7857 | 0.7551 | 0.7755 | 0.7857 | 0.7755 | 0.7959 |
| **Kappa Index** | 0.5714 | 0.5102 | 0.551 | 0.5714 | 0.551 | 0.5918 |
| **AUC** | 0.8848 | 0.8751 | 0.9017 | 0.8834 | 0.9017 | 0.9038 |
| **RMSE** | 0.3721 | 0.3919 | 0.3593 | 0.3724 | 0.3601 | 0.3593 |

TP and TN are the numbers of correctly classified pixels for landslide and non-landslide, respectively(Bui *et al.*, 2016). The FR, FR-IOE, and WOE-FR correspond to the highest correctly classified landslide pixel (39 landslide points) while IOE corresponds to the highest correctly classified non-landslide pixel (40 non-landslide points). On the other hand, FN and FP are the numbers of pixels erroneously classified

for landslide and non-landslide, respectively (Tien Bui *et al.*, 2018). The highest misclassification for the landslide pixel corresponds to IOE with FN of 15 landslide points while the maximum non-landslide misclassification corresponds to FR, WOE, FR-IOE, and IOE-WOE with FP of 11 non-landslide points.

Sensitivity is the proportion of landslide pixels that are correctly classified as landslide occurrences (Bui *et al.*, 2016). The highest correctly classified landslide pixel corresponds to LSM developed using FR and hybrid FR LSM namely FR, FR-IOE, and WOE-FR with a sensitivity of 0.7959. The least correctly classified landslide pixel corresponds to LSM developed by IOE (0.6939).

Specificity is the proportion of the non-landslide pixels that are correctly classified as non-landslide (Tien Bui *et al.*, 2018). Since the validation is carried out by 49 landslide pixels (30%) and an equal number of non- landslide pixels, the specificity shows the capability of non-landslide pixels classification. The highest correctly classified non-landslide pixel corresponds to LSM developed by IOE with a specificity of 0.8163 followed by WOE-FR with a specificity of 0.7959. Rest all the models has an equal specificity of 0.7755.

Accuracy is the proportion of landslide and non-landslide pixels that are correctly classified for both landslide and non-slide pixels (Bui *et al.*, 2016). The highest accuracy corresponds to WOE-FR (0.7959), followed by FR and FR-IOE (0.7857). The least accuracy corresponds to LSM developed using the IOE with an accuracy of 0.7551.

### II. Kappa Index

The Kappa index shows the reliability of the model and its value varies from −1 (non-reliable) to 1 (reliable) (Tien Bui *et al.*, 2018). As per Landis and Koch (1977), all the models fall under the moderate agreement (0.41-0.6) between the ground-truthing and predicted value. However, while comparing with the moderate agreement, WOE-FR has the highest kappa value (0.5918) while IOE has the least Kappa value (0.5102).

### III. Receiver Operating Characteristic (ROC) curve

The AUC from the ROC curve gives the predictive capability of the LSM. The ROC curve is plotted using the False Positive Rate (1-specificity) on X-axis and True Positive Rate (sensitivity) on Y-axis (Shirzadi *et al.*, 2017). The prediction rate is used to evaluate the future predictive power of the LSM (Wang *et al.*, 2015) and it was calculated using the validation dataset. The ROC curve for 12.5m spatial resolution is shown in Figure 17. The highest predictive capability corresponds to WOE-FR (0.9038), followed by WOE and IOE-WOE (0.9017), FR (0.8848), FR-IOE (0.8834), and (0.8751). As per the Shirani *et al.* (2018), the WOE, WOE-FR, and IOE-WOE fall under the excellent category (0.9-1.0), and the remaining LSM falls under the very good category (0.8-0.9) for 12.5m spatial resolution.

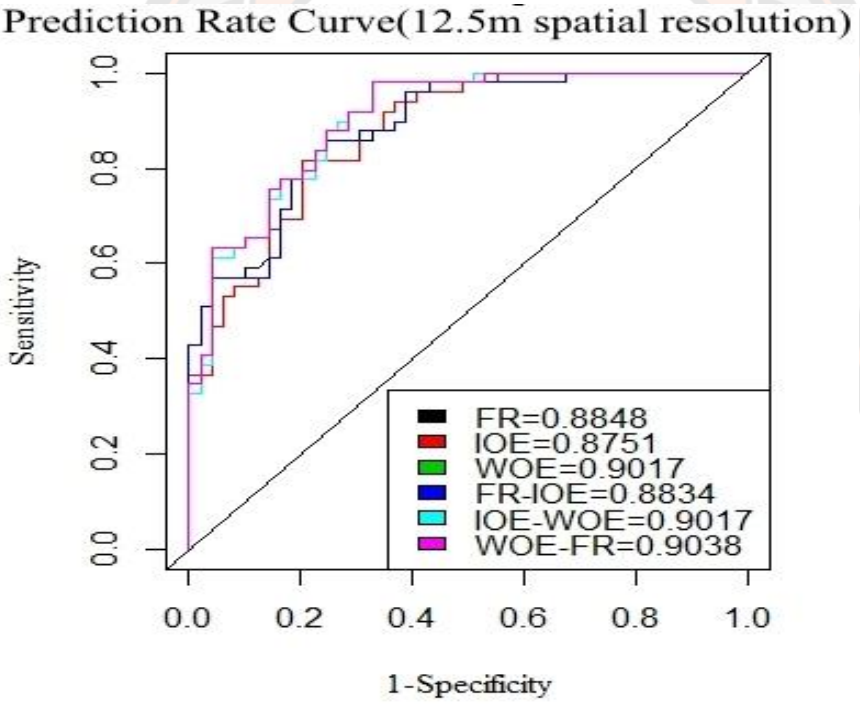


**Figure 17 ROC curve of different models using 12.5m spatial resolution**

### IV. Root Means Square Error (RMSE)

The Root Mean Square Error (RMSE) is defined as the differences between values predicted values for the landslides by the models and the observed values from the actual ground. When the RMSE value is 0, it is considered as no error which corresponds to correlation coefficient 1 and vice versa (Barnston, 1992). The highest

RMSE corresponds to LSM developed using IOE (0.3919), followed by FR-IOE (0.3724), FR (0.3721), IOE-WOE (0.3601), and the least RMSE corresponds to WOE and WOE-FR (0.3593).

### 4.5.2 Validation of LSM produced by 30m spatial resolution

#### I. Confusion Matrix

The confusion matrix calculates TP, TN, FP, and FN which will be ultimately used for calculation of sensitivity, specificity, accuracy, kappa index, and AUC. The summary of the statistical indices is given in Table 20.

**Table 20 Validation for 30m spatial resolution LSM**

| | FR | IOE | WOE | FR-IOE | IOE-WOE | WOE-FR |
|---|---|---|---|---|---|---|
| **TP** | 37 | 33 | 42 | 37 | 42 | 41 |
| **TN** | 39 | 40 | 38 | 39 | 38 | 38 |
| **FP** | 10 | 9 | 11 | 10 | 11 | 11 |
| **FN** | 12 | 16 | 7 | 12 | 7 | 8 |
| **Sensitivity** | 0.7551 | 0.6735 | 0.8571 | 0.7551 | 0.8571 | 0.8367 |
| **Specificity** | 0.7959 | 0.8163 | 0.7755 | 0.7959 | 0.7755 | 0.7755 |
| **Accuracy** | 0.7755 | 0.7449 | 0.8163 | 0.7755 | 0.8163 | 0.8061 |
| **Kappa Index** | 0.551 | 0.4898 | 0.6327 | 0.551 | 0.6327 | 0.6122 |
| **AUC** | 0.8844 | 0.8825 | 0.8905 | 0.8846 | 0.8905 | 0.8905 |
| **RMSE** | 0.3744 | 0.3831 | 0.3628 | 0.3742 | 0.3628 | 0.3628 |

The WOE and IOE-WOE correspond to the highest correctly classified landslide pixel with a TP of 42 while IOE corresponds to the highest correctly classified non-landslide pixel with a TN of 40. On the other hand, the highest misclassification for the landslide pixel corresponds to IOE with FN of 16 landslide points while the maximum misclassified non-landslide pixel corresponds to WOE, IOE-WOE, and WOE-FR with FP of 11 non-landslide points.

The correctly highest classified landslide pixel corresponds to LSM developed using WOE and IOE-WOE with a sensitivity of 0.8571. The least correctly classified landslide pixel corresponds to LSM developed by IOE with a sensitivity of 0.6735.

The IOE classified maximum correct classification with non-landslide pixels with a specificity of 0.8163 followed by FR and FR-IOE (0.7959), and WOE, IOE-WOE, and WOE-FR (0.7755).

The highest accuracy corresponds to WOE-FR and WOE (0.8163), followed by WOE-FR (0.8061), FR, and FR-IOE (0.7755). The least accuracy corresponds to LSM developed using the IOE with an accuracy of 0.7449.

**II. Kappa Index**

As per Landis and Koch (1977), FR (0.551), IOE(0.4898), FR-IOE(0.551) falls under the moderate agreement (0.41-0.6), while WOE(0.6327), IOE-WOE(0.6327), WOE-FR(0.6122) falls under Substantial agreement (0.61-0.80) between the ground-truthing and predicted value. While comparing with within the models, all the models related to WOE are more reliable compared to other models with minimum kappa value ranging from 0.6122 to 0.6327. On the other hand, the least reliable mode corresponds to IOE with Kapp value of 0.4898.

**III. Receiver Operating Characteristic (ROC) curve**

The ROC curve for the 30m spatial resolution LSM is shown in Figure 18. The highest predictive capability corresponds to WOE, WOE-FR and IOE-WOE (0.8905), followed by FR-IOE (0.8846), FR (0.8844) and IOE (0.8825). As per the Shirani *et al.* (2018), all the LSM falls under the Very good category (0.8-0.9) for the 30m spatial resolution.

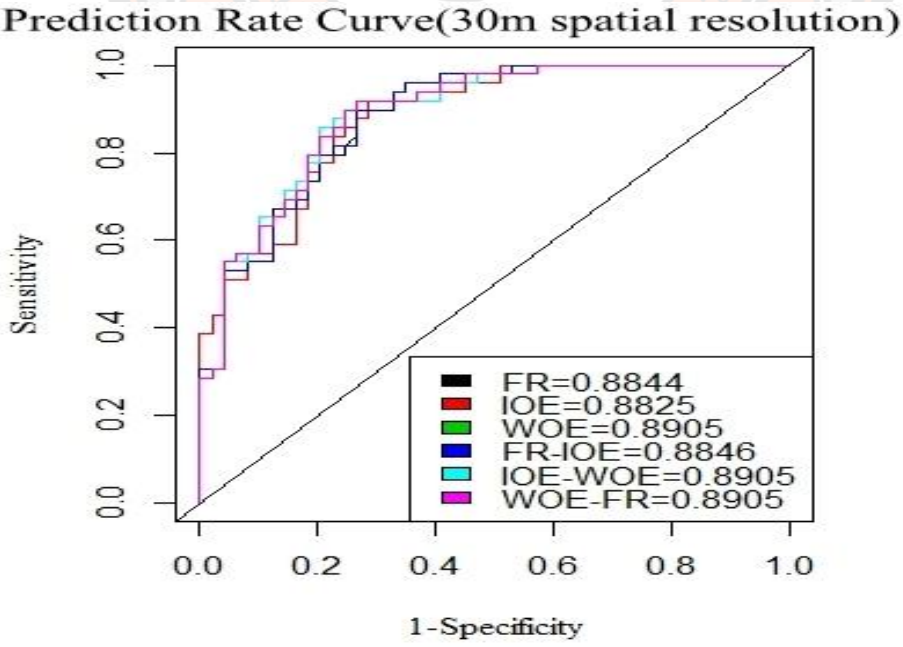


**Figure 18 ROC curve of different models using 30m spatial resolution**

**IV. Root Means Square Error (RMSE)**

The Root Mean Square Error (RMSE) is defined as the differences between values predicted values for the landslides by the models and the observed values from the actual ground. The highest RMSE corresponds to LSM developed using IOE (0.3831), followed by FR (0.3744), FR-IOE (0.3742) and the least error corresponds to three LSM namely, WOE, IOE-WOR, and FR-WOE with RMSE of 0.3628.

### 4.5.3 Validation of LSM produced by 90m spatial resolution

**I. Confusion Matrix**

The result of the confusion matrix showing TP, TN, FP, and FN are shown in Table 21. The TP, TN, FP, and FN are used for calculation of sensitivity, specificity, accuracy, kappa index, and AUC. The summary of the statistical indices is given in Table 21.

**Table 21 Validation for 90m spatial resolution LSM**

| | FR | IOE | WOE | FR-IOE | IOE-WOE | WOE-FR |
|---|---|---|---|---|---|---|
| **TP** | 36 | 38 | 39 | 36 | 39 | 39 |
| **TN** | 36 | 37 | 37 | 36 | 37 | 37 |
| **FP** | 13 | 12 | 12 | 13 | 12 | 12 |
| **FN** | 13 | 11 | 10 | 13 | 10 | 10 |
| **Sensitivity** | 0.7347 | 0.7755 | 0.7959 | 0.7347 | 0.7959 | 0.7959 |
| **Specificity** | 0.7347 | 0.7551 | 0.7551 | 0.7347 | 0.7551 | 0.7551 |
| **Accuracy** | 0.7347 | 0.7653 | 0.7755 | 0.7347 | 0.7755 | 0.7755 |
| **Kappa Index** | 0.4694 | 0.5306 | 0.551 | 0.4694 | 0.551 | 0.551 |
| **AUC** | 0.8324 | 0.8259 | 0.853 | 0.833 | 0.853 | 0.8505 |
| **RMSE** | 0.4094 | 0.4097 | 0.3946 | 0.409 | 0.3946 | 0.3956 |

The WOE, IOE-WOE, and IOE-WOE correspond to the highest correctly classified landslide pixel with a TP of 39. On the other hand, the highest misclassification for the landslide pixel corresponds to FR, and FR-IOE with FN of 13

The highest correctly classified landslide pixel corresponds to LSM developed using WOE, IOE-WOE, and WOE-FR with a sensitivity of 0.7959. The least correctly classified landslide pixel corresponds to LSM developed by FR and FR-IOE with a sensitivity of 0.7347.

The highest correctly classified non-landslide pixel are links to LSM developed by four models which include IOE, WOE, IOE-WOE, and WOE-FR with a specificity

of 0.7551. The FR and FR-IOE had the least specificity of 0.7347 indicating the lowest classified non-landslide point.

The LSM related to WOE has the highest accuracy (0.7755) which includes in WOE, IOE-WOE, and WOE-FR. On the other hand, the FR and FR-IOE correspond to the lowest accuracy (0.7347) for the 90m spatial resolution.

### II. Kappa Index

The Kappa index for WOE, IOE-WOE, and WOE-FR are 0.5510, IOE is 0.5306, and FR and FR-IOE are 0.4694. As per Landis and Koch (1977), all the models fall under the moderate agreement (0.41-0.6) between the ground-truthing and predicted value.

### III. Receiver Operating Characteristic (ROC) curve

The ROC curve for the 30m spatial resolution LSM is shown in Figure 19. The best predictive LSM is developed using the WOE and IOE-WOE with AUC of 0.8530 and the least prediction rate is developed using the IOE with AUC of 0.8259. THE AUC for the FR is 0.8324, FR-IOE is 0.8330 and WOE-FR is 0.8505. As per the Shirani *et al.* (2018), all the LSM falls under the Very good category (0.8-0.9) for the 90m spatial resolution.

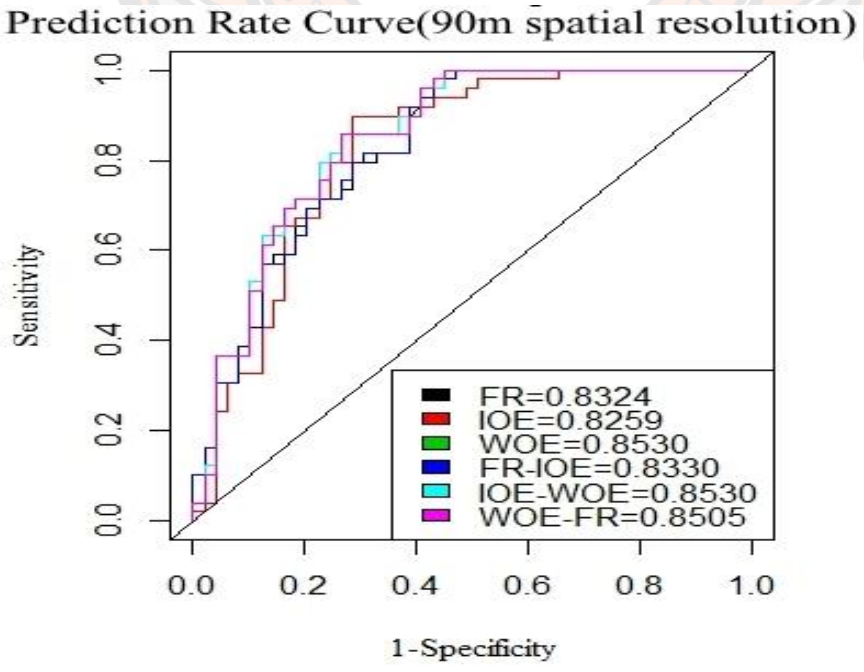


**Figure 19 ROC curves of different models using 90m spatial resolution.**

**IV. Root Means Square Error (RMSE)**

The accuracy is said to be lower when the RMSE is higher. The lowest accuracy with RMSE of 0.4097 corresponds to IOE, followed by FR (0.4094), FR-IOE (0.4090), WOE-FR (0.3956). The highest accuracy with the least RMSE corresponds to WOE and IOE-WOE (0.3946).

### 4.5.4 Relationship between the spatial resolution and the different validation parameters

The Figure 20 shows the relationship between the spatial resolution with the statistical parameters such as sensitivity, specificity, accuracy, Cohen's kappa index, prediction rate, and the root mean square error (RMSE). The value of the statistical parameters was calculated from the average of the FR, IOE, WOE, FR-IOE, IOE-WOE, and WOE-FR for individual spatial resolutions (12.5m, 30m, and 90m). Generally, it is observed that the correlation between the spatial resolution and the statistical parameters is negative except the RMSE. The negative correlation indicates that the sensitivity, specificity, accuracy, Cohen's kappa index, and prediction rate decreases with an increase in the grid size from 12.5m to 90m. However, the RMSE increases with an increase in grid size indicating the smaller grid size are better for the LSM.

Regarding the relationship between the spatial resolution and the sensitivity (Figure 20(a)), it is noticed that the sensitivity decreases as the spatial resolution becomes courser (increasing grid size). This shows that the capability of correctly classified landslide pixels is decreasing as the spatial resolution becomes courser.

Similarly, the relationship between the specificity and the grid size also shows a negative correlation (Figure 20(b)) indicating the potential of classifying the non-landslides is decreasing as the cell size increases.

The accuracy shows the proportion of correctly landslide and non-landslide. From Figure 20(c), it is noticed that the accuracy decreases as the grid size increases. This clearly indicate the coarse spatial resolution has less strength of classifying the landslide and the non-landslide pixel.

The kappa index (Figure 20(d)) indicates the reliability of the models and the LSM. The kappa index also follows a similar pattern as that of the sensitivity,

specificity, and accuracy. The reliability of classification decreases as the spatial resolution becomes courser.

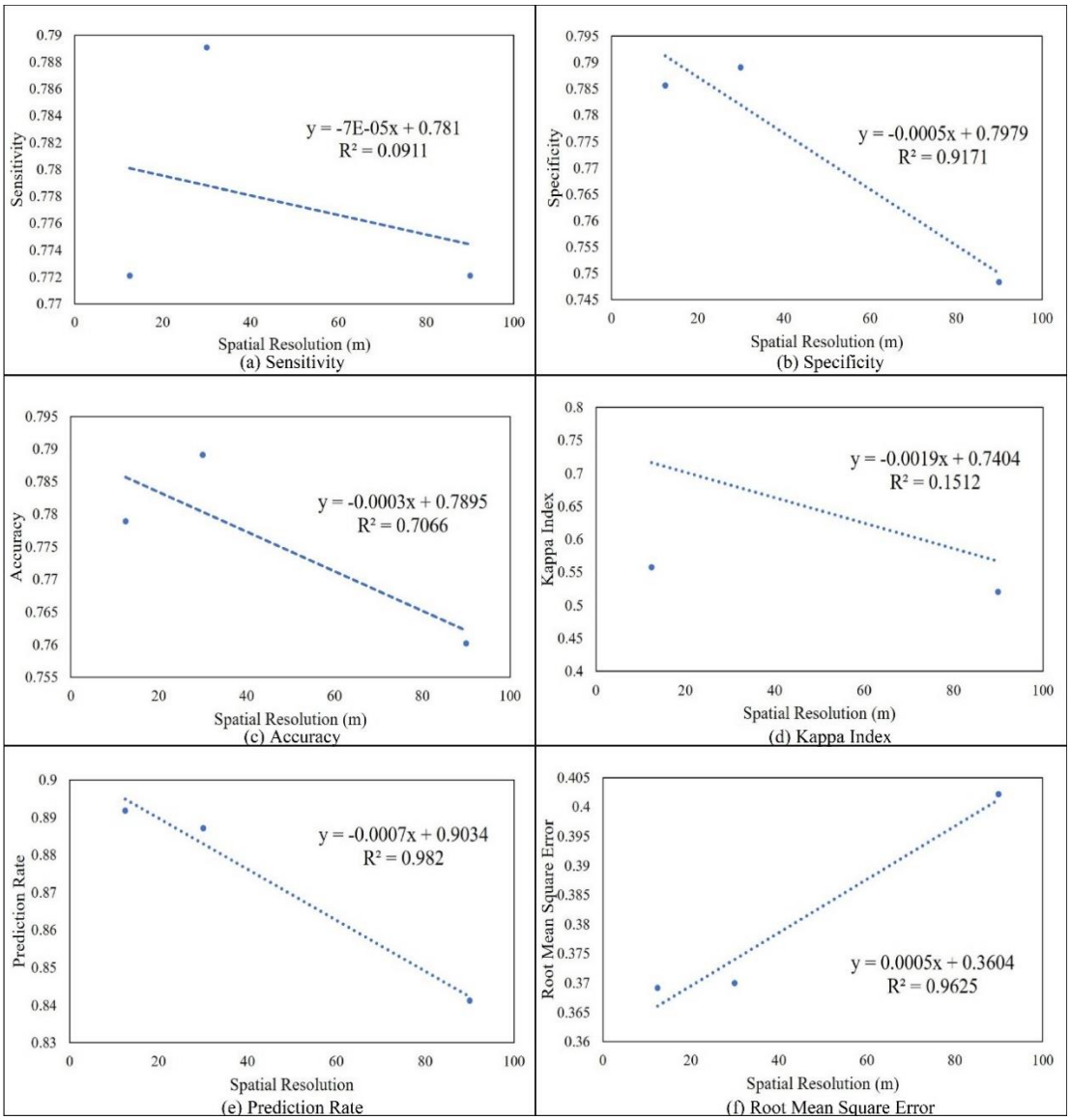


**Figure 20 Relationship between the different validation parameters and spatial resolutions**

The prediction capability also decreases as the spatial resolution becomes courser. From (Figure 20(e)) it clearly shows that the higher spatial resolution is relatively better for the prediction of the LSM.

On contrary to all other statistical parameters, the value of RMSE increases as the spatial resolution becomes courser (Figure 20(f)). The RMSE is the difference between values predicted values for the landslides by the models and the observed values from

the actual ground. When the RMSE value is 0, it is considered as no error. This study clearly indicates the RMSE value increases with an increase in spatial resolution value (course spatial resolution).

From all the statistical parameters, it indicates that it is not advisable to use the course resolution as it compromises the classification of the landslide pixel (sensitivity), classification of the non-landslide pixel (specificity), classification of both landslide and non-landslide pixel (accuracy), reliability of the LSM (Kappa index), deceases prediction capability (prediction rate) and the increases the RMSE value.

### 4.5.5 Comparison of bivariate models for the validation parameters

The Figure 21 shows the average of the statistical parameters of the three different spatial resolutions (12.5m, 30m, and 90m). It is observed that the WOE and its hybrid models (IOE-WOE and WOE-FR) have the highest sensitivity (0.8095) while LSM developed by IOE has the lowest sensitivity (0.7143). This shows that the WOE and its hybrid models have the best capacity to classify the landslide pixels.

Regarding the specificity, the IOE classified relatively better non-slide pixels for this study with a specificity of 0.7959, followed by WOE-FR with specificity of 0.7755. The remaining four models classified the least non-slide pixel with a specificity of 0.7687 for this study.

The accuracy is the capability classification of landslides and non-landslides by the different models. The highest accuracy corresponds to WOE-FR (0.7925), followed by WOE and IOE-WOE (0.7891). The accuracy of FR and FR-IOE is 0.7653 and the least accurate of all the models corresponds to IOE (0.7551).

The reliability of the different model is decided by Cohen's kappa index. The WOE-FR is considered to be the highest reliable model with the highest kappa index of 0.5850, followed by WOE and IOE-WOE with a kappa index of 0.5782. The kappa index of FR and FR-IOE is 0.5306 and the least reliable model is IOE with a kappa index of 0.5102.

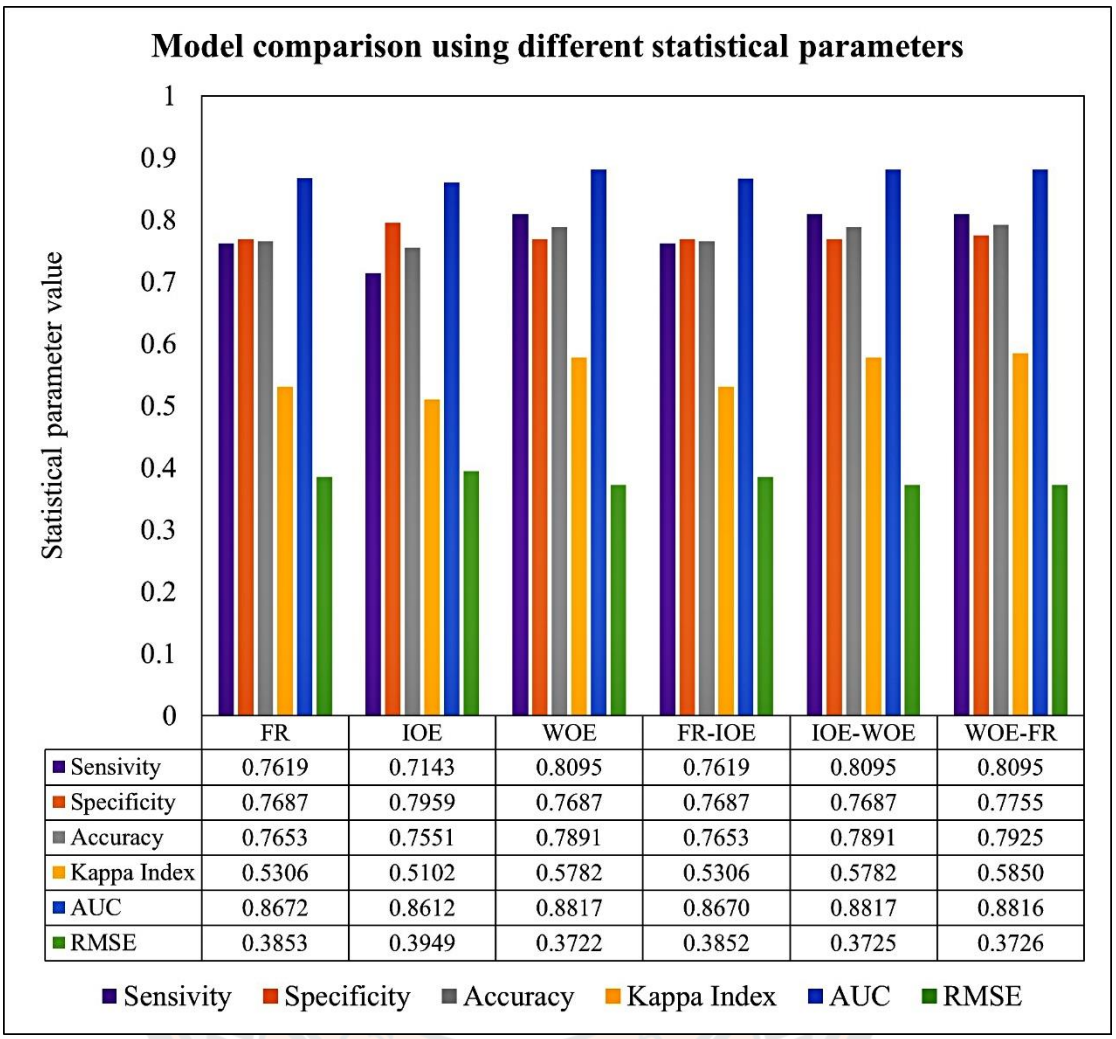


| | FR | IOE | WOE | FR-IOE | IOE-WOE | WOE-FR |
|---|---|---|---|---|---|---|
| Sensivity | 0.7619 | 0.7143 | 0.8095 | 0.7619 | 0.8095 | 0.8095 |
| Specificity | 0.7687 | 0.7959 | 0.7687 | 0.7687 | 0.7687 | 0.7755 |
| Accuracy | 0.7653 | 0.7551 | 0.7891 | 0.7653 | 0.7891 | 0.7925 |
| Kappa Index | 0.5306 | 0.5102 | 0.5782 | 0.5306 | 0.5782 | 0.5850 |
| AUC | 0.8672 | 0.8612 | 0.8817 | 0.8670 | 0.8817 | 0.8816 |
| RMSE | 0.3853 | 0.3949 | 0.3722 | 0.3852 | 0.3725 | 0.3726 |

**Figure 21 Comparison between the validation parameters and the different models**

The value of AUC of the ROC is used as a prediction rate which shows the strength of LSM to predict the future LSM. The WOE and IOE-WOE have the highest prediction rate (0.8817), followed by WOE-FR (0.8816), FR(0.8672), FR-IOE (0.8670), and IOE (0.8612).

The RMSE shows the degree of error and the highest error in classification corresponds to IOE with RMSE of 0.3949, followed by FR (0.3853), FR-IOE (0.3852), WOE-FR (0.3726), and IOE-WOE (0.3725). The WOE (0.3722) has the least RMSE.

# CHAPTER V
# CONCLUSION

## 5.1 Argument

The LSM was developed using the three primary models and three hybrid models. The hybrids models are derived from the primary models for three different spatial resolutions (12m, 30m, and 90m). The most accurate model for developing the LSM among the three models is WOE, followed by the FR and IOE. The accuracy of WOE is 0.7891, followed by FR with an accuracy of 0.7653 and IOE with an accuracy of 0.7551. The combination of the models to form new hybrid models. The accuracy of the hybrid model has better or equivalent to the highest primary model. For example, the accuracy of the hybrid model WOE-FR has an accuracy of 0.7925 while its primary model WOE has an accuracy of just 0.7891, and the accuracy of FR is just 0.7653. Similarly, IOE-WOE has an accuracy of 0.7891 which is higher than its primary model IOE (0.7551) or equal to WOE (0.7891). The hybrid model FR-IOE has an accuracy of 7653 which is higher than its primary model IOE (0.7551) and equivalent to FR (0.7653).

Among the primary models, the WOE has the highest reliability of the model with a kappa index of 0.5782, followed by FR with a kappa index of 0.5306 and IOE with a kappa index of 0.5102. It is noticed that the hybrid models improve the reliability because it increases the kappa index or the hybrid model has the reliability of the highest primary model. The hybrid model WOE-FR has a kappa index of 0.5850 while its primary model FR has a kappa index of 0.55306 and WOE has a kappa index of 0.5782. Similarly, the kappa index of hybrid model FR-IOE is 0.5306 which is better than its primary model IOE(0.5102) and equal to FR (0.5302). The hybrid model IOE-WOE has a kappa index of 0.5782 which is higher than IOE (0.5102) and equal to WOE(0.5782).

While comparing the future predictive power among the primary models, the WOE has the highest predictive power of the LSM with an AUC of 0.8817, followed by FR (0.8672) and IOE (0.8612). There is a slight improvement in the predictive power in the hybrid models for all three hybrid models with higher AUC.

The lowest RMSE among the primary models corresponds to WOE(0.3722), followed by FR(0.3853) and IOE(0.3949). It was noticed that the hybrid models decrease the RMSE. For instance, the FR-IOE has a RMSE of 0.3852 while its primary model FR has RMSE of 0.3853, and IOE has a RMSE of 0.3949.

In general, the WOE is much better than FR and IOE for developing the LSM in terms of accuracy, reliability, and predictive power. Furthermore, the hybrid models which are formed by combining the primary models improve the accuracy, reliability, predictive power, and minimizes the RMSE. Although the comparison between the accuracy between the bivariate statistical methods are debatable, most of the studies shows that weight of evidence methods is better than the index of model (Li and Wang, 2019; Liu and Duan, 2018). Youssef *et al.* (2015) has found that the frequency ratio is better than Index of entropy. Overall, the performance of the model follow the order of Weight of Evidence, Frequency ratio and Index of entropy which is similarly to the result of Nohani *et al.* (2019).

In terms of spatial resolutions, the finer resolution produces higher accuracy LSM compared to the courser resolution in terms of accuracy, reliability, predictive power, and RMSE. The result is agreed with the analysis of (Lee, Choi, and Woo, 2004)

## 5.2 Conclusion

A total of fifteen landslide influencing factors were used for this study which includes elevation, slope, aspect, slope curvature, topographic wetness index, stream power index, drainage density, Normalized Difference Vegetation Index, Normalized Difference Soil Index, proximity to the river, proximity to the fault, average annual rainfall, and lithology, land use land cover, and proximity to the road. The elevation, slope, aspect, slope curvature, topographic wetness index, stream power index, and drainage density were derived from ALOS PALSAR DEM (12.5m) and SRTM DEM (30m and 90m). The Normalized Difference Vegetation Index, Normalized Difference Soil Index, and land use land cover were derived from sentinel-2. The Geological map of Bhutan is used to derive the lithological map and proximity to the fault map. The rainfall map of 21 years (1996-2017) from 20 rainfall stations across Bhutan were used to derive a rainfall map which was developed using the IDW interpolation. The Digital Topographic Map of Bhutan was used to derive the map of road and river.

The landslide inventory was done using the interpretation of sentinel image, google earth, and field investigation. A total of 164 landslide locations were identified of which 70% (115) were used for the training dataset while the remaining 30% (49) were used for the validation dataset. All the factors were classified into classes and then trained using the existing landslide locations from the training dataset which will ultimately be used in the analysis of FR, IOE, and WOE.

The average magnitude of contribution from the individual classes of the factors of three spatial resolution was calculated using the frequency ratio, landslide density of the Index of Entropy, Contrast of the Weight of Evidence. The Index of Entropy model also calculates the amount of contribution from the individual influencing factors. The $W_j$ of Table 15 indicates the magnitude of influence of the influencing factors on the landslide occurrences (Mondal and Mandal, 2019). Among the fifteen factors, the most dominant five factors were the Normalized Difference Vegetation Index (0.394), followed by the land use land cover (0.176), rainfall (0.163), elevation (0.158), Normalized Difference Soil Index (0.134), and lithology (0.125). The least significant factor was the Topographic Wetness Index with a weight of 0.008.

All the developed LSM were classified into five zones using the natural break classification for all the three different models and three different spatial for the individual models. As per the natural break classification, it was noticed that the size of an area increases as the landslide zone moves from a very high susceptibility zone to a low susceptibility zone and then decreases as it reached a very low susceptibility zone for most of the models.

The validation of the LSM was conducted using 30% of the total landslide which was collected during the landslide inventory. The sensitivity, specificity, accuracy, kappa index, the area under the curve (AUC) and root mean square error (RMSE) was used for the validation of the LSM. The best classified landslide pixel corresponds to WOE and its hybrid models (IOE-WOE and WOE-FR) with a sensitivity of 0.8095 each while the IOE model classifies the best non-landslide pixel with a specificity of 0.7959. The highest accuracy model is linked to WOE-FR with an accuracy of 0.7925 and the most reliable for the landslide study was performed by WOE-FR with a kappa index of 0.5850. As per Landis and Koch (1977), all the models fall under the moderate agreement the predicted and observed landslide due to its kappa

values falling in between the 0.41-0.60. The highest prediction rate of LSM corresponds to WOE and IOE-WOE with an AUC of 0.8817. The predictive power of all the LSM developed by different models falls under a very good category (0.8-0.9) (Shirani *et al.*, 2018). The least RMSE corresponds to IOE-WOE and is considered to be the least error among the various models.

It is noted that all finer resolution gives better accuracy for developing landslide susceptibility studies. The relationship between the different validation parameters and spatial resolution (12.5m) corresponds to higher sensitivity, specificity, accuracy, kappa index, and the prediction rate compared to coarser spatial resolution (90m). At the same time, the error least error also corresponds to finer resolution with lesser RMSE value.

### 5.3 Limitations and suggestions

The following are the limitations and suggestions for the future studies.

1. Since the initial landslide inventory mapping was done using the sentinel-2, and google earth image, it is recommended to use a higher resolution satellite image/aerial photograph to gain more accurate landslide susceptibility mapping.
2. Since this study uses only geostatistical analysis, it is recommended to use machine learning techniques and compare how the accuracy is deviating compared to machine learning techniques.
3. Most of the studies used IDW interpolation for landslide susceptibility mapping. Similarly, this study also used IDW interpolation to develop a rainfall map. It is recommended to use different interpolation techniques for the landslide studies and compare the accuracy assessment.
4. This study used geospatial techniques for the landslide studies which were developed using the training dataset of the landslide inventory. It is recommended to use geotechnical field tests in selected sites to confirm and validate the landslide susceptibility map which was developed using geospatial techniques.
5. Only three spatial resolutions were used for deriving relation between the different validation parameters which is not very accurate graph. It is recommended to use

more number of spatial resolution to derive the more accurate relationship between spatial resolution and validation parameters.

6. It is noticed that the high and very high landslide prone area are located the physical geography such as which is made up of combination of steep terrain, lower elevation, closer to the river, weak lithology (Tsm and pCd) and heavy precipitated area. Therefore, Bhutanese government, engineers and decision makers are suggested to minimize future planning in such area which is considered as the high and very landslide prone area. The high and very high landslide prone area are indicated by orange and red color, respectively.

# REFERENCES


Achour, Y., Boumezbeur, A., Hadji, R., Chouabbi, A., Cavaleiro, V., & Bendaoud, E. A. (2017). Landslide susceptibility mapping using analytic hierarchy process and information value methods along a highway road section in Constantine, Algeria. *Arabian Journal of Geosciences, 10*(8), 194.

Action, N. A. P. o. (2014). Addressing the Risks of Climate-induced Disasters through Enhanced National and Local Capacity for Effective Actions.

Akgun, A., Kıncal, C., & Pradhan, B. (2012). Application of remote sensing data and GIS for landslide risk assessment as an environmental threat to Izmir city (west Turkey). *Environmental monitoring and assessment, 184*(9), 5453-5470.

Aleotti, P., & Chowdhury, R. (1999). Landslide hazard assessment: summary review and new perspectives. *Bulletin of Engineering Geology and the Environment, 58*(1), 21-44.

Alex, E. C., Ramesh, K., & Sridevi, H. (2017). Quantification and understanding The observed changes in land cover Patterns in bangalore. *International Journal of Civil Engineering and Technology, 8*(4), 597-603.

Ayalew, L., & Yamagishi, H. (2005). The application of GIS-based logistic regression for landslide susceptibility mapping in the Kakuda-Yahiko Mountains, Central Japan. *Geomorphology, 65*(1-2), 15-31.

Ayalew, L., Yamagishi, H., & Ugawa, N. (2004). Landslide susceptibility mapping using GIS-based weighted linear combination, the case in Tsugawa area of Agano River, Niigata Prefecture, Japan. *Landslides, 1*(1), 73-81.

Bai, S.-B., Wang, J., Lü, G.-N., Zhou, P.-G., Hou, S.-S., & Xu, S.-N. (2010). GIS-based logistic regression for landslide susceptibility mapping of the Zhongxian segment in the Three Gorges area, China. *Geomorphology, 115*(1-2), 23-31.

Barella, C. F., Sobreira, F. G., & Zêzere, J. L. (2019). A comparative analysis of statistical landslide susceptibility mapping in the southeast region of Minas Gerais state, Brazil. *Bulletin of Engineering Geology and the Environment, 78*(5), 3205-3221.

Barnston, A. G. (1992). Correspondence among the correlation, RMSE, and Heidke forecast verification measures; refinement of the Heidke score. *Weather and Forecasting, 7*(4), 699-709.

Bonham-Carter, G., Agterberg, F., & Wright, D. (1988). Integration of geological datasets for gold exploration in Nova Scotia. *Photogrammetric Engineering and Remote Sensing, 54*(11), 1585-1592.

Bui, D. T., Tuan, T. A., Klempe, H., Pradhan, B., & Revhaug, I. (2016). Spatial prediction models for shallow landslide hazards: a comparative assessment of the efficacy of support vector machines, artificial neural networks, kernel logistic regression, and logistic model tree. *Landslides, 13*(2), 361-378.

Cao, C., Xu, P., Wang, Y., Chen, J., Zheng, L., & Niu, C. (2016). Flash flood hazard susceptibility mapping using frequency ratio and statistical index methods in coalmine subsidence areas. *Sustainability, 8*(9), 948.

Carranza, E. J. M. (2004). Weights of evidence modeling of mineral potential: a case study using small number of prospects, Abra, Philippines. *Natural Resources Research, 13*(3), 173-187.

Carrara, A., Guzzetti, F., Cardinali, M., & Reichenbach, P. (1999). Use of GIS technology in the prediction and monitoring of landslide hazard. *Natural hazards, 20*(2-3), 117-135.

Chand, D. S. (2008). *Landslide monitoring in space and time using optical satellite imagery and DEM derived parameters: case study from Garhwal Himalaya, Uttarakhand, India.* ITC.

Cheki, D., & Shibayama, T. (2008). Method for landslide risk evaluation and road operation management: a case study of Bhutan. *Journal of Construction Management, JSCE, 15*, 23-31.

Chen, F.-W., & Liu, C.-W. (2012). Estimation of the spatial rainfall distribution using inverse distance weighting (IDW) in the middle of Taiwan. *Paddy Water Environ, 10*(3), 209-222.

Clague, J. J., & Stead, D. (2012). *Landslides: types, mechanisms and modeling*: Cambridge University Press.

Constantin, M., Bednarik, M., Jurchescu, M. C., & Vlaicu, M. (2011). Landslide susceptibility assessment using the bivariate statistical analysis and the index of entropy in the Sibiciu Basin (Romania). *Environ Earth Sci, 63*(2), 397-406.

Cruden, D., & VanDine, D. (2013). CLASSIFICATION, DESCRIPTION, CAUSES AND INDIRECT EFFECTS Canadian Technical Guidelines and Best Practices related to Landslides: a national initiative for loss reduction. *Geol Surv Can Open File, 7359*, 2013.

Cruden, D. M., & Varnes, D. J. (1996). Landslides: investigation and mitigation. Chapter 3-Landslide types and processes. *Transportation research board special report*(247).

Dahal, R. K., Hasegawa, S., Nonomura, A., Yamanaka, M., Dhakal, S., & Paudyal, P. (2008). Predictive modelling of rainfall-induced landslide hazard in the Lesser Himalaya of Nepal based on weights-of-evidence. *Geomorphology, 102*(3-4), 496-510.

Dahal, R. K., Hasegawa, S., Nonomura, A., Yamanaka, M., Masuda, T., & Nishino, K. (2008). GIS-based weights-of-evidence modelling of rainfall-induced landslides in small catchments for landslide susceptibility mapping. *Environ Geol, 54*(2), 311-324.

Dawson, A., Neves, L., Sarkar, R., & Dijkstra, T. (2018). Bhutanese road and bridge resilience to floods and landslides–first suggestions for assessment and response.

Devkota, K. C., Regmi, A. D., Pourghasemi, H. R., Yoshida, K., Pradhan, B., Ryu, I. C., . . . Althuwaynee, O. F. (2013). Landslide susceptibility mapping using certainty factor, index of entropy and logistic regression models in GIS and their comparison at Mugling–Narayanghat road section in Nepal Himalaya. *Natural hazards, 65*(1), 135-165.

EM-DAT, C. (2020). The International Disaster Database. Brussels, Belgium: UCLouvain.

Foumelis, M., Lekkas, E., & Parcharidis, I. (2004). Landslide susceptibility mapping by GIS-based qualitative weighting procedure in Corinth area. *Bulletin of the Geological Society of Greece, 36*(2), 904-912.

Gupta, M., Ghose, M., & Sharma, L. (2009). Application of remote sensing and GIS for landslides hazard and assessment of their probabilistic occurrence—a case study of NH31A between Rangpo and Singtam. *J Geomatics, 3*(1), 13-17.

Guzzetti, F., Carrara, A., Cardinali, M., & Reichenbach, P. (1999). Landslide hazard evaluation: a review of current techniques and their application in a multi-scale study, Central Italy. *Geomorphology, 31*(1-4), 181-216.

He, H., Hu, D., Sun, Q., Zhu, L., & Liu, Y. (2019). A landslide susceptibility assessment method based on GIS technology and an AHP-weighted information content method: A case study of southern Anhui, China. *ISPRS International Journal of Geo-Information, 8*(6), 266.

Highland, L., & Bobrowsky, P. T. (2008). *The landslide handbook: a guide to understanding landslides*: US Geological Survey Reston.

Jaafari, A., Najafi, A., Pourghasemi, H., Rezaeian, J., & Sattarian, A. (2014). GIS-based frequency ratio and index of entropy models for landslide susceptibility assessment in the Caspian forest, northern Iran. *International Journal of Environmental Science and Technology, 11*(4), 909-926.

Karagianni, A., Lazos, I., & Chatzipetros, A. (2018). *Remote sensing techniques in disaster management: Amynteon mine landslides, Greece.* Paper presented at the GeoInformation for Disaster Management Conference.

Kaur, H., Gupta, S., Parkash, S., Thapa, R., Gupta, A., & Khanal, G. C. (2019). Evaluation of landslide susceptibility in a hill city of Sikkim Himalaya with the perspective of hybrid modelling techniques. *Annals of GIS, 25*(2), 113-132.

Kayastha, P., Dhital, M. R., & De Smedt, F. (2012). Landslide susceptibility mapping using the weight of evidence method in the Tinau watershed, Nepal. *Nat hazards, 63*(2), 479-498.

Kayastha, P., Dhital, M. R., & Smedt, F. (2012). Landslide susceptibility mapping using the weight of evidence method in the Tinau watershed, Nepal. *Natural hazards, 63*(2), 479-498.

Kelarestaghi, A., & Ahmadi, H. (2009). Landslide susceptibility analysis with a bivariate approach and GIS in Northern Iran. *Arabian Journal of Geosciences, 2*(1), 95-101.

Keunza, K., Dorji, Y., & Wangda, D. (2004). Landslides in Bhutan. *Country Report, Department of Geology and Mines, Royal Government of Bhutan, Thimpu, 8*.

Khan, H., Shafique, M., Khan, M. A., Bacha, M. A., Shah, S. U., & Calligaris, C. (2019). Landslide susceptibility assessment using Frequency Ratio, a case study of northern Pakistan. *The Egyptian Journal of Remote Sensing and Space Science, 22*(1), 11-24.

Kumar, R., & Anbalagan, R. (2015). Landslide susceptibility zonation in part of Tehri reservoir region using frequency ratio, fuzzy logic and GIS. *Journal of Earth System Science, 124*(2), 431-448.

Landis, J. R., & Koch, G. G. (1977). The measurement of observer agreement for categorical data. *biometrics*, 159-174.

Lee, S., Choi, J., & Woo, I. (2004). The effect of spatial resolution on the accuracy of landslide susceptibility mapping: a case study in Boun, Korea. *Geosciences Journal*, *8*(1), 51.

Li, R., & Wang, N. (2019). Landslide susceptibility mapping for the Muchuan county (China): A comparison between bivariate statistical models (woe, ebf, and ioe) and their ensembles with logistic regression. *Symmetry*, *11*(6), 762.

Liu, J., & Duan, Z. (2018). Quantitative assessment of landslide susceptibility comparing statistical index, index of entropy, and weights of evidence in the Shangnan area, China. *Entropy*, *20*(11), 868.

Long, S., McQuarrie, N., Tobgay, T., Grujic, D., & Hollister, L. (2011). Geologic map of Bhutan. *Journal of Maps*, *7*(1), 184-192.

Mahalingam, R., & Olsen, M. J. (2016). Evaluation of the influence of source and spatial resolution of DEMs on derivative products used in landslide mapping. *Geomatics, Natural Hazards and Risk*, *7*(6), 1835-1855.

Mandal, S., & Mandal, K. (2018). Bivariate statistical index for landslide susceptibility mapping in the Rorachu river basin of eastern Sikkim Himalaya, India. *Spatial Information Research*, *26*(1), 59-75.

Metternicht, G., Hurni, L., & Gogu, R. (2005). Remote sensing of landslides: An analysis of the potential contribution to geo-spatial systems for hazard

assessment in mountainous environments. *Remote sensing of Environment, 98*(2-3), 284-303.

Mind'je, R., Li, L., Amanambu, A. C., Nahayo, L., Nsengiyumva, J. B., Gasirabo, A., & Mindje, M. (2019). Flood susceptibility modeling and hazard perception in Rwanda. *International Journal of Disaster Risk Reduction, 38*, 101211.

Moazzam, M. F. U., Vansarochana, A., Boonyanuphap, J., & Choosumrong, S. (2018). LANDSLIDE ASSESSMENT USING GIS-BASED FREQUENCY RATIO METHOD: A CASE STUDY OF MAE-PHUN SUB-DISTRICT, LAPLAE DISTRICT, UTTARADIT PROVINCE, THAILAND.

Mondal, S., & Mandal, S. (2019). Landslide susceptibility mapping of Darjeeling Himalaya, India using index of entropy (IOE) model. *Applied Geomatics, 11*(2), 129-146.

Moore, I. D., Grayson, R., & Ladson, A. (1991). Digital terrain modelling: a review of hydrological, geomorphological, and biological applications. *Hydrological processes, 5*(1), 3-30.

Mora, O., Lenzano, M., Toth, C., & Grejner, D. (2014). ANALYZING THE EFFECTS OF SPATIAL RESOLUTION FOR SMALL LANDSLIDE SUSCEPTIBILITY AND HAZARD MAPPING. *International Archives of the Photogrammetry, Remote Sensing & Spatial Information Sciences*.

Neuhäuser, B., Damm, B., & Terhorst, B. (2012). GIS-based assessment of landslide susceptibility on the base of the weights-of-evidence model. *Landslides, 9*(4), 511-528.

Nguyen, V. V., Pham, B. T., Vu, B. T., Prakash, I., Jha, S., Shahabi, H., . . . Chatterjee, J. M. (2019). Hybrid machine learning approaches for landslide susceptibility modeling. *Forests, 10*(2), 157.

Nohani, E., Moharrami, M., Sharafi, S., Khosravi, K., Pradhan, B., Pham, B. T., . . . M Melesse, A. (2019). Landslide susceptibility mapping using different GIS-based bivariate models. *Water, 11*(7), 1402.

Osaragi, T. (2002). Classification methods for spatial data representation. University College London, London: Center for Advanced Spatial Analysis.

Pardeshi, S. D., Autade, S. E., & Pardeshi, S. S. (2013). Landslide hazard assessment: recent trends and techniques. *SpringerPlus, 2*(1), 523.

Pasang, S., & Kubíček, P. (2018). Information Value Model based Landslide Susceptibility Mapping at Phuentsholing, Bhutan.

Pourghasemi, H. R., Mohammady, M., & Pradhan, B. (2012). Landslide susceptibility mapping using index of entropy and conditional probability models in GIS: Safarood Basin, Iran. *Catena, 97*, 71-84.

Pradhan, B., Oh, H.-J., & Buchroithner, M. (2010). Weights-of-evidence model applied to landslide susceptibility mapping in a tropical hilly area. *Geomatics, Natural Hazards and Risk, 1*(3), 199-223.

Regmi, A. D., Devkota, K. C., Yoshida, K., Pradhan, B., Pourghasemi, H. R., Kumamoto, T., & Akgun, A. (2014). Application of frequency ratio, statistical index, and weights-of-evidence models and their comparison in landslide susceptibility mapping in Central Nepal Himalaya. *Arabian Journal of Geosciences, 7*(2), 725-742.

Rodriguez, E., Morris, C. S., & Belz, J. E. (2006). A global assessment of the SRTM performance. *Photogrammetric Engineering & Remote Sensing, 72*(3), 249-260.

Roy, J., Saha, S., Arabameri, A., Blaschke, T., & Bui, D. T. (2019). A Novel Ensemble Approach for Landslide Susceptibility Mapping (LSM) in Darjeeling and Kalimpong Districts, West Bengal, India. *Remote Sens, 11*(23), 2866.

Saadatkhah, N., Kassim, A., & Lee, L. M. (2014). Qualitative and quantitative landslide susceptibility assessments in Hulu Kelang area, Malaysia. *EJGE, 19*(47), 545-563.

Samanta, S., Pal, D. K., & Palsamanta, B. (2018). Flood susceptibility analysis through remote sensing, GIS and frequency ratio model. *Applied Water Science, 8*(2), 66.

Santillan, J., & Makinano-Santillan, M. (2016). VERTICAL ACCURACY ASSESSMENT OF 30-M RESOLUTION ALOS, ASTER, AND SRTM GLOBAL DEMS OVER NORTHEASTERN MINDANAO, PHILIPPINES. *International Archives of the Photogrammetry, Remote Sensing & Spatial Information Sciences, 41*.

Sarkar, R., & Dorji, K. (2019). Determination of the Probabilities of Landslide Events—A Case Study of Bhutan. *Hydrology, 6*(2), 52.

Sarkar, R., Kurar, R., Zangmo, S., Dema, U., Subba, S., & Sharma, D. (2017). Application of soil nailing for landslide mitigation in Bhutan: a case study at Sorchen Bypass. *Electron J Geotech Eng, 22*(13), 4963-4980.

Shafapour Tehrany, M., Kumar, L., Neamah Jebur, M., & Shabani, F. (2019). Evaluating the application of the statistical index method in flood susceptibility mapping and its comparison with frequency ratio and logistic regression methods. *Geomatics, Natural Hazards and Risk, 10*(1), 79-101.

Shahabi, H., Ahmad, B., & Khezri, S. (2013). Evaluation and comparison of bivariate and multivariate statistical methods for landslide susceptibility mapping (case study: Zab basin). *Arabian Journal of Geosciences, 6*(10), 3885-3907.

Shirani, K., Pasandi, M., & Arabameri, A. (2018). Landslide susceptibility assessment by dempster–shafer and index of entropy models, Sarkhoun basin, southwestern Iran. *Natural hazards, 93*(3), 1379-1418.

Shirzadi, A., Bui, D. T., Pham, B. T., Solaimani, K., Chapi, K., Kavian, A., . . . Revhaug, I. (2017). Shallow landslide susceptibility assessment using a novel hybrid intelligence approach. *Environ Earth Sci, 76*(2), 60.

Sun, X., Chen, J., Bao, Y., Han, X., Zhan, J., & Peng, W. (2018). Landslide susceptibility mapping using logistic regression analysis along the jinsha river and its tributaries close to Derong and Deqin County, Southwestern China. *ISPRS International Journal of Geo-Information, 7*(11), 438.

Thongley, & Vansarochana, C. (2020). Weight of Evidence Approach for Landslide Susceptibility Mapping: A Case Study at Ossay Watershed Area in Bhutan. *Disaster Advances, 13*(9), 1-9.

Thongley, T., & Vansarochana, C. (2020). Spatial Zonation of Landslide Prone Area Using Information Value in the Geologically Fragile Region of Samdrup Jongkhar-Tashigang National Highway in Bhutan. *Environment and Natural Resources Journal*, xx-xx.

Thongley, T., & Vansarochana, C. (2021a). Landslide Identification and Zonation Using the Index of Entropy Technique at Ossey Watershed Area in Bhutan. *Applied Environmental Research, 43*(1), 102-115.

Thongley, T., & Vansarochana, C. (2021b). Landslide susceptibility assessment using frequency ratio model at Ossey watershed area in Bhutan. *Engineering and Applied Science Research, 48*(1), 56-64.

Tien Bui, D., Shahabi, H., Shirzadi, A., Chapi, K., Alizadeh, M., Chen, W., . . . Hong, H. (2018). Landslide detection and susceptibility mapping by airsar data using support vector machine and index of entropy models in cameron highlands, malaysia. *Remote Sensing, 10*(10), 1527.

Tofani, V., Segoni, S., Agostini, A., Catani, F., & Casagli, N. (2013). Use of remote sensing for landslide studies in Europe. *Natural Hazards & Earth System Sciences, 13*(2).

Van Westen, C. (2002). Use of weights of evidence modeling for landslide susceptibility mapping. *International Institute for Geoinformation Science and Earth Observation: Enschede, The Netherlands*, 21.

Van Westen, C., Van Asch, T. W., & Soeters, R. (2006). Landslide hazard and risk zonation—why is it still so difficult? *Bulletin of Engineering Geology and the Environment, 65*(2), 167-184.

Varnes, D., & Eckel, E. (1958). Landslide types and processes: Landslides and Engineering Practice by the Committee on Landslide Investigations: Highway Research Board Special Report.

Varnes, D. J. (1958). Landslide types and processes. *Landslides and engineering practice, 24*, 20-47.

Varnes, D. J. (1978). Slope movement types and processes. *Special report, 176*, 11-33.

Varnes, D. J. (1984). *Landslide hazard zonation: a review of principles and practice*.

Wang, L., Sawada, K., & Moriguchi, S. (2011). Landslide susceptibility mapping by using logistic regression model with neighborhood analysis: A case study in Mizunami City. *Int. J. GEOMATE, 1*, 99-104.

Wang, Q., Li, W., Chen, W., & Bai, H. (2015). GIS-based assessment of landslide susceptibility using certainty factor and index of entropy models for the

Qianyang County of Baoji city, China. *Journal of Earth System Science, 124*(7), 1399-1415.

Yang, L., Meng, X., & Zhang, X. (2011). SRTM DEM and its application advances. *International Journal of Remote Sensing, 32*(14), 3875-3896.

Youssef, A. M., Al-Kathery, M., & Pradhan, B. (2015). Landslide susceptibility mapping at Al-Hasher area, Jizan (Saudi Arabia) using GIS-based frequency ratio and index of entropy models. *Geosciences Journal, 19*(1), 113-134.

Zhang, T., Han, L., Han, J., Li, X., Zhang, H., & Wang, H. (2019). Assessment of Landslide Susceptibility Using Integrated Ensemble Fractal Dimension with Kernel Logistic Regression Model. *Entropy, 21*(2), 218.

Zhao, Y., Wang, R., Jiang, Y., Liu, H., & Wei, Z. (2019). GIS-based logistic regression for rainfall-induced landslide susceptibility mapping under different grid sizes in Yueqing, Southeastern China. *Engineering Geology, 259*, 105147.

Zhu, L., & Huang, J.-f. (2006). GIS-based logistic regression method for landslide susceptibility mapping in regional scale. *Journal of Zhejiang University-Science A, 7*(12), 2007-2017.

# APPENDIX

## Appendix A: Detail of landslide types at Ossey Watershed Area

The explanation of the types of landslides are were explained in Table 2 and Figure 1. The following are the landslide types in various locations which was noted during the landslide inventory.

| Landslide Id | Location | | | Types of Landslide | Remark |
|---|---|---|---|---|---|
| | Latitude | Longitude | Elevation | | |
| 1 | 90.48 | 27.02 | 911 | Debris flow | |
| 2 | 90.53 | 27.01 | 851 | Earth flow | |
| 3 | 90.52 | 27.02 | 1003 | Earth flow | |
| 4 | 90.48 | 27.03 | 1123 | Debris flow | |
| 5 | 90.63 | 27.03 | 1709 | Debris flow | |
| 6 | 90.57 | 27.03 | 1015 | Earth flow | |
| 7 | 90.54 | 26.97 | 1035 | Debris flow | |
| 8 | 90.46 | 26.98 | 955 | Earth flow | |
| 9 | 90.51 | 27.00 | 1029 | Debris flow | |
| 10 | 90.50 | 27.00 | 718 | Earth flow | |
| 11 | 90.52 | 26.99 | 851 | Debris flow | |
| 12 | 90.39 | 27.01 | 1877 | Earth flow | |
| 13 | 90.41 | 27.01 | 1000 | Earth flow | |
| 14 | 90.42 | 27.01 | 923 | Earth flow | |
| 15 | 90.52 | 27.01 | 998 | Debris flow | |
| 16 | 90.50 | 26.95 | 762 | Earth flow | |
| 17 | 90.57 | 26.95 | 874 | Earth flow | |
| 18 | 90.56 | 26.94 | 698 | Earth flow | |
| 19 | 90.57 | 26.94 | 851 | Earth flow | |
| 20 | 90.57 | 26.93 | 773 | Earth flow | |
| 21 | 90.55 | 26.94 | 551 | Earth flow | |
| 22 | 90.56 | 26.95 | 789 | Earth flow | |
| 23 | 90.55 | 26.94 | 574 | Earth flow | |
| 24 | 90.49 | 26.95 | 996 | Debris flow | |
| 25 | 90.54 | 26.95 | 480 | Earth flow | |
| 26 | 90.54 | 26.96 | 527 | Debris flow | |
| 27 | 90.54 | 26.95 | 589 | Earth flow | |
| 28 | 90.55 | 26.96 | 709 | Earth flow | |
| 29 | 90.55 | 26.96 | 688 | Translational Slide | |
| 30 | 90.55 | 26.96 | 786 | Earth flow | |
| 31 | 90.49 | 26.97 | 551 | Earth flow | |
| 32 | 90.47 | 26.97 | 730 | Debris flow | |
| 33 | 90.48 | 26.92 | 551 | Earth flow | |
| 34 | 90.48 | 26.92 | 399 | Earth flow | |
| 35 | 90.49 | 26.92 | 348 | Debris flow | |
| 36 | 90.56 | 26.94 | 578 | Earth flow | |

| | | | | | |
|---|---|---|---|---|---|
| 37 | 90.53 | 27.06 | 1851 | Earth flow | |
| 38 | 90.57 | 27.05 | 1254 | Translational Slide | |
| 39 | 90.45 | 27.05 | 1257 | Earth flow | |
| 40 | 90.48 | 26.93 | 671 | Earth flow | |
| 41 | 90.47 | 26.93 | 936 | Rock fall | |
| 42 | 90.48 | 26.95 | 860 | Debris Avalanche | |
| 43 | 90.45 | 26.98 | 1045 | Earth flow | |
| 44 | 90.46 | 26.98 | 836 | Earth flow | |
| 45 | 90.46 | 26.98 | 659 | Earth flow | |
| 46 | 90.52 | 26.98 | 477 | Debris flow | |
| 47 | 90.53 | 26.96 | 598 | Earth flow | |
| 48 | 90.53 | 26.95 | 667 | Earth flow | |
| 49 | 90.55 | 26.97 | 1287 | Earth flow | |
| 50 | 90.53 | 26.95 | 720 | Debris flow | |
| 51 | 90.48 | 26.97 | 522 | Earth flow | |
| 52 | 90.48 | 27.03 | 1032 | Earth flow | |
| 53 | 90.64 | 27.08 | 2092 | Earth flow | |
| 54 | 90.64 | 27.07 | 1982 | Earth flow | |
| 55 | 90.68 | 27.03 | 2222 | Debris flow | |
| 56 | 90.68 | 27.00 | 2134 | Earth flow | |
| 57 | 90.63 | 27.01 | 1452 | Debris flow | |
| 58 | 90.61 | 27.00 | 1402 | Earth flow | |
| 59 | 90.58 | 27.06 | 1730 | Earth flow | |
| 60 | 90.56 | 27.07 | 1611 | Earth flow | |
| 61 | 90.28 | 27.07 | 2078 | Earth flow | |
| 62 | 90.30 | 27.08 | 1850 | Earth flow | |
| 63 | 90.31 | 27.09 | 1643 | Debris flow | |
| 64 | 90.33 | 27.11 | 1671 | Earth flow | |
| 65 | 90.33 | 27.14 | 2899 | Earth flow | |
| 66 | 90.34 | 27.18 | 3339 | Earth flow | |
| 67 | 90.36 | 27.21 | 3327 | Debris flow | |
| 68 | 90.38 | 27.20 | 2738 | Debris Avalanche | |
| 69 | 90.39 | 27.19 | 2314 | Earth flow | |
| 70 | 90.41 | 27.18 | 1934 | Earth flow | |
| 71 | 90.43 | 27.17 | 2280 | Earth flow | |
| 72 | 90.44 | 27.15 | 2429 | Earth flow | |
| 73 | 90.45 | 27.09 | 1464 | Debris flow | |
| 74 | 90.50 | 27.14 | 2431 | Earth flow | |
| 75 | 90.50 | 27.13 | 2113 | Earth flow | |
| 76 | 90.53 | 27.09 | 1929 | Earth flow | |
| 77 | 90.64 | 27.00 | 2045 | Earth flow | |
| 78 | 90.37 | 27.14 | 2169 | Earth flow | |
| 79 | 90.33 | 27.20 | 3685 | Earth flow | |
| 80 | 90.65 | 27.01 | 1820 | Debris flow | |
| 81 | 90.66 | 27.06 | 1989 | Earth flow | |

| | | | | | |
|---|---|---|---|---|---|
| 82 | 90.55 | 27.08 | 1821 | Earth flow | |
| 83 | 90.40 | 27.01 | 1554 | Earth flow | |
| 84 | 90.46 | 26.96 | 801 | Earth flow | |
| 85 | 90.45 | 26.96 | 1182 | Earth flow | |
| 86 | 90.51 | 26.94 | 252 | Earth flow | |
| 87 | 90.51 | 26.94 | 409 | Earth flow | |
| 88 | 90.51 | 26.95 | 406 | Earth flow | |
| 89 | 90.53 | 26.97 | 531 | Creep | |
| 90 | 90.54 | 26.97 | 768 | Earth flow | |
| 91 | 90.55 | 26.95 | 997 | Earth flow | |
| 92 | 90.54 | 26.93 | 432 | Earth flow | |
| 93 | 90.51 | 27.00 | 889 | Earth flow | |
| 94 | 90.50 | 27.01 | 683 | Debris flow | |
| 95 | 90.48 | 27.03 | 1365 | Earth flow | |
| 96 | 90.45 | 27.04 | 1148 | Earth flow | |
| 97 | 90.45 | 27.04 | 1058 | Earth flow | |
| 98 | 90.44 | 27.04 | 1149 | Earth flow | |
| 99 | 90.59 | 26.98 | 1602 | Debris Avalanche | |
| 100 | 90.59 | 26.98 | 1636 | Earth flow | |
| 101 | 90.45 | 26.98 | 903 | Earth flow | |
| 102 | 90.36 | 27.01 | 1729 | Earth flow | |
| 103 | 90.37 | 27.03 | 1549 | Debris Avalanche | |
| 104 | 90.37 | 27.03 | 1421 | Earth flow | |
| 105 | 90.46 | 27.01 | 1003 | Earth flow | |
| 106 | 90.64 | 27.04 | 1745 | Earth flow | |
| 107 | 90.54 | 27.06 | 1559 | Earth flow | |
| 108 | 90.62 | 27.02 | 1885 | Debris flow | |
| 109 | 90.56 | 26.95 | 635 | Debris flow | |
| 110 | 90.45 | 27.02 | 1153 | Earth flow | |
| 111 | 90.52 | 26.93 | 366 | Earth flow | |
| 112 | 90.56 | 26.94 | 798 | Debris flow | |
| 113 | 90.44 | 27.02 | 858 | Earth flow | |
| 114 | 90.37 | 27.01 | 1731 | Earth flow | |
| 115 | 90.52 | 26.94 | 540 | Debris flow | |
| 116 | 90.40 | 27.19 | 2269 | Earth flow | |
| 117 | 90.35 | 27.17 | 3199 | Earth flow | |
| 118 | 90.40 | 27.03 | 1069 | Debris flow | |
| 119 | 90.57 | 27.05 | 1120 | Debris flow | |
| 120 | 90.53 | 27.06 | 1578 | Earth flow | |
| 121 | 90.52 | 27.02 | 967 | Debris flow | |
| 122 | 90.52 | 27.01 | 910 | Earth flow | |
| 123 | 90.51 | 27.00 | 911 | Earth flow | |
| 124 | 90.55 | 27.00 | 1194 | Debris flow | |
| 125 | 90.56 | 26.98 | 1398 | Earth flow | |
| 126 | 90.53 | 26.98 | 489 | Earth flow | |

| | | | | | |
|---|---|---|---|---|---|
| 127 | 90.51 | 26.98 | 746 | Debris flow | |
| 128 | 90.40 | 27.01 | 1315 | Debris flow | |
| 129 | 90.41 | 27.01 | 894 | Earth flow | |
| 130 | 90.44 | 26.97 | 1251 | Earth flow | |
| 131 | 90.46 | 26.98 | 739 | Earth flow | |
| 132 | 90.55 | 26.98 | 1154 | Earth flow | |
| 133 | 90.54 | 26.96 | 643 | Debris flow | |
| 134 | 90.54 | 26.95 | 494 | Earth flow | |
| 135 | 90.53 | 26.96 | 511 | Earth flow | |
| 136 | 90.51 | 26.95 | 406 | Earth flow | |
| 137 | 90.50 | 26.95 | 611 | Earth flow | |
| 138 | 90.51 | 26.94 | 357 | Debris flow | |
| 139 | 90.53 | 26.93 | 490 | Earth flow | |
| 140 | 90.56 | 26.93 | 710 | Earth flow | |
| 141 | 90.55 | 26.94 | 683 | Earth flow | |
| 142 | 90.48 | 26.93 | 818 | Debris flow | |
| 143 | 90.48 | 26.92 | 597 | Earth flow | |
| 144 | 90.48 | 26.92 | 506 | Earth flow | |
| 145 | 90.49 | 26.92 | 412 | Debris Avalanche | |
| 146 | 90.54 | 26.93 | 421 | Earth flow | |
| 147 | 90.56 | 26.95 | 931 | Earth flow | |
| 148 | 90.56 | 26.93 | 636 | Earth flow | |
| 149 | 90.49 | 26.95 | 788 | Debris flow | |
| 150 | 90.50 | 26.97 | 521 | Debris flow | |
| 151 | 90.49 | 26.97 | 778 | Debris flow | |
| 152 | 90.48 | 26.95 | 851 | Earth flow | |
| 153 | 90.46 | 26.96 | 1128 | Earth flow | |
| 154 | 90.47 | 26.94 | 1151 | Earth flow | |
| 155 | 90.57 | 26.94 | 1069 | Debris Avalanche | |
| 156 | 90.45 | 27.04 | 940 | Earth flow | |
| 157 | 90.44 | 27.02 | 845 | Earth flow | |
| 158 | 90.48 | 27.03 | 1201 | Earth flow | |
| 159 | 90.45 | 27.04 | 1132 | Earth flow | |
| 160 | 90.36 | 27.01 | 1784 | Debris flow | |
| 161 | 90.47 | 27.01 | 1003 | Debris flow | |
| 162 | 90.59 | 26.98 | 1629 | Earth flow | |
| 163 | 90.51 | 27.02 | 1112 | Earth flow | |
| 664 | 90.63 | 26.93 | 1523 | Earth flow | |

## Appendix B: Detail of Frequency Ratio calculation using three different spatial resolution

The following Table shows the detail calculation of individual spatial resolution (12.5m, 30m and 90m) using the Frequency Ratio.

| Spatial Resolution | Class | No of pixel in class | % of landslide pixel in class | No of landslide in class | % of landslide in class | Frequency Ratio |
|---|---|---|---|---|---|---|
| Elevation(m) | | | | | | |
| 12.5m | < 854.00 | 711123 | 13.54 | 44 | 38.26 | 2.83 |
| | 854.00 - 1455 | 1278941 | 24.35 | 32 | 27.83 | 1.14 |
| | 1455.01 - 1949 | 1697050 | 32.31 | 21 | 18.26 | 0.57 |
| | 1949.01 - 2619 | 1285804 | 24.48 | 13 | 11.3 | 0.46 |
| | 2619 < | 279682 | 5.32 | 5 | 4.35 | 0.82 |
| 30m | < 854.00 | 113694 | 12.47 | 37 | 32.17 | 2.58 |
| | 854.00 - 1455 | 209113 | 22.93 | 37 | 32.17 | 1.4 |
| | 1455.01 - 1949 | 292274 | 32.05 | 21 | 18.26 | 0.57 |
| | 1949.01 - 2619 | 243245 | 26.67 | 15 | 13.04 | 0.49 |
| | 2619 < | 53621 | 5.88 | 5 | 4.35 | 0.74 |
| 90m | < 854.00 | 12614 | 12.47 | 38 | 33.04 | 2.65 |
| | 854.00 - 1455 | 23263 | 22.99 | 36 | 31.3 | 1.36 |
| | 1455.01 - 1949 | 32472 | 32.09 | 22 | 19.13 | 0.6 |
| | 1949.01 - 2619 | 26898 | 26.58 | 14 | 12.17 | 0.46 |
| | 2619 < | 5936 | 5.87 | 5 | 4.35 | 0.74 |
| Slope (Degree) | | | | | | |
| 12.5m | 0 - 13.00 | 503807 | 9.59 | 9 | 7.83 | 0.82 |
| | 13.01 - 23.00 | 1027159 | 19.56 | 13 | 11.3 | 0.58 |
| | 23.01 - 32.00 | 1575077 | 29.99 | 33 | 28.7 | 0.96 |
| | 32.01 - 42.00 | 1537245 | 29.27 | 34 | 29.57 | 1.01 |
| | 42 < | 609312 | 11.6 | 26 | 22.61 | 1.95 |
| 30m | 0 - 13.00 | 93299 | 10.23 | 6 | 5.22 | 0.51 |
| | 13.01 - 23.00 | 195676 | 21.46 | 20 | 17.39 | 0.81 |
| | 23.01 - 32.00 | 275372 | 30.2 | 28 | 24.35 | 0.81 |
| | 32.01 - 42.00 | 255827 | 28.05 | 31 | 26.96 | 0.96 |
| | 42 < | 91773 | 10.06 | 30 | 26.09 | 2.59 |
| 90m | 0 - 13.00 | 11472 | 11.34 | 11 | 9.57 | 0.84 |
| | 13.01 - 23.00 | 27384 | 27.06 | 29 | 25.22 | 0.93 |
| | 23.01 - 32.00 | 35491 | 35.08 | 33 | 28.7 | 0.82 |
| | 32.01 - 42.00 | 23855 | 23.58 | 31 | 26.96 | 1.14 |
| | 42 < | 2981 | 2.95 | 11 | 9.57 | 3.25 |
| Aspect | | | | | | |
| 12.5m | Flat | 47614 | 0.91 | 0 | 0 | 0 |
| | North | 636941 | 12.13 | 5 | 4.35 | 0.36 |
| | NorthEast | 589967 | 11.23 | 9 | 7.83 | 0.7 |
| | East | 599110 | 11.41 | 15 | 13.04 | 1.14 |
| | SouthEast | 758507 | 14.44 | 33 | 28.7 | 1.99 |
| | South | 681513 | 12.97 | 19 | 16.52 | 1.27 |
| | SouthWest | 749811 | 14.28 | 15 | 13.04 | 0.91 |
| | West | 604243 | 11.5 | 8 | 6.96 | 0.6 |
| | NorthWest | 584894 | 11.14 | 11 | 9.57 | 0.86 |
| 30m | Flat | 285 | 0.03 | 0 | 0 | 0 |
| | North | 118174 | 12.96 | 6 | 5.22 | 0.4 |
| | NorthEast | 97997 | 10.75 | 9 | 7.83 | 0.73 |
| | East | 110602 | 12.13 | 14 | 12.17 | 1 |
| | SouthEast | 129200 | 14.17 | 33 | 28.7 | 2.03 |
| | South | 120454 | 13.21 | 18 | 15.65 | 1.19 |
| | SouthWest | 126820 | 13.91 | 18 | 15.65 | 1.13 |
| | West | 111498 | 12.23 | 7 | 6.09 | 0.5 |
| | NorthWest | 96917 | 10.63 | 10 | 8.7 | 0.82 |
| 90m | Flat | 6 | 0.01 | 0 | 0 | 0 |
| | North | 11739 | 11.6 | 6 | 5.22 | 0.45 |
| | NorthEast | 10792 | 10.67 | 5 | 4.35 | 0.41 |

| | | | | | | |
|---|---|---|---|---|---|---|
| | East | 13004 | 12.85 | 16 | 13.91 | 1.08 |
| | SouthEast | 14659 | 14.49 | 29 | 25.22 | 1.74 |
| | South | 13247 | 13.09 | 24 | 20.87 | 1.59 |
| | SouthWest | 14400 | 14.23 | 13 | 11.3 | 0.79 |
| | West | 12655 | 12.51 | 10 | 8.7 | 0.7 |
| | NorthWest | 10681 | 10.56 | 12 | 10.43 | 0.99 |
| Curvature | | | | | | |
| 12.5m | Concave | 2214763 | 42.17 | 47 | 40.87 | 0.97 |
| | Flat | 802326 | 15.27 | 17 | 14.78 | 0.97 |
| | Convex | 2235511 | 42.56 | 51 | 44.35 | 1.04 |
| 30m | Concave | 434525 | 47.65 | 70 | 60.87 | 1.28 |
| | Flat | 36424 | 3.99 | 3 | 2.61 | 0.65 |
| | Convex | 440998 | 48.36 | 42 | 36.52 | 0.76 |
| 90m | Concave | 50045 | 49.46 | 73 | 63.48 | 1.28 |
| | Flat | 1309 | 1.29 | 0 | 0 | 0 |
| | Convex | 49829 | 49.25 | 42 | 36.52 | 0.74 |
| Topographic wetness index | | | | | | |
| 12.5m | < 0.999 | 529278 | 10.08 | 12 | 10.43 | 1.04 |
| | 0.999 - 3.219 | 1520949 | 28.96 | 35 | 30.43 | 1.05 |
| | 3.220 - 6.688 | 486118 | 9.25 | 7 | 6.09 | 0.66 |
| | 6.688 < | 2716255 | 51.71 | 61 | 53.04 | 1.03 |
| 30m | < 0.999 | 200164 | 21.95 | 27 | 23.48 | 1.07 |
| | 0.999 - 3.219 | 217946 | 23.9 | 31 | 26.96 | 1.13 |
| | 3.220 - 6.688 | 37006 | 4.06 | 5 | 4.35 | 1.07 |
| | 6.688 < | 456831 | 50.09 | 52 | 45.22 | 0.9 |
| 90m | < 0.999 | 38278 | 37.83 | 46 | 40 | 1.06 |
| | 0.999 - 3.219 | 11135 | 11 | 11 | 9.57 | 0.87 |
| | 3.220 - 6.688 | 1358 | 1.34 | 1 | 0.87 | 0.65 |
| | 6.688 < | 50412 | 49.82 | 57 | 49.57 | 0.99 |
| Stream Power Index | | | | | | |
| 12.5m | < -4.052 | 850701 | 16.2 | 16 | 13.91 | 0.86 |
| | -4.052 - 0.886 | 1638515 | 31.19 | 31 | 26.96 | 0.86 |
| | 0.887 - 3.529 | 2336225 | 44.48 | 59 | 51.3 | 1.15 |
| | 3.529 < | 427159 | 8.13 | 9 | 7.83 | 0.96 |
| 30m | < -4.052 | 233485 | 25.6 | 18 | 15.65 | 0.61 |
| | -4.052 - 0.886 | 344021 | 37.72 | 44 | 38.26 | 1.01 |
| | 0.887 - 3.529 | 274078 | 30.05 | 39 | 33.91 | 1.13 |
| | 3.529 < | 60363 | 6.62 | 14 | 12.17 | 1.84 |
| 90m | < -4.052 | 32999 | 32.61 | 28 | 24.35 | 0.75 |
| | -4.052 - 0.886 | 42295 | 41.8 | 45 | 39.13 | 0.94 |
| | 0.887 - 3.529 | 20832 | 20.59 | 37 | 32.17 | 1.56 |
| | 3.529 < | 5057 | 5 | 5 | 4.35 | 0.87 |
| Drainage Density | | | | | | |
| 12.5m | < 0.545 | 964147 | 18.36 | 6 | 5.22 | 0.28 |
| | 0.545 - 0.854 | 1329522 | 25.31 | 37 | 32.17 | 1.27 |
| | 0.855 - 1.153 | 1269392 | 24.17 | 44 | 38.26 | 1.58 |
| | 1.154 - 1.462 | 1111965 | 21.17 | 21 | 18.26 | 0.86 |
| | 1.462 < | 577574 | 11 | 7 | 6.09 | 0.55 |
| 30m | < 0.545 | 167456 | 18.36 | 6 | 5.22 | 0.28 |
| | 0.545 - 0.854 | 230872 | 25.32 | 37 | 32.17 | 1.27 |
| | 0.855 - 1.153 | 220395 | 24.17 | 44 | 38.26 | 1.58 |
| | 1.154 - 1.462 | 192998 | 21.16 | 21 | 18.26 | 0.86 |
| | 1.462 < | 100226 | 10.99 | 7 | 6.09 | 0.55 |
| 90m | < 0.545 | 18485 | 18.27 | 7 | 6.09 | 0.33 |
| | 0.545 - 0.854 | 25650 | 25.35 | 36 | 31.3 | 1.23 |
| | 0.855 - 1.153 | 24516 | 24.23 | 43 | 37.39 | 1.54 |
| | 1.154 - 1.462 | 21420 | 21.17 | 22 | 19.13 | 0.9 |
| | 1.462 < | 11112 | 10.98 | 7 | 6.09 | 0.55 |
| Normalized Difference Vegetation Index | | | | | | |
| 12.5m | < 0.223 | 219873 | 4.19 | 32 | 27.83 | 6.65 |
| | 0.223 - 0.407 | 574346 | 10.93 | 19 | 16.52 | 1.51 |
| | 0.408 - 0.562 | 877493 | 16.71 | 20 | 17.39 | 1.04 |
| | 0.563 - 0.688 | 1492466 | 28.41 | 25 | 21.74 | 0.77 |
| | 0.688 < | 2088422 | 39.76 | 19 | 16.52 | 0.42 |

| | | | | | | |
|---|---|---|---|---|---|---|
| 30m | < 0.223 | 38264 | 4.2 | 22 | 19.13 | 4.56 |
| | 0.223 - 0.407 | 99842 | 10.95 | 28 | 24.35 | 2.22 |
| | 0.408 - 0.562 | 152092 | 16.68 | 17 | 14.78 | 0.89 |
| | 0.563 - 0.688 | 259052 | 28.41 | 26 | 22.61 | 0.8 |
| | 0.688 < | 362697 | 39.77 | 22 | 19.13 | 0.48 |
| 90m | < 0.223 | 4269 | 4.22 | 17 | 14.78 | 3.5 |
| | 0.223 - 0.407 | 11050 | 10.92 | 21 | 18.26 | 1.67 |
| | 0.408 - 0.562 | 16732 | 16.54 | 18 | 15.65 | 0.95 |
| | 0.563 - 0.688 | 29073 | 28.73 | 26 | 22.61 | 0.79 |
| | 0.688 < | 40059 | 39.59 | 33 | 28.7 | 0.72 |
| Normalized Difference Soil Index | | | | | | |
| 12.5m | < -0.516 | 484543 | 9.22 | 8 | 6.96 | 0.75 |
| | -0.516 - -0.273 | 946456 | 18.02 | 10 | 8.7 | 0.48 |
| | -0.274 - -0.097 | 1471428 | 28.01 | 16 | 13.91 | 0.5 |
| | -0.098 - 0.078 | 1655777 | 31.52 | 43 | 37.39 | 1.19 |
| | 0.078 < | 694396 | 13.22 | 38 | 33.04 | 2.5 |
| 30m | < -0.516 | 84053 | 9.22 | 8 | 6.96 | 0.755 |
| | -0.516 - -0.273 | 164589 | 18.05 | 12 | 10.43 | 0.578 |
| | -0.274 - -0.097 | 255238 | 27.99 | 13 | 11.3 | 0.404 |
| | -0.098 - 0.078 | 287262 | 31.5 | 43 | 37.39 | 1.187 |
| | 0.078 < | 120805 | 13.25 | 39 | 33.91 | 2.56 |
| 90m | < -0.516 | 9379 | 9.27 | 9 | 7.83 | 0.84 |
| | -0.516 - -0.273 | 18265 | 18.05 | 10 | 8.7 | 0.48 |
| | -0.274 - -0.097 | 28423 | 28.09 | 22 | 19.13 | 0.68 |
| | -0.098 - 0.078 | 31704 | 31.33 | 38 | 33.04 | 1.05 |
| | 0.078 < | 13412 | 13.26 | 36 | 31.3 | 2.36 |
| Distance from the river (m) | | | | | | |
| 12.5m | 0-100 | 176948 | 3.37 | 6 | 5.22 | 1.55 |
| | 100-200 | 162601 | 3.1 | 2 | 1.74 | 0.56 |
| | 200-300 | 158292 | 3.01 | 4 | 3.48 | 1.15 |
| | 300-400 | 157852 | 3.01 | 4 | 3.48 | 1.16 |
| | 400< | 4596907 | 87.52 | 99 | 86.09 | 0.98 |
| 30m | 0-100 | 31639 | 3.47 | 7 | 6.09 | 1.75 |
| | 100-200 | 27341 | 3 | 1 | 0.87 | 0.29 |
| | 200-300 | 29785 | 3.27 | 4 | 3.48 | 1.06 |
| | 300-400 | 25379 | 2.78 | 4 | 3.48 | 1.25 |
| | 400< | 797803 | 87.48 | 99 | 86.09 | 0.98 |
| 90m | 0-100 | 4349 | 4.3 | 8 | 6.96 | 1.62 |
| | 100-200 | 2476 | 2.45 | 1 | 0.87 | 0.36 |
| | 200-300 | 3448 | 3.41 | 4 | 3.48 | 1.02 |
| | 300-400 | 2799 | 2.77 | 4 | 3.48 | 1.26 |
| | 400< | 88111 | 87.08 | 98 | 85.22 | 0.98 |
| Distance from the Fault(m) | | | | | | |
| 12.5m | 0-100 | 219126 | 4.17 | 1 | 0.87 | 0.21 |
| | 100-200 | 206180 | 3.93 | 5 | 4.35 | 1.11 |
| | 200-300 | 198818 | 3.79 | 6 | 5.22 | 1.38 |
| | 300-400 | 180361 | 3.43 | 5 | 4.35 | 1.27 |
| | 400< | 4448115 | 84.68 | 98 | 85.22 | 1.01 |
| 30m | 0-100 | 39885 | 4.37 | 1 | 0.87 | 0.2 |
| | 100-200 | 33632 | 3.69 | 5 | 4.35 | 1.18 |
| | 200-300 | 37929 | 4.16 | 7 | 6.09 | 1.46 |
| | 300-400 | 29107 | 3.19 | 3 | 2.61 | 0.82 |
| | 400< | 771394 | 84.59 | 99 | 86.09 | 1.02 |
| 90m | 0-100 | 5536 | 5.47 | 4 | 3.48 | 0.64 |
| | 100-200 | 3333 | 3.29 | 4 | 3.48 | 1.06 |
| | 200-300 | 4076 | 4.03 | 5 | 4.35 | 1.08 |
| | 300-400 | 3028 | 2.99 | 6 | 5.22 | 1.74 |
| | 400< | 85210 | 84.21 | 96 | 83.48 | 0.99 |
| Distance from the road(m) | | | | | | |
| 12.5m | 0-100 | 166121 | 3.16 | 5 | 4.35 | 1.37 |
| | 100-200 | 136503 | 2.6 | 2 | 1.74 | 0.67 |
| | 200-300 | 126201 | 2.4 | 6 | 5.22 | 2.17 |
| | 300-400 | 120319 | 2.29 | 2 | 1.74 | 0.76 |
| | 400< | 4703456 | 89.55 | 100 | 86.96 | 0.97 |

| | | | | | | |
|---|---|---|---|---|---|---|
| 30m | 0-100 | 30136 | 3.3 | 5 | 4.35 | 1.32 |
| | 100-200 | 22593 | 2.48 | 3 | 2.61 | 1.05 |
| | 200-300 | 23374 | 2.56 | 6 | 5.22 | 2.04 |
| | 300-400 | 19606 | 2.15 | 1 | 0.87 | 0.4 |
| | 400< | 816238 | 89.5 | 100 | 86.96 | 0.97 |
| 90m | 0-100 | 4024 | 3.977 | 5 | 4.35 | 1.09 |
| | 100-200 | 2011 | 1.987 | 2 | 1.74 | 0.88 |
| | 200-300 | 2740 | 2.708 | 7 | 6.09 | 2.25 |
| | 300-400 | 2082 | 2.058 | 2 | 1.74 | 0.85 |
| | 400< | 90326 | 89.27 | 99 | 86.09 | 0.96 |
| Lithology | | | | | | |
| 12.5m | Tsm | 555267 | 10.57 | 32 | 27.83 | 2.63 |
| | Pzc | 55299 | 1.05 | 1 | 0.87 | 0.83 |
| | pCd | 199124 | 3.79 | 12 | 10.43 | 2.75 |
| | GHlml | 132280 | 2.52 | 5 | 4.35 | 1.73 |
| | GHlo | 936177 | 17.82 | 23 | 20 | 1.12 |
| | Tgr | 3374453 | 64.24 | 42 | 36.52 | 0.57 |
| 30m | Tsm | 96424 | 10.57 | 32 | 26.02 | 2.46 |
| | Pzc | 9617 | 1.05 | 1 | 0.87 | 0.82 |
| | pCd | 34574 | 3.79 | 12 | 10.43 | 2.75 |
| | GHlml | 22953 | 2.52 | 5 | 4.35 | 1.73 |
| | GHlo | 162532 | 17.82 | 23 | 20 | 1.12 |
| | Tgr | 585847 | 64.24 | 42 | 36.52 | 0.57 |
| 90m | Tsm | 10716 | 10.59 | 32 | 27.83 | 2.63 |
| | Pzc | 18107 | 17.9 | 23 | 20 | 1.12 |
| | pCd | 3846 | 3.8 | 12 | 10.43 | 2.75 |
| | GHlml | 2549 | 2.52 | 5 | 4.35 | 1.73 |
| | GHlo | 64931 | 64.17 | 42 | 36.52 | 0.57 |
| | Tgr | 1034 | 1.02 | 1 | 0.87 | 0.85 |
| Rainfall (mm) | | | | | | |
| 12.5m | 1786.79 - 2434.61 | 1345852 | 25.62 | 19 | 16.52 | 0.64 |
| | 2434.62 - 2930.01 | 1499293 | 28.54 | 15 | 13.04 | 0.46 |
| | 2930.02 - 3539.74 | 1065871 | 20.29 | 16 | 13.91 | 0.69 |
| | 3539.75 - 4225.67 | 710092 | 13.52 | 39 | 33.91 | 2.51 |
| | 4225.68 - 5025.93 | 631492 | 12.02 | 26 | 22.61 | 1.88 |
| 30m | 1786.79 - 2434.61 | 233498 | 25.6 | 19 | 16.52 | 0.65 |
| | 2434.62 - 2930.01 | 260364 | 28.55 | 14 | 12.17 | 0.43 |
| | 2930.02 - 3539.74 | 185119 | 20.3 | 17 | 14.78 | 0.73 |
| | 3539.75 - 4225.67 | 123357 | 13.53 | 39 | 33.91 | 2.51 |
| | 4225.68 - 5025.93 | 109609 | 12.02 | 26 | 22.61 | 1.88 |
| 90m | 1786.79 - 2434.61 | 25797 | 25.5 | 19 | 16.52 | 0.65 |
| | 2434.62 - 2930.01 | 28937 | 28.6 | 14 | 12.17 | 0.43 |
| | 2930.02 - 3539.74 | 20564 | 20.32 | 16 | 13.91 | 0.68 |
| | 3539.75 - 4225.67 | 13715 | 13.55 | 40 | 34.78 | 2.57 |
| | 4225.68 - 5025.93 | 12170 | 12.03 | 26 | 22.61 | 1.88 |
| Land Use Land Cover | | | | | | |
| 12.5m | Agricultural Land | 172063 | 3.28 | 2 | 1.74 | 0.53 |
| | Built Up Area | 4943 | 0.09 | 0 | 0 | 0 |
| | Forest | 4863000 | 92.58 | 110 | 95.65 | 1.03 |
| | Shrub | 130659 | 2.49 | 3 | 2.61 | 1.05 |
| | Water Bodies | 81935 | 1.56 | 0 | 0 | 0 |
| 30m | Agricultural Land | 29903 | 3.28 | 2 | 1.74 | 0.53 |
| | Built Up Area | 851 | 0.09 | 0 | 0 | 0 |
| | Forest | 844305 | 92.58 | 110 | 95.65 | 1.03 |
| | Shrub | 22629 | 2.48 | 3 | 2.61 | 1.05 |
| | Water Bodies | 14259 | 1.56 | 0 | 0 | 0 |
| 90m | Agricultural Land | 3261 | 3.22 | 2 | 1.74 | 0.54 |
| | Built Up Area | 96 | 0.09 | 0 | 0 | 0 |
| | Forest | 93764 | 92.67 | 107 | 93.04 | 1 |
| | Shrub | 2467 | 2.44 | 5 | 4.35 | 1.78 |
| | Water Bodies | 1595 | 1.58 | 1 | 0.87 | 0.55 |

## Appendix C: Detail of Index of Entropy calculation using three different spatial resolution

The following Table shows the detail calculation of individual spatial resolution (12.5m, 30m and 90m) using the Index of Entropy

| Spatial Resolution | Class | No of pixel in class | % of landslide pixel in class | No of landslide in class | % of landslide in class | Pij | (Pij) | Hj | Hjmax | Ij | Pj | Wij |
|---|---|---|---|---|---|---|---|---|---|---|---|---|
| Elevation(m) | | | | | | | | | | | | |
| 12.5m | < 854.00 | 711123 | 13.54 | 44 | 38.26 | 2.83 | 0.49 | 1.982 | 2.322 | 0.146 | 1.162 | 0.17 |
| | 854.00 - 1455 | 1278941 | 24.35 | 32 | 27.83 | 1.14 | 0.20 | | | | | |
| | 1455.01 - 1949 | 1697050 | 32.31 | 21 | 18.26 | 0.57 | 0.10 | | | | | |
| | 1949.01 - 2619 | 1285804 | 24.48 | 13 | 11.30 | 0.46 | 0.08 | | | | | |
| | 2619 < | 279682 | 5.32 | 5 | 4.35 | 0.82 | 0.14 | | | | | |
| 30m | < 854.00 | 113694 | 12.47 | 37 | 32.17 | 2.58 | 0.45 | 2.025 | 2.322 | 0.128 | 1.156 | 0.148 |
| | 854.00 - 1455 | 209113 | 22.93 | 37 | 32.17 | 1.40 | 0.24 | | | | | |
| | 1455.01 - 1949 | 292274 | 32.05 | 21 | 18.26 | 0.57 | 0.10 | | | | | |
| | 1949.01 - 2619 | 243245 | 26.67 | 15 | 13.04 | 0.49 | 0.08 | | | | | |
| | 2619 < | 53621 | 5.88 | 5 | 4.35 | 0.74 | 0.13 | | | | | |
| 90m | < 854.00 | 12614 | 12.47 | 38 | 33.04 | 2.65 | 0.46 | 2.012 | 2.322 | 0.133 | 1.161 | 0.155 |
| | 854.00 - 1455 | 23263 | 22.99 | 36 | 31.30 | 1.36 | 0.23 | | | | | |
| | 1455.01 - 1949 | 32472 | 32.09 | 22 | 19.13 | 0.60 | 0.10 | | | | | |
| | 1949.01 - 2619 | 26898 | 26.58 | 14 | 12.17 | 0.46 | 0.08 | | | | | |
| | 2619 < | 5936 | 5.87 | 5 | 4.35 | 0.74 | 0.13 | | | | | |
| Slope (Degree) | | | | | | | | | | | | |
| 12.5m | 0 - 13.00 | 503807 | 9.59 | 9 | 7.83 | 0.82 | 0.15 | 2.195 | 2.322 | 0.055 | 1.062 | 0.058 |
| | 13.01 - 23.00 | 1027159 | 19.56 | 13 | 11.30 | 0.58 | 0.11 | | | | | |
| | 23.01 - 32.00 | 1575077 | 29.99 | 33 | 28.70 | 0.96 | 0.18 | | | | | |
| | 32.01 - 42.00 | 1537245 | 29.27 | 34 | 29.57 | 1.01 | 0.19 | | | | | |
| | 42 < | 609312 | 11.60 | 26 | 22.61 | 1.95 | 0.37 | | | | | |
| 30m | 0 - 13.00 | 93299 | 10.23 | 6 | 5.22 | 0.51 | 0.09 | 2.063 | 2.322 | 0.112 | 1.136 | 0.127 |
| | 13.01 - 23.00 | 195676 | 21.46 | 20 | 17.39 | 0.81 | 0.14 | | | | | |
| | 23.01 - 32.00 | 275372 | 30.20 | 28 | 24.35 | 0.81 | 0.14 | | | | | |
| | 32.01 - 42.00 | 255827 | 28.05 | 31 | 26.96 | 0.96 | 0.17 | | | | | |
| | 42 < | 91773 | 10.06 | 30 | 26.09 | 2.59 | 0.46 | | | | | |
| 90m | 0 - 13.00 | 11472 | 11.34 | 11 | 9.57 | 0.84 | 0.12 | 2.06 | 2.322 | 0.113 | 1.397 | 0.158 |
| | 13.01 - 23.00 | 27384 | 27.06 | 29 | 25.22 | 0.93 | 0.13 | | | | | |
| | 23.01 - 32.00 | 35491 | 35.08 | 33 | 28.70 | 0.82 | 0.12 | | | | | |
| | 32.01 - 42.00 | 23855 | 23.58 | 31 | 26.96 | 1.14 | 0.16 | | | | | |
| | 42 < | 2981 | 2.95 | 11 | 9.57 | 3.25 | 0.46 | | | | | |
| Aspect | | | | | | | | | | | | |
| 12.5m | Flat | 47614 | 0.91 | 0 | 0.00 | 0.00 | 0.00 | 2.843 | 3.17 | 0.103 | 0.871 | 0.09 |
| | North | 636941 | 12.13 | 5 | 4.35 | 0.36 | 0.05 | | | | | |
| | NorthEast | 589967 | 11.23 | 9 | 7.83 | 0.70 | 0.09 | | | | | |
| | East | 599110 | 11.41 | 15 | 13.04 | 1.14 | 0.15 | | | | | |
| | SouthEast | 758507 | 14.44 | 33 | 28.70 | 1.99 | 0.25 | | | | | |
| | South | 681513 | 12.97 | 19 | 16.52 | 1.27 | 0.16 | | | | | |
| | SouthWest | 749811 | 14.28 | 15 | 13.04 | 0.91 | 0.12 | | | | | |
| | West | 604243 | 11.50 | 8 | 6.96 | 0.60 | 0.08 | | | | | |
| | NorthWest | 584894 | 11.14 | 11 | 9.57 | 0.86 | 0.11 | | | | | |
| 30m | Flat | 285 | 0.03 | 0 | 0.00 | 0.00 | 0.00 | 2.839 | 3.17 | 0.104 | 0.865 | 0.09 |
| | North | 118174 | 12.96 | 6 | 5.22 | 0.40 | 0.05 | | | | | |
| | NorthEast | 97997 | 10.75 | 9 | 7.83 | 0.73 | 0.09 | | | | | |
| | East | 110602 | 12.13 | 14 | 12.17 | 1.00 | 0.13 | | | | | |
| | SouthEast | 129200 | 14.17 | 33 | 28.70 | 2.03 | 0.26 | | | | | |
| | South | 120454 | 13.21 | 18 | 15.65 | 1.19 | 0.15 | | | | | |
| | SouthWest | 126820 | 13.91 | 18 | 15.65 | 1.13 | 0.14 | | | | | |
| | West | 111498 | 12.23 | 7 | 6.09 | 0.50 | 0.06 | | | | | |
| | NorthWest | 96917 | 10.63 | 10 | 8.70 | 0.82 | 0.11 | | | | | |
| 90m | Flat | 6 | 0.01 | 0 | 0.00 | 0.00 | 0.00 | 2.839 | 3.17 | 0.104 | 0.861 | 0.09 |
| | North | 11739 | 11.60 | 6 | 5.22 | 0.45 | 0.06 | | | | | |
| | NorthEast | 10792 | 10.67 | 5 | 4.35 | 0.41 | 0.05 | | | | | |
| | East | 13004 | 12.85 | 16 | 13.91 | 1.08 | 0.14 | | | | | |
| | SouthEast | 14659 | 14.49 | 29 | 25.22 | 1.74 | 0.22 | | | | | |
| | South | 13247 | 13.09 | 24 | 20.87 | 1.59 | 0.21 | | | | | |
| | SouthWest | 14400 | 14.23 | 13 | 11.30 | 0.79 | 0.10 | | | | | |
| | West | 12655 | 12.51 | 10 | 8.70 | 0.70 | 0.09 | | | | | |
| | NorthWest | 10681 | 10.56 | 12 | 10.43 | 0.99 | 0.13 | | | | | |
| Curvature | | | | | | | | | | | | |
| 12.5m | Concave | 2214763 | 42.17 | 47 | 40.87 | 0.97 | 0.33 | 1.584 | 1.585 | 0.001 | 0.993 | 0.001 |
| | Flat | 802326 | 15.27 | 17 | 14.78 | 0.97 | 0.32 | | | | | |
| | Convex | 2235511 | 42.56 | 51 | 44.35 | 1.04 | 0.35 | | | | | |
| 30m | Concave | 434525 | 47.65 | 70 | 60.87 | 1.28 | 0.48 | 1.521 | 1.585 | 0.04 | 0.895 | 0.036 |
| | Flat | 36424 | 3.99 | 3 | 2.61 | 0.65 | 0.24 | | | | | |
| | Convex | 440998 | 48.36 | 42 | 36.52 | 0.76 | 0.28 | | | | | |
| 90m | Concave | 50045 | 49.46 | 73 | 63.48 | 1.28 | 0.63 | 0.948 | 1.585 | 0.402 | 0.675 | 0.271 |
| | Flat | 1309 | 1.29 | 0 | 0.00 | 0.00 | 0.00 | | | | | |
| | Convex | 49829 | 49.25 | 42 | 36.52 | 0.74 | 0.37 | | | | | |
| Topographic Wetness Index | | | | | | | | | | | | |
| 12.5m | < 0.999 | 529278 | 10.08 | 12 | 10.43 | 1.04 | 0.27 | 1.976 | 2 | 0.012 | 0.943 | 0.011 |

| | | | | | | | | | | | | |
|---|---|---|---|---|---|---|---|---|---|---|---|---|
| | 0.999 - 3.219 | 1520949 | 28.96 | 35 | 30.43 | 1.05 | 0.28 | | | | | |
| | 3.220 - 6.688 | 486118 | 9.25 | 7 | 6.09 | 0.66 | 0.17 | | | | | |
| | 6.688 < | 2716255 | 51.71 | 61 | 53.04 | 1.03 | 0.27 | | | | | |
| 30m | < 0.999 | 200164 | 21.95 | 27 | 23.48 | 1.07 | 0.26 | 1.995 | 2 | 0.002 | 1.043 | 0.003 |
| | 0.999 - 3.219 | 217946 | 23.90 | 31 | 26.96 | 1.13 | 0.27 | | | | | |
| | 3.220 - 6.688 | 37006 | 4.06 | 5 | 4.35 | 1.07 | 0.26 | | | | | |
| | 6.688 < | 456831 | 50.09 | 52 | 45.22 | 0.90 | 0.22 | | | | | |
| 90m | < 0.999 | 38278 | 37.83 | 46 | 40.00 | 1.06 | 0.30 | 1.977 | 2 | 0.012 | 0.892 | 0.01 |
| | 0.999 - 3.219 | 11135 | 11.00 | 11 | 9.57 | 0.87 | 0.24 | | | | | |
| | 3.220 - 6.688 | 1358 | 1.34 | 1 | 0.87 | 0.65 | 0.18 | | | | | |
| | 6.688 < | 50412 | 49.82 | 57 | 49.57 | 0.99 | 0.28 | | | | | |
| Stream Power Index | | | | | | | | | | | | |
| 12.5m | < -4.052 | 850701 | 16.20 | 16 | 13.91 | 0.86 | 0.22 | 1.989 | 2 | 0.005 | 0.96 | 0.005 |
| | -4.052 - 0.886 | 1638515 | 31.19 | 31 | 26.96 | 0.86 | 0.23 | | | | | |
| | 0.887 - 3.529 | 2336225 | 44.48 | 59 | 51.30 | 1.15 | 0.30 | | | | | |
| | 3.529 < | 427159 | 8.13 | 9 | 7.83 | 0.96 | 0.25 | | | | | |
| 30m | < -4.052 | 233485 | 25.60 | 18 | 15.65 | 0.61 | 0.13 | 1.895 | 2 | 0.053 | 1.148 | 0.06 |
| | -4.052 - 0.886 | 344021 | 37.72 | 44 | 38.26 | 1.01 | 0.22 | | | | | |
| | 0.887 - 3.529 | 274078 | 30.05 | 39 | 33.91 | 1.13 | 0.25 | | | | | |
| | 3.529 < | 60363 | 6.62 | 14 | 12.17 | 1.84 | 0.40 | | | | | |
| 90m | < -4.052 | 32999 | 32.61 | 28 | 24.35 | 0.75 | 0.18 | 1.937 | 2 | 0.032 | 1.029 | 0.032 |
| | -4.052 - 0.886 | 42295 | 41.80 | 45 | 39.13 | 0.94 | 0.23 | | | | | |
| | 0.887 - 3.529 | 20832 | 20.59 | 37 | 32.17 | 1.56 | 0.38 | | | | | |
| | 3.529 < | 5057 | 5.00 | 5 | 4.35 | 0.87 | 0.21 | | | | | |
| Drainage Density | | | | | | | | | | | | |
| 12.5m | < 0.545 | 964147 | 18.36 | 6 | 5.22 | 0.28 | 0.06 | 2.118 | 2.322 | 0.088 | 0.911 | 0.08 |
| | 0.545 - 0.854 | 1329522 | 25.31 | 37 | 32.17 | 1.27 | 0.28 | | | | | |
| | 0.855 - 1.153 | 1269392 | 24.17 | 44 | 38.26 | 1.58 | 0.35 | | | | | |
| | 1.154 - 1.462 | 1111965 | 21.17 | 21 | 18.26 | 0.86 | 0.19 | | | | | |
| | 1.462 < | 577574 | 11.00 | 7 | 6.09 | 0.55 | 0.12 | | | | | |
| 30m | < 0.545 | 167456 | 18.36 | 6 | 5.22 | 0.28 | 0.06 | 2.118 | 2.322 | 0.088 | 0.911 | 0.08 |
| | 0.545 - 0.854 | 230872 | 25.32 | 37 | 32.17 | 1.27 | 0.28 | | | | | |
| | 0.855 - 1.153 | 220395 | 24.17 | 44 | 38.26 | 1.58 | 0.35 | | | | | |
| | 1.154 - 1.462 | 192998 | 21.16 | 21 | 18.26 | 0.86 | 0.19 | | | | | |
| | 1.462 < | 100226 | 10.99 | 7 | 6.09 | 0.55 | 0.12 | | | | | |
| 90m | < 0.545 | 18485 | 18.27 | 7 | 6.09 | 0.33 | 0.07 | 2.146 | 2.322 | 0.076 | 0.914 | 0.069 |
| | 0.545 - 0.854 | 25650 | 25.35 | 36 | 31.30 | 1.23 | 0.27 | | | | | |
| | 0.855 - 1.153 | 24516 | 24.23 | 43 | 37.39 | 1.54 | 0.34 | | | | | |
| | 1.154 - 1.462 | 21420 | 21.17 | 22 | 19.13 | 0.90 | 0.20 | | | | | |
| | 1.462 < | 11112 | 10.98 | 7 | 6.09 | 0.55 | 0.12 | | | | | |
| Normalized Difference Vegetation Index | | | | | | | | | | | | |
| 12.5m | <223 | 219873 | 4.19 | 32 | 27.83 | 6.65 | 0.64 | 1.612 | 2.322 | 0.306 | 2.076 | 0.635 |
| | 0.223 - 0.407 | 574346 | 10.93 | 19 | 16.52 | 1.51 | 0.15 | | | | | |
| | 0.408 - 0.562 | 877493 | 16.71 | 20 | 17.39 | 1.04 | 0.10 | | | | | |
| | 0.563 - 0.688 | 1492466 | 28.41 | 25 | 21.74 | 0.77 | 0.07 | | | | | |
| | 0.688 < | 2088422 | 39.76 | 19 | 16.52 | 0.42 | 0.04 | | | | | |
| 30m | <223 | 38264 | 4.20 | 22 | 19.13 | 4.56 | 0.51 | 1.863 | 2.322 | 0.198 | 1.789 | 0.354 |
| | 0.223 - 0.407 | 99842 | 10.95 | 28 | 24.35 | 2.22 | 0.25 | | | | | |
| | 0.408 - 0.562 | 152092 | 16.68 | 17 | 14.78 | 0.89 | 0.10 | | | | | |
| | 0.563 - 0.688 | 259052 | 28.41 | 26 | 22.61 | 0.80 | 0.09 | | | | | |
| | 0.688 < | 362697 | 39.77 | 22 | 19.13 | 0.48 | 0.05 | | | | | |
| 90m | <223 | 4269 | 4.22 | 17 | 14.78 | 3.50 | 0.46 | 2.029 | 2.322 | 0.126 | 1.527 | 0.193 |
| | 0.223 - 0.407 | 11050 | 10.92 | 21 | 18.26 | 1.67 | 0.22 | | | | | |
| | 0.408 - 0.562 | 16732 | 16.54 | 18 | 15.65 | 0.95 | 0.12 | | | | | |
| | 0.563 - 0.688 | 29073 | 28.73 | 26 | 22.61 | 0.79 | 0.10 | | | | | |
| | 0.688 < | 40059 | 39.59 | 33 | 28.70 | 0.72 | 0.09 | | | | | |
| Normalized Difference Soil Index | | | | | | | | | | | | |
| 12.5m | < -0.516 | 484543 | 9.22 | 8 | 6.96 | 0.75 | 0.14 | 2.017 | 2.322 | 0.131 | 1.084 | 0.142 |
| | -0.516 - -0.273 | 946456 | 18.02 | 10 | 8.70 | 0.48 | 0.09 | | | | | |
| | -0.274 - -0.097 | 1471428 | 28.01 | 16 | 13.91 | 0.50 | 0.09 | | | | | |
| | -0.098 - 0.078 | 1655777 | 31.52 | 43 | 37.39 | 1.19 | 0.22 | | | | | |
| | 0.078 < | 694396 | 13.22 | 38 | 33.04 | 2.50 | 0.46 | | | | | |
| 30m | < -0.516 | 84053 | 9.22 | 8 | 6.96 | 0.76 | 0.14 | 2.004 | 2.322 | 0.137 | 1.097 | 0.15 |
| | -0.516 - -0.273 | 164589 | 18.05 | 12 | 10.43 | 0.58 | 0.11 | | | | | |
| | -0.274 - -0.097 | 255238 | 27.99 | 13 | 11.30 | 0.40 | 0.07 | | | | | |
| | -0.098 - 0.078 | 287262 | 31.50 | 43 | 37.39 | 1.19 | 0.22 | | | | | |
| | 0.078 < | 120805 | 13.25 | 39 | 33.91 | 2.56 | 0.47 | | | | | |
| 90m | < -0.516 | 9379 | 9.27 | 9 | 7.83 | 0.84 | 0.16 | 2.086 | 2.322 | 0.102 | 1.085 | 0.11 |
| | -0.516 - -0.273 | 18265 | 18.05 | 10 | 8.70 | 0.48 | 0.09 | | | | | |
| | -0.274 - -0.097 | 28423 | 28.09 | 22 | 19.13 | 0.68 | 0.13 | | | | | |
| | -0.098 - 0.078 | 31704 | 31.33 | 38 | 33.04 | 1.05 | 0.19 | | | | | |
| | 0.078 < | 13412 | 13.26 | 36 | 31.30 | 2.36 | 0.44 | | | | | |
| Distance from the river(m) | | | | | | | | | | | | |
| 12.5m | 0-100 | 176948 | 3.37 | 6 | 5.22 | 1.55 | 0.29 | 2.255 | 2.322 | 0.029 | 1.081 | 0.031 |
| | 100-200 | 162601 | 3.10 | 2 | 1.74 | 0.56 | 0.10 | | | | | |
| | 200-300 | 158292 | 3.01 | 4 | 3.48 | 1.15 | 0.21 | | | | | |
| | 300-400 | 157852 | 3.01 | 4 | 3.48 | 1.16 | 0.21 | | | | | |
| | 400< | 4596907 | 87.52 | 99 | 86.09 | 0.98 | 0.18 | | | | | |
| 30m | 0-100 | 31639 | 3.47 | 7 | 6.09 | 1.75 | 0.33 | 2.159 | 2.322 | 0.07 | 1.069 | 0.075 |
| | 100-200 | 27341 | 3.00 | 1 | 0.87 | 0.29 | 0.05 | | | | | |
| | 200-300 | 29785 | 3.27 | 4 | 3.48 | 1.07 | 0.20 | | | | | |
| | 300-400 | 25379 | 2.78 | 4 | 3.48 | 1.25 | 0.23 | | | | | |
| | 400< | 797803 | 87.48 | 99 | 86.09 | 0.98 | 0.18 | | | | | |
| 90m | 0-100 | 4349 | 4.30 | 8 | 6.96 | 1.62 | 0.31 | 2.194 | 2.322 | 0.055 | 1.046 | 0.058 |

| | | | | | | | | | | | | |
|---|---|---|---|---|---|---|---|---|---|---|---|---|
| | 100-200 | 2476 | 2.45 | 1 | 0.87 | 0.36 | 0.07 | | | | | |
| | 200-300 | 3448 | 3.41 | 4 | 3.48 | 1.02 | 0.20 | | | | | |
| | 300-400 | 2799 | 2.77 | 4 | 3.48 | 1.26 | 0.24 | | | | | |
| | 400< | 88111 | 87.08 | 98 | 85.22 | 0.98 | 0.19 | | | | | |
| Distance from the fault(m) | | | | | | | | | | | | |
| | 0-100 | 219126 | 4.17 | 1 | 0.87 | 0.21 | 0.04 | | | | | |
| | 100-200 | 206180 | 3.93 | 5 | 4.35 | 1.11 | 0.22 | | | | | |
| 12.5m | 200-300 | 198818 | 3.79 | 6 | 5.22 | 1.38 | 0.28 | 2.157 | 2.322 | 0.071 | 0.993 | 0.071 |
| | 300-400 | 180361 | 3.43 | 5 | 4.35 | 1.27 | 0.25 | | | | | |
| | 400< | 4448115 | 84.68 | 98 | 85.22 | 1.01 | 0.20 | | | | | |
| | 0-100 | 39885 | 4.37 | 1 | 0.87 | 0.20 | 0.04 | | | | | |
| | 100-200 | 33632 | 3.69 | 5 | 4.35 | 1.18 | 0.25 | | | | | |
| 30m | 200-300 | 37929 | 4.16 | 7 | 6.09 | 1.46 | 0.31 | 2.138 | 2.322 | 0.079 | 0.935 | 0.074 |
| | 300-400 | 29107 | 3.19 | 3 | 2.61 | 0.82 | 0.17 | | | | | |
| | 400< | 771394 | 84.59 | 99 | 86.09 | 1.02 | 0.22 | | | | | |
| | 0-100 | 5536 | 5.47 | 4 | 3.48 | 0.64 | 0.12 | | | | | |
| | 100-200 | 3333 | 3.29 | 4 | 3.48 | 1.06 | 0.19 | | | | | |
| 90m | 200-300 | 4076 | 4.03 | 5 | 4.35 | 1.08 | 0.20 | 2.248 | 2.322 | 0.032 | 1.101 | 0.035 |
| | 300-400 | 3028 | 2.99 | 6 | 5.22 | 1.74 | 0.32 | | | | | |
| | 400< | 85210 | 84.21 | 96 | 83.48 | 0.99 | 0.18 | | | | | |
| Distance from the road(m) | | | | | | | | | | | | |
| | 0-100 | 166121 | 3.16 | 5 | 4.35 | 1.37 | 0.23 | | | | | |
| | 100-200 | 136503 | 2.60 | 2 | 1.74 | 0.67 | 0.11 | | | | | |
| 12.5m | 200-300 | 126201 | 2.40 | 6 | 5.22 | 2.17 | 0.37 | 2.18 | 2.322 | 0.061 | 1.189 | 0.073 |
| | 300-400 | 120319 | 2.29 | 2 | 1.74 | 0.76 | 0.13 | | | | | |
| | 400< | 4703456 | 89.55 | 100 | 86.96 | 0.97 | 0.16 | | | | | |
| | 0-100 | 30136 | 3.30 | 5 | 4.35 | 1.32 | 0.23 | | | | | |
| | 100-200 | 22593 | 2.48 | 3 | 2.61 | 1.05 | 0.18 | | | | | |
| 30m | 200-300 | 23374 | 2.56 | 6 | 5.22 | 2.04 | 0.35 | 2.165 | 2.322 | 0.068 | 1.156 | 0.078 |
| | 300-400 | 19606 | 2.15 | 1 | 0.87 | 0.40 | 0.07 | | | | | |
| | 400< | 816238 | 89.50 | 100 | 86.96 | 0.97 | 0.17 | | | | | |
| | 0-100 | 4024 | 3.98 | 5 | 4.35 | 1.09 | 0.18 | | | | | |
| | 100-200 | 2011 | 1.99 | 2 | 1.74 | 0.88 | 0.15 | | | | | |
| 90m | 200-300 | 2740 | 2.71 | 7 | 6.09 | 2.25 | 0.37 | 2.202 | 2.322 | 0.052 | 1.205 | 0.062 |
| | 300-400 | 2082 | 2.06 | 2 | 1.74 | 0.85 | 0.14 | | | | | |
| | 400< | 90326 | 89.27 | 99 | 86.09 | 0.96 | 0.16 | | | | | |
| Lithology | | | | | | | | | | | | |
| | Tsm | 555267 | 10.57 | 32 | 27.83 | 2.63 | 0.27 | | | | | |
| | Pzc | 55299 | 1.05 | 1 | 0.87 | 0.83 | 0.09 | | | | | |
| 12.5m | pCd | 199124 | 3.79 | 12 | 10.43 | 2.75 | 0.29 | 2.379 | 2.585 | 0.08 | 1.605 | 0.128 |
| | GHlml | 132280 | 2.52 | 5 | 4.35 | 1.73 | 0.18 | | | | | |
| | GHlo | 936177 | 17.82 | 23 | 20.00 | 1.12 | 0.12 | | | | | |
| | Tgr | 3374453 | 64.24 | 42 | 36.52 | 0.57 | 0.06 | | | | | |
| | Tsm | 96424 | 10.57 | 32 | 26.02 | 2.46 | 0.26 | | | | | |
| | Pzc | 9617 | 1.05 | 1 | 0.87 | 0.83 | 0.09 | | | | | |
| 30m | pCd | 34574 | 3.79 | 12 | 10.43 | 2.75 | 0.29 | 2.387 | 2.585 | 0.077 | 1.576 | 0.121 |
| | GHlml | 22953 | 2.52 | 5 | 4.35 | 1.73 | 0.18 | | | | | |
| | GHlo | 162532 | 17.82 | 23 | 20.00 | 1.12 | 0.12 | | | | | |
| | Tgr | 585847 | 64.24 | 42 | 36.52 | 0.57 | 0.06 | | | | | |
| | Tsm | 10716 | 10.59 | 32 | 27.83 | 2.63 | 0.27 | | | | | |
| | Pzc | 18107 | 17.90 | 23 | 20.00 | 1.12 | 0.12 | | | | | |
| 90m | pCd | 3846 | 3.80 | 12 | 10.43 | 2.75 | 0.28 | 2.382 | 2.585 | 0.079 | 1.606 | 0.126 |
| | GHlml | 2549 | 2.52 | 5 | 4.35 | 1.73 | 0.18 | | | | | |
| | GHlo | 64931 | 64.17 | 42 | 36.52 | 0.57 | 0.06 | | | | | |
| | Tgr | 1034 | 1.02 | 1 | 0.87 | 0.85 | 0.09 | | | | | |
| Rainfall(mm) | | | | | | | | | | | | |
| | 1786.79 - 2434.61 | 1345852 | 25.62 | 19 | 16.52 | 0.64 | 0.10 | | | | | |
| | 2434.62 - 2930.01 | 1499293 | 28.54 | 15 | 13.04 | 0.46 | 0.07 | | | | | |
| 12.5m | 2930.02 - 3539.74 | 1065871 | 20.29 | 16 | 13.91 | 0.69 | 0.11 | 2.021 | 2.322 | 0.13 | 1.235 | 0.16 |
| | 3539.75 - 4225.67 | 710092 | 13.52 | 39 | 33.91 | 2.51 | 0.41 | | | | | |
| | 4225.68 - 5025.93 | 631492 | 12.02 | 26 | 22.61 | 1.88 | 0.30 | | | | | |
| | 1786.79 - 2434.61 | 233498 | 25.60 | 19 | 16.52 | 0.65 | 0.10 | | | | | |
| | 2434.62 - 2930.01 | 260364 | 28.55 | 14 | 12.17 | 0.43 | 0.07 | | | | | |
| 30m | 2930.02 - 3539.74 | 185119 | 20.30 | 17 | 14.78 | 0.73 | 0.12 | 2.02 | 2.322 | 0.13 | 1.238 | 0.161 |
| | 3539.75 - 4225.67 | 123357 | 13.53 | 39 | 33.91 | 2.51 | 0.41 | | | | | |
| | 4225.68 - 5025.93 | 109609 | 12.02 | 26 | 22.61 | 1.88 | 0.30 | | | | | |
| | 1786.79 - 2434.61 | 25797 | 25.50 | 19 | 16.52 | 0.65 | 0.10 | | | | | |
| | 2434.62 - 2930.01 | 28937 | 28.60 | 14 | 12.17 | 0.43 | 0.07 | | | | | |
| 90m | 2930.02 - 3539.74 | 20564 | 20.32 | 16 | 13.91 | 0.68 | 0.11 | 2.005 | 2.322 | 0.137 | 1.241 | 0.169 |
| | 3539.75 - 4225.67 | 13715 | 13.55 | 40 | 34.78 | 2.57 | 0.41 | | | | | |
| | 4225.68 - 5025.93 | 12170 | 12.03 | 26 | 22.61 | 1.88 | 0.30 | | | | | |
| Land use land cover | | | | | | | | | | | | |
| | Agricultural Land | 172063 | 3.28 | 2 | 1.74 | 0.53 | 0.20 | | | | | |
| | Built Up Area | 4943 | 0.09 | 0 | 0.00 | 0.00 | 0.00 | | | | | |
| 12.5m | Forest | 4863000 | 92.58 | 110 | 95.65 | 1.03 | 0.40 | 1.525 | 2.322 | 0.343 | 0.523 | 0.179 |
| | Shrub | 130659 | 2.49 | 3 | 2.61 | 1.05 | 0.40 | | | | | |
| | Water Bodies | 81935 | 1.56 | 0 | 0.00 | 0.00 | 0.00 | | | | | |
| | Agricultural Land | 29903 | 3.28 | 2 | 1.74 | 0.53 | 0.20 | | | | | |
| | Built Up Area | 851 | 0.09 | 0 | 0.00 | 0.00 | 0.00 | | | | | |
| 30m | Forest | 844305 | 92.58 | 110 | 95.65 | 1.03 | 0.40 | 1.525 | 2.322 | 0.343 | 0.523 | 0.179 |
| | Shrub | 22629 | 2.48 | 3 | 2.61 | 1.05 | 0.40 | | | | | |
| | Water Bodies | 14259 | 1.56 | 0 | 0.00 | 0.00 | 0.00 | | | | | |
| 90m | Agricultural Land | 3261 | 3.22 | 2 | 1.74 | 0.54 | 0.14 | 1.816 | 2.322 | 0.218 | 0.776 | 0.169 |
| | Built Up Area | 96 | 0.09 | 0 | 0.00 | 0.00 | 0.00 | | | | | |

| | | | | | | | | | | | | |
|---|---|---|---|---|---|---|---|---|---|---|---|---|
| | Forest | 93764 | 92.67 | 107 | 93.04 | 1.00 | 0.26 | | | | | |
| | Shrub | 2467 | 2.44 | 5 | 4.35 | 1.78 | 0.46 | | | | | |
| | Water Bodies | 1595 | 1.58 | 1 | 0.87 | 0.55 | 0.14 | | | | | |

## Appendix D: Detail of Weight of Evidence calculation using three different spatial resolution

The following Table shows the detail calculation of individual spatial resolution (12.5m, 30m and 90m) using the Weight of Evidence

| Spatial Resolution | Class | No of pixel in class | % of landslide pixel in class | No of landslide in class | % of landslide in class | W+ | W- | C | S2(W+) | S2(W-) | S(C ) | Cs |
|---|---|---|---|---|---|---|---|---|---|---|---|---|
| Elevation(m) | | | | | | | | | | | | |
| 12.5m | < 854.00 | 711123 | 13.54 | 44 | 38.26 | 1.039 | -0.337 | 1.376 | 0.023 | 0.014 | 0.192 | 7.170 |
| | 854.00 - 1455 | 1278941 | 24.35 | 32 | 27.83 | 0.133 | -0.047 | 0.181 | 0.031 | 0.012 | 0.208 | 0.868 |
| | 1455.01 - 1949 | 1697050 | 32.31 | 21 | 18.26 | -0.571 | 0.189 | -0.759 | 0.048 | 0.011 | 0.241 | -3.145 |
| | 1949.01 - 2619 | 1285804 | 24.48 | 13 | 11.30 | -0.773 | 0.161 | -0.933 | 0.077 | 0.010 | 0.294 | -3.170 |
| | 2619 < | 279682 | 5.32 | 5 | 4.35 | -0.203 | 0.010 | -0.213 | 0.200 | 0.009 | 0.457 | -0.466 |
| 30m | < 854.00 | 113694 | 12.47 | 37 | 32.17 | 0.948 | -0.255 | 1.203 | 0.027 | 0.013 | 0.200 | 6.027 |
| | 854.00 - 1455 | 209113 | 22.93 | 37 | 32.17 | 0.339 | -0.128 | 0.466 | 0.027 | 0.013 | 0.200 | 2.337 |
| | 1455.01 - 1949 | 292274 | 32.05 | 21 | 18.26 | -0.563 | 0.185 | -0.747 | 0.048 | 0.011 | 0.241 | -3.096 |
| | 1949.01 - 2619 | 243245 | 26.67 | 15 | 13.04 | -0.715 | 0.170 | -0.886 | 0.067 | 0.010 | 0.277 | -3.199 |
| | 2619 < | 53621 | 5.88 | 5 | 4.35 | -0.302 | 0.016 | -0.318 | 0.200 | 0.009 | 0.457 | -0.695 |
| 90m | < 854.00 | 12614 | 12.47 | 38 | 33.04 | 0.975 | -0.268 | 1.243 | 0.026 | 0.013 | 0.198 | 6.269 |
| | 854.00 - 1455 | 23263 | 22.99 | 36 | 31.30 | 0.309 | -0.114 | 0.423 | 0.028 | 0.013 | 0.201 | 2.103 |
| | 1455.01 - 1949 | 32472 | 32.09 | 22 | 19.13 | -0.517 | 0.175 | -0.692 | 0.045 | 0.011 | 0.237 | -2.919 |
| | 1949.01 - 2619 | 26898 | 26.58 | 14 | 12.17 | -0.781 | 0.179 | -0.960 | 0.071 | 0.010 | 0.285 | -3.367 |
| | 2619 < | 5936 | 5.87 | 5 | 4.35 | -0.300 | 0.016 | -0.316 | 0.200 | 0.009 | 0.457 | -0.690 |
| Slope(Degree) | | | | | | | | | | | | |
| 12.5m | 0 - 13.00 | 503807 | 9.59 | 9 | 7.83 | -0.203 | 0.019 | -0.223 | 0.111 | 0.009 | 0.347 | -0.642 |
| | 13.01 - 23.00 | 1027159 | 19.56 | 13 | 11.30 | -0.548 | 0.098 | -0.646 | 0.077 | 0.010 | 0.294 | -2.193 |
| | 23.01 - 32.00 | 1575077 | 29.99 | 33 | 28.70 | -0.044 | 0.018 | -0.062 | 0.030 | 0.012 | 0.206 | -0.302 |
| | 32.01 - 42.00 | 1537245 | 29.27 | 34 | 29.57 | 0.010 | -0.004 | 0.014 | 0.029 | 0.012 | 0.204 | 0.070 |
| | 42 < | 609312 | 11.60 | 26 | 22.61 | 0.667 | -0.133 | 0.800 | 0.038 | 0.011 | 0.223 | 3.590 |
| 30m | 0 - 13.00 | 93299 | 10.23 | 6 | 5.22 | -0.673 | 0.054 | -0.728 | 0.167 | 0.009 | 0.419 | -1.735 |
| | 13.01 - 23.00 | 195676 | 21.46 | 20 | 17.39 | -0.210 | 0.050 | -0.261 | 0.050 | 0.011 | 0.246 | -1.059 |
| | 23.01 - 32.00 | 275372 | 30.20 | 28 | 24.35 | -0.215 | 0.080 | -0.296 | 0.036 | 0.011 | 0.217 | -1.361 |
| | 32.01 - 42.00 | 255827 | 28.05 | 31 | 26.96 | -0.040 | 0.015 | -0.055 | 0.032 | 0.012 | 0.210 | -0.262 |
| | 42 < | 91773 | 10.06 | 30 | 26.09 | 0.953 | -0.196 | 1.149 | 0.033 | 0.012 | 0.212 | 5.409 |
| 90m | 0 - 13.00 | 11472 | 11.34 | 11 | 9.57 | -0.170 | 0.020 | -0.190 | 0.091 | 0.010 | 0.317 | -0.599 |
| | 13.01 - 23.00 | 27384 | 27.06 | 29 | 25.22 | -0.071 | 0.025 | -0.096 | 0.034 | 0.012 | 0.215 | -0.446 |
| | 23.01 - 32.00 | 35491 | 35.08 | 33 | 28.70 | -0.201 | 0.094 | -0.295 | 0.030 | 0.012 | 0.206 | -1.429 |
| | 32.01 - 42.00 | 23855 | 23.58 | 31 | 26.96 | 0.134 | -0.045 | 0.179 | 0.032 | 0.012 | 0.210 | 0.853 |
| | 42 < | 2981 | 2.95 | 11 | 9.57 | 1.178 | -0.071 | 1.248 | 0.091 | 0.010 | 0.317 | 3.937 |
| Aspect | | | | | | | | | | | | |
| 12.5m | Flat | 47614 | 0.91 | 0 | 0.00 | 0.000 | 0.009 | -0.009 | 0.000 | 0.009 | 0.000 | 0.000 |
| | North | 636941 | 12.13 | 5 | 4.35 | -1.026 | 0.085 | -1.111 | 0.200 | 0.009 | 0.457 | -2.429 |
| | NorthEast | 589967 | 11.23 | 9 | 7.83 | -0.361 | 0.038 | -0.399 | 0.111 | 0.009 | 0.347 | -1.149 |
| | East | 599110 | 11.41 | 15 | 13.04 | 0.134 | -0.019 | 0.153 | 0.067 | 0.010 | 0.277 | 0.552 |
| | SouthEast | 758507 | 14.44 | 33 | 28.70 | 0.687 | -0.182 | 0.869 | 0.030 | 0.012 | 0.206 | 4.215 |
| | South | 681513 | 12.97 | 19 | 16.52 | 0.242 | -0.042 | 0.283 | 0.053 | 0.010 | 0.251 | 1.128 |
| | SouthWest | 749811 | 14.28 | 15 | 13.04 | -0.090 | 0.014 | -0.104 | 0.067 | 0.010 | 0.277 | -0.377 |
| | West | 604243 | 11.50 | 8 | 6.96 | -0.503 | 0.050 | -0.553 | 0.125 | 0.009 | 0.367 | -1.509 |
| | NorthWest | 584894 | 11.14 | 11 | 9.57 | -0.152 | 0.018 | -0.170 | 0.091 | 0.010 | 0.317 | -0.535 |
| 30m | Flat | 285 | 0.03 | 0 | 0.00 | 0.000 | 0.000 | 0.000 | 0.000 | 0.009 | 0.093 | -0.003 |
| | North | 118174 | 12.96 | 6 | 5.22 | -0.910 | 0.085 | -0.995 | 0.167 | 0.009 | 0.419 | -2.373 |
| | NorthEast | 97997 | 10.75 | 9 | 7.83 | -0.317 | 0.032 | -0.349 | 0.111 | 0.009 | 0.347 | -1.006 |
| | East | 110602 | 12.13 | 14 | 12.17 | 0.004 | -0.001 | 0.004 | 0.071 | 0.010 | 0.285 | 0.015 |
| | SouthEast | 129200 | 14.17 | 33 | 28.70 | 0.706 | -0.185 | 0.891 | 0.030 | 0.012 | 0.206 | 4.323 |
| | South | 120454 | 13.21 | 18 | 15.65 | 0.170 | -0.029 | 0.198 | 0.056 | 0.010 | 0.257 | 0.773 |
| | SouthWest | 126820 | 13.91 | 18 | 15.65 | 0.118 | -0.020 | 0.139 | 0.056 | 0.010 | 0.257 | 0.541 |
| | West | 111498 | 12.23 | 7 | 6.09 | -0.697 | 0.068 | -0.765 | 0.143 | 0.009 | 0.390 | -1.962 |
| | NorthWest | 96917 | 10.63 | 10 | 8.70 | -0.201 | 0.021 | -0.222 | 0.100 | 0.010 | 0.331 | -0.671 |
| 90m | Flat | 6 | 0.01 | 0 | 0.00 | 0.000 | 0.000 | 0.000 | 0.000 | 0.009 | 0.093 | -0.001 |
| | North | 11739 | 11.60 | 6 | 5.22 | -0.799 | 0.070 | -0.869 | 0.167 | 0.009 | 0.419 | -2.072 |
| | NorthEast | 10792 | 10.67 | 5 | 4.35 | -0.897 | 0.068 | -0.966 | 0.200 | 0.009 | 0.457 | -2.112 |
| | East | 13004 | 12.85 | 16 | 13.91 | 0.079 | -0.012 | 0.092 | 0.063 | 0.010 | 0.269 | 0.340 |
| | SouthEast | 14659 | 14.49 | 29 | 25.22 | 0.554 | -0.134 | 0.688 | 0.034 | 0.012 | 0.215 | 3.205 |
| | South | 13247 | 13.09 | 24 | 20.87 | 0.466 | -0.094 | 0.560 | 0.042 | 0.011 | 0.229 | 2.441 |
| | SouthWest | 14400 | 14.23 | 13 | 11.30 | -0.230 | 0.034 | -0.264 | 0.077 | 0.010 | 0.294 | -0.896 |
| | West | 12655 | 12.51 | 10 | 8.70 | -0.363 | 0.043 | -0.406 | 0.100 | 0.010 | 0.331 | -1.227 |
| | NorthWest | 10681 | 10.56 | 12 | 10.43 | -0.012 | 0.001 | -0.013 | 0.083 | 0.010 | 0.305 | -0.042 |
| Curvature | | | | | | | | | | | | |
| 12.5m | Concave | 2214763 | 42.17 | 47 | 40.87 | -0.031 | 0.022 | -0.053 | 0.021 | 0.015 | 0.190 | -0.281 |
| | Flat | 802326 | 15.27 | 17 | 14.78 | -0.033 | 0.006 | -0.039 | 0.059 | 0.010 | 0.263 | -0.147 |
| | Convex | 2235511 | 42.56 | 51 | 44.35 | 0.041 | -0.032 | 0.073 | 0.020 | 0.016 | 0.188 | 0.388 |
| 30m | Concave | 434525 | 47.65 | 70 | 60.87 | 0.245 | -0.291 | 0.536 | 0.014 | 0.022 | 0.191 | 2.805 |
| | Flat | 36424 | 3.99 | 3 | 2.61 | -0.426 | 0.014 | -0.440 | 0.333 | 0.009 | 0.585 | -0.753 |
| | Convex | 440998 | 48.36 | 42 | 36.52 | -0.281 | 0.206 | -0.487 | 0.024 | 0.014 | 0.194 | -2.515 |
| 90m | Concave | 50045 | 49.46 | 73 | 63.48 | 0.250 | -0.325 | 0.574 | 0.014 | 0.024 | 0.194 | 2.966 |
| | Flat | 1309 | 1.29 | 0 | 0.00 | 0.000 | 0.013 | -0.013 | 0.000 | 0.009 | 0.093 | -0.140 |
| | Convex | 49829 | 49.25 | 42 | 36.52 | -0.299 | 0.224 | -0.523 | 0.024 | 0.014 | 0.194 | -2.699 |
| Toppographic Wetness Index | | | | | | | | | | | | |
| 12.5m | < 0.999 | 529278 | 10.08 | 12 | 10.43 | 0.035 | -0.004 | 0.039 | 0.083 | 0.010 | 0.305 | 0.128 |
| | 0.999 - 3.219 | 1520949 | 28.96 | 35 | 30.43 | 0.050 | -0.021 | 0.071 | 0.029 | 0.013 | 0.203 | 0.350 |
| | 3.220 - 6.688 | 486118 | 9.25 | 7 | 6.09 | -0.419 | 0.034 | -0.453 | 0.143 | 0.009 | 0.390 | -1.162 |
| | 6.688 < | 2716255 | 51.71 | 61 | 53.04 | 0.025 | -0.028 | 0.053 | 0.016 | 0.019 | 0.187 | 0.286 |
| 30m | < 0.999 | 200164 | 21.95 | 27 | 23.48 | 0.067 | -0.020 | 0.087 | 0.037 | 0.011 | 0.220 | 0.396 |
| | 0.999 - 3.219 | 217946 | 23.90 | 31 | 26.96 | 0.120 | -0.041 | 0.161 | 0.032 | 0.012 | 0.210 | 0.768 |
| | 3.220 - 6.688 | 37006 | 4.06 | 5 | 4.35 | 0.069 | -0.003 | 0.072 | 0.200 | 0.009 | 0.457 | 0.158 |
| | 6.688 < | 456831 | 50.09 | 52 | 45.22 | -0.102 | 0.093 | -0.196 | 0.019 | 0.016 | 0.187 | -1.044 |
| 90m | < 0.999 | 38278 | 37.83 | 46 | 40.00 | 0.056 | -0.036 | 0.091 | 0.022 | 0.014 | 0.190 | 0.480 |
| | 0.999 - 3.219 | 11135 | 11.00 | 11 | 9.57 | -0.140 | 0.016 | -0.156 | 0.091 | 0.010 | 0.317 | -0.493 |
| | 3.220 - 6.688 | 1358 | 1.34 | 1 | 0.87 | -0.434 | 0.005 | -0.439 | 1.000 | 0.009 | 1.004 | -0.437 |

| | | | | | | | | | | | | |
|---|---|---|---|---|---|---|---|---|---|---|---|---|
| | 6.688 < | 50412 | 49.82 | 57 | 49.57 | -0.005 | 0.005 | -0.010 | 0.018 | 0.017 | 0.187 | -0.055 |
| Stream Power Index | | | | | | | | | | | | |
| 12.5m | < -4.052 | 850701 | 16.20 | 16 | 13.91 | -0.152 | 0.027 | -0.179 | 0.063 | 0.010 | 0.269 | -0.664 |
| | -4.052 - 0.886 | 1638515 | 31.19 | 31 | 26.96 | -0.146 | 0.060 | -0.206 | 0.032 | 0.012 | 0.210 | -0.979 |
| | 0.887 - 3.529 | 2336225 | 44.48 | 59 | 51.30 | 0.143 | -0.131 | 0.274 | 0.017 | 0.018 | 0.187 | 1.469 |
| | 3.529 < | 427159 | 8.13 | 9 | 7.83 | -0.038 | 0.003 | -0.042 | 0.111 | 0.009 | 0.347 | -0.120 |
| 30m | < -4.052 | 233485 | 25.60 | 18 | 15.65 | -0.492 | 0.126 | -0.618 | 0.056 | 0.010 | 0.257 | -2.407 |
| | -4.052 - 0.886 | 344021 | 37.72 | 44 | 38.26 | 0.014 | -0.009 | 0.023 | 0.023 | 0.014 | 0.192 | 0.119 |
| | 0.887 - 3.529 | 274078 | 30.05 | 39 | 33.91 | 0.121 | -0.057 | 0.178 | 0.026 | 0.013 | 0.197 | 0.901 |
| | 3.529 < | 60363 | 6.62 | 14 | 12.17 | 0.609 | -0.061 | 0.671 | 0.071 | 0.010 | 0.285 | 2.352 |
| 90m | < -4.052 | 32999 | 32.61 | 28 | 24.35 | -0.292 | 0.116 | -0.408 | 0.036 | 0.011 | 0.217 | -1.878 |
| | -4.052 - 0.886 | 42295 | 41.80 | 45 | 39.13 | -0.066 | 0.045 | -0.111 | 0.022 | 0.014 | 0.191 | -0.580 |
| | 0.887 - 3.529 | 20832 | 20.59 | 37 | 32.17 | 0.446 | -0.158 | 0.604 | 0.027 | 0.013 | 0.200 | 3.026 |
| | 3.529 < | 5057 | 5.00 | 5 | 4.35 | -0.139 | 0.007 | -0.146 | 0.200 | 0.009 | 0.457 | -0.320 |
| Drainage Density | | | | | | | | | | | | |
| 12.5m | < 0.545 | 964147 | 18.36 | 6 | 5.22 | -1.258 | 0.149 | -1.407 | 0.167 | 0.009 | 0.419 | -3.356 |
| | 0.545 - 0.854 | 1329522 | 25.31 | 37 | 32.17 | 0.240 | -0.096 | 0.336 | 0.027 | 0.013 | 0.200 | 1.685 |
| | 0.855 - 1.153 | 1269392 | 24.17 | 44 | 38.26 | 0.459 | -0.206 | 0.665 | 0.023 | 0.014 | 0.192 | 3.466 |
| | 1.154 - 1.462 | 1111965 | 21.17 | 21 | 18.26 | -0.148 | 0.036 | -0.184 | 0.048 | 0.011 | 0.241 | -0.763 |
| | 1.462 < | 577574 | 11.00 | 7 | 6.09 | -0.591 | 0.054 | -0.645 | 0.143 | 0.009 | 0.390 | -1.654 |
| 30m | < 0.545 | 167456 | 18.36 | 6 | 5.22 | -1.258 | 0.149 | -1.408 | 0.167 | 0.009 | 0.419 | -3.357 |
| | 0.545 - 0.854 | 230872 | 25.32 | 37 | 32.17 | 0.240 | -0.096 | 0.336 | 0.027 | 0.013 | 0.200 | 1.683 |
| | 0.855 - 1.153 | 220395 | 24.17 | 44 | 38.26 | 0.459 | -0.206 | 0.665 | 0.023 | 0.014 | 0.192 | 3.466 |
| | 1.154 - 1.462 | 192998 | 21.16 | 21 | 18.26 | -0.148 | 0.036 | -0.184 | 0.048 | 0.011 | 0.241 | -0.761 |
| | 1.462 < | 100226 | 10.99 | 7 | 6.09 | -0.591 | 0.054 | -0.644 | 0.143 | 0.009 | 0.390 | -1.652 |
| 90m | < 0.545 | 18485 | 18.27 | 7 | 6.09 | -1.099 | 0.139 | -1.238 | 0.143 | 0.009 | 0.390 | -3.174 |
| | 0.545 - 0.854 | 25650 | 25.35 | 36 | 31.3 | 0.211 | -0.083 | 0.294 | 0.028 | 0.013 | 0.201 | 1.463 |
| | 0.855 - 1.153 | 24516 | 24.23 | 43 | 37.39 | 0.434 | -0.191 | 0.625 | 0.023 | 0.014 | 0.193 | 3.241 |
| | 1.154 - 1.462 | 21420 | 21.17 | 22 | 19.13 | -0.101 | 0.026 | -0.127 | 0.045 | 0.011 | 0.237 | -0.535 |
| | 1.462 < | 11112 | 10.98 | 7 | 6.09 | -0.590 | 0.054 | -0.644 | 0.143 | 0.009 | 0.390 | -1.650 |
| Normalized Difference Vegetation Index | | | | | | | | | | | | |
| 12.5m | <223 | 219873 | 4.19 | 32 | 27.83 | 1.894 | -0.283 | 2.178 | 0.031 | 0.012 | 0.208 | 10.465 |
| | 0.223 - 0.407 | 574346 | 10.93 | 19 | 16.52 | 0.413 | -0.065 | 0.478 | 0.053 | 0.010 | 0.251 | 1.902 |
| | 0.408 - 0.562 | 877493 | 16.71 | 20 | 17.39 | 0.040 | -0.008 | 0.048 | 0.050 | 0.011 | 0.246 | 0.197 |
| | 0.563 - 0.688 | 1492466 | 28.41 | 25 | 21.74 | -0.268 | 0.089 | -0.357 | 0.040 | 0.011 | 0.226 | -1.579 |
| | 0.688 < | 2088422 | 39.76 | 19 | 16.52 | -0.878 | 0.326 | -1.204 | 0.053 | 0.010 | 0.251 | -4.797 |
| 30m | <223 | 38264 | 4.20 | 22 | 19.13 | 1.517 | -0.169 | 1.687 | 0.045 | 0.011 | 0.237 | 7.114 |
| | 0.223 - 0.407 | 99842 | 10.95 | 28 | 24.35 | 0.799 | -0.163 | 0.962 | 0.036 | 0.011 | 0.217 | 4.429 |
| | 0.408 - 0.562 | 152092 | 16.68 | 17 | 14.78 | -0.121 | 0.022 | -0.143 | 0.059 | 0.010 | 0.263 | -0.545 |
| | 0.563 - 0.688 | 259052 | 28.41 | 26 | 22.61 | -0.228 | 0.078 | -0.306 | 0.038 | 0.011 | 0.223 | -1.373 |
| | 0.688 < | 362697 | 39.77 | 22 | 19.13 | -0.732 | 0.295 | -1.027 | 0.045 | 0.011 | 0.237 | -4.330 |
| 90m | <223 | 4269 | 4.22 | 17 | 14.78 | 1.254 | -0.117 | 1.371 | 0.059 | 0.010 | 0.263 | 5.217 |
| | 0.223 - 0.407 | 11050 | 10.92 | 21 | 18.26 | 0.514 | -0.086 | 0.600 | 0.048 | 0.011 | 0.241 | 2.486 |
| | 0.408 - 0.562 | 16732 | 16.54 | 18 | 15.65 | -0.055 | 0.011 | -0.065 | 0.056 | 0.010 | 0.257 | -0.255 |
| | 0.563 - 0.688 | 29073 | 28.73 | 26 | 22.61 | -0.240 | 0.082 | -0.322 | 0.038 | 0.011 | 0.223 | -1.445 |
| | 0.688 < | 40059 | 39.59 | 33 | 28.70 | -0.322 | 0.166 | -0.488 | 0.030 | 0.012 | 0.206 | -2.366 |
| Normalized Difference Soil Index | | | | | | | | | | | | |
| 12.5m | < -0.516 | 484543 | 9.22 | 8 | 6.96 | -0.282 | 0.025 | -0.307 | 0.125 | 0.009 | 0.367 | -0.837 |
| | -0.516 - -0.273 | 946456 | 18.02 | 10 | 8.70 | -0.729 | 0.108 | -0.836 | 0.100 | 0.010 | 0.331 | -2.527 |
| | -0.274 - -0.097 | 1471428 | 28.01 | 16 | 13.91 | -0.700 | 0.179 | -0.879 | 0.063 | 0.010 | 0.269 | -3.261 |
| | -0.098 - 0.078 | 1655777 | 31.52 | 43 | 37.39 | 0.171 | -0.090 | 0.260 | 0.023 | 0.014 | 0.193 | 1.351 |
| | 0.078 < | 694396 | 13.22 | 38 | 33.04 | 0.916 | -0.259 | 1.175 | 0.026 | 0.013 | 0.198 | 5.929 |
| 30m | < -0.516 | 84053 | 9.22 | 8 | 6.96 | -0.281 | 0.025 | -0.306 | 0.125 | 0.009 | 0.367 | -0.835 |
| | -0.516 - -0.273 | 164589 | 18.05 | 12 | 10.43 | -0.548 | 0.089 | -0.637 | 0.083 | 0.010 | 0.305 | -2.087 |
| | -0.274 - -0.097 | 255238 | 27.99 | 13 | 11.30 | -0.907 | 0.208 | -1.115 | 0.077 | 0.010 | 0.294 | -3.786 |
| | -0.098 - 0.078 | 287262 | 31.5 | 43 | 37.39 | 0.171 | -0.090 | 0.261 | 0.023 | 0.014 | 0.193 | 1.356 |
| | 0.078 < | 120805 | 13.25 | 39 | 33.91 | 0.940 | -0.272 | 1.212 | 0.026 | 0.013 | 0.197 | 6.154 |
| 90m | < -0.516 | 9379 | 9.27 | 9 | 7.83 | -0.169 | 0.016 | -0.185 | 0.111 | 0.009 | 0.347 | -0.533 |
| | -0.516 - -0.273 | 18265 | 18.05 | 10 | 8.70 | -0.730 | 0.108 | -0.839 | 0.100 | 0.010 | 0.331 | -2.534 |
| | -0.274 - -0.097 | 28423 | 28.09 | 22 | 19.13 | -0.384 | 0.117 | -0.502 | 0.045 | 0.011 | 0.237 | -2.116 |
| | -0.098 - 0.078 | 31704 | 31.33 | 38 | 33.04 | 0.053 | -0.025 | 0.078 | 0.026 | 0.013 | 0.198 | 0.395 |
| | 0.078 < | 13412 | 13.26 | 36 | 31.30 | 0.859 | -0.233 | 1.093 | 0.028 | 0.013 | 0.201 | 5.434 |
| Distance from the river(m) | | | | | | | | | | | | |
| 12.5m | 0-100 | 176948 | 3.37 | 6 | 5.22 | 0.437 | -0.019 | 0.457 | 0.167 | 0.009 | 0.419 | 1.089 |
| | 100-200 | 162601 | 3.10 | 2 | 1.74 | -0.577 | 0.014 | -0.591 | 0.500 | 0.009 | 0.713 | -0.828 |
| | 200-300 | 158292 | 3.01 | 4 | 3.48 | 0.143 | -0.005 | 0.148 | 0.250 | 0.009 | 0.509 | 0.291 |
| | 300-400 | 157852 | 3.01 | 4 | 3.48 | 0.146 | -0.005 | 0.151 | 0.250 | 0.009 | 0.509 | 0.297 |
| | 400< | 4596907 | 87.52 | 99 | 86.09 | -0.016 | 0.108 | -0.125 | 0.010 | 0.063 | 0.269 | -0.464 |
| 30m | 0-100 | 31639 | 3.47 | 7 | 6.09 | 0.562 | -0.027 | 0.590 | 0.143 | 0.009 | 0.390 | 1.512 |
| | 100-200 | 27341 | 3.00 | 1 | 0.87 | -1.238 | 0.022 | -1.259 | 1.000 | 0.009 | 1.004 | -1.254 |
| | 200-300 | 29785 | 3.27 | 4 | 3.48 | 0.063 | -0.002 | 0.065 | 0.250 | 0.009 | 0.509 | 0.128 |
| | 300-400 | 25379 | 2.78 | 4 | 3.48 | 0.223 | -0.007 | 0.230 | 0.250 | 0.009 | 0.509 | 0.452 |
| | 400< | 797803 | 87.48 | 99 | 86.09 | -0.016 | 0.106 | -0.122 | 0.010 | 0.063 | 0.269 | -0.452 |
| 90m | 0-100 | 4349 | 4.30 | 8 | 6.96 | 0.481 | -0.028 | 0.510 | 0.125 | 0.009 | 0.367 | 1.391 |
| | 100-200 | 2476 | 2.45 | 1 | 0.87 | -1.035 | 0.016 | -1.051 | 1.000 | 0.009 | 1.004 | -1.046 |
| | 200-300 | 3448 | 3.41 | 4 | 3.48 | 0.020 | -0.001 | 0.021 | 0.250 | 0.009 | 0.509 | 0.042 |
| | 300-400 | 2799 | 2.77 | 4 | 3.48 | 0.229 | -0.007 | 0.236 | 0.250 | 0.009 | 0.509 | 0.464 |
| | 400< | 88111 | 87.08 | 98 | 85.22 | -0.022 | 0.135 | -0.156 | 0.010 | 0.059 | 0.263 | -0.595 |
| Distance from the fault(m) | | | | | | | | | | | | |
| 12.5m | 0-100 | 219126 | 4.17 | 1 | 0.87 | -1.568 | 0.034 | -1.602 | 1.000 | 0.009 | 1.004 | -1.595 |
| | 100-200 | 206180 | 3.93 | 5 | 4.35 | 0.102 | -0.004 | 0.107 | 0.200 | 0.009 | 0.457 | 0.233 |
| | 200-300 | 198818 | 3.79 | 6 | 5.22 | 0.321 | -0.015 | 0.336 | 0.167 | 0.009 | 0.419 | 0.801 |
| | 300-400 | 180361 | 3.43 | 5 | 4.35 | 0.236 | -0.010 | 0.246 | 0.200 | 0.009 | 0.457 | 0.537 |
| | 400< | 4448115 | 84.68 | 98 | 85.22 | 0.006 | -0.035 | 0.042 | 0.010 | 0.059 | 0.263 | 0.159 |
| 30m | 0-100 | 39885 | 4.37 | 1 | 0.87 | -1.615 | 0.036 | -1.651 | 1.000 | 0.009 | 1.004 | -1.644 |
| | 100-200 | 33632 | 3.69 | 5 | 4.35 | 0.165 | -0.007 | 0.171 | 0.200 | 0.009 | 0.457 | 0.375 |
| | 200-300 | 37929 | 4.16 | 7 | 6.09 | 0.381 | -0.020 | 0.401 | 0.143 | 0.009 | 0.390 | 1.029 |
| | 300-400 | 29107 | 3.19 | 3 | 2.61 | -0.202 | 0.006 | -0.208 | 0.333 | 0.009 | 0.585 | -0.355 |
| | 400< | 771394 | 84.59 | 99 | 86.09 | 0.018 | -0.102 | 0.120 | 0.010 | 0.063 | 0.269 | 0.445 |
| 90m | 0-100 | 5536 | 5.47 | 4 | 3.48 | -0.453 | 0.021 | -0.474 | 0.250 | 0.009 | 0.509 | -0.931 |
| | 100-200 | 3333 | 3.29 | 4 | 3.48 | 0.054 | -0.002 | 0.056 | 0.250 | 0.009 | 0.509 | 0.111 |
| | 200-300 | 4076 | 4.03 | 5 | 4.35 | 0.076 | -0.003 | 0.080 | 0.200 | 0.009 | 0.457 | 0.174 |
| | 300-400 | 3028 | 2.99 | 6 | 5.22 | 0.556 | -0.023 | 0.579 | 0.167 | 0.009 | 0.419 | 1.381 |
| | 400< | 85210 | 84.21 | 96 | 83.48 | -0.009 | 0.046 | -0.054 | 0.010 | 0.053 | 0.251 | -0.216 |
| Distance from the road(m) | | | | | | | | | | | | |
| 12.5m | 0-100 | 166121 | 3.16 | 5 | 4.35 | 0.318 | -0.012 | 0.331 | 0.200 | 0.009 | 0.457 | 0.723 |

| | | | | | | | | | | | | |
|---|---|---|---|---|---|---|---|---|---|---|---|---|
| | 100-200 | 136503 | 2.60 | 2 | 1.74 | -0.402 | 0.009 | -0.410 | 0.500 | 0.009 | 0.713 | -0.575 |
| | 200-300 | 126201 | 2.40 | 6 | 5.22 | 0.775 | -0.029 | 0.805 | 0.167 | 0.009 | 0.419 | 1.919 |
| | 300-400 | 120319 | 2.29 | 2 | 1.74 | -0.275 | 0.006 | -0.281 | 0.500 | 0.009 | 0.713 | -0.394 |
| | 400< | 4703456 | 89.55 | 100 | 86.96 | -0.029 | 0.221 | -0.251 | 0.010 | 0.067 | 0.277 | -0.905 |
| 30m | 0-100 | 30136 | 3.30 | 5 | 4.35 | 0.274 | -0.011 | 0.285 | 0.200 | 0.009 | 0.457 | 0.624 |
| | 100-200 | 22593 | 2.48 | 3 | 2.61 | 0.052 | -0.001 | 0.053 | 0.333 | 0.009 | 0.585 | 0.091 |
| | 200-300 | 23374 | 2.56 | 6 | 5.22 | 0.711 | -0.028 | 0.738 | 0.167 | 0.009 | 0.419 | 1.761 |
| | 300-400 | 19606 | 2.15 | 1 | 0.87 | -0.905 | 0.013 | -0.918 | 1.000 | 0.009 | 1.004 | -0.914 |
| | 400< | 816238 | 89.50 | 100 | 86.96 | -0.029 | 0.217 | -0.246 | 0.010 | 0.067 | 0.277 | -0.889 |
| 90m | 0-100 | 4024 | 3.98 | 5 | 4.35 | 0.089 | -0.004 | 0.093 | 0.200 | 0.009 | 0.457 | 0.203 |
| | 100-200 | 2011 | 1.99 | 2 | 1.74 | -0.133 | 0.003 | -0.136 | 0.500 | 0.009 | 0.713 | -0.191 |
| | 200-300 | 2740 | 2.71 | 7 | 6.09 | 0.810 | -0.035 | 0.845 | 0.143 | 0.009 | 0.390 | 2.167 |
| | 300-400 | 2082 | 2.06 | 2 | 1.74 | -0.168 | 0.003 | -0.171 | 0.500 | 0.009 | 0.713 | -0.240 |
| | 400< | 90326 | 89.27 | 99 | 86.09 | -0.036 | 0.260 | -0.296 | 0.010 | 0.063 | 0.269 | -1.099 |
| Lithology | | | | | | | | | | | | |
| 12.5m | Tsm | 555267 | 10.57 | 32 | 27.83 | 0.968 | -0.214 | 1.182 | 0.031 | 0.012 | 0.208 | 5.681 |
| | Pzc | 55299 | 1.05 | 1 | 0.87 | -0.191 | 0.002 | -0.193 | 1.000 | 0.009 | 1.004 | -0.192 |
| | pCd | 199124 | 3.79 | 12 | 10.43 | 1.013 | -0.072 | 1.084 | 0.083 | 0.010 | 0.305 | 3.554 |
| | GHlml | 132280 | 2.52 | 5 | 4.35 | 0.546 | -0.019 | 0.565 | 0.200 | 0.009 | 0.457 | 1.236 |
| | GHlo | 936177 | 17.82 | 23 | 20.00 | 0.115 | -0.027 | 0.142 | 0.043 | 0.011 | 0.233 | 0.609 |
| | Tgr | 3374453 | 64.24 | 42 | 36.52 | -0.565 | 0.574 | -1.139 | 0.024 | 0.014 | 0.194 | -5.880 |
| 30m | Tsm | 96424 | 10.57 | 32 | 26.02 | 0.900 | -0.190 | 1.090 | 0.031 | 0.012 | 0.208 | 5.238 |
| | Pzc | 9617 | 1.05 | 1 | 0.87 | -0.193 | 0.002 | -0.195 | 1.000 | 0.009 | 1.004 | -0.194 |
| | pCd | 34574 | 3.79 | 12 | 10.43 | 1.012 | -0.072 | 1.084 | 0.083 | 0.010 | 0.305 | 3.554 |
| | GHlml | 22953 | 2.52 | 5 | 4.35 | 0.547 | -0.019 | 0.566 | 0.200 | 0.009 | 0.457 | 1.237 |
| | GHlo | 162532 | 17.82 | 23 | 20.00 | 0.115 | -0.027 | 0.142 | 0.043 | 0.011 | 0.233 | 0.610 |
| | Tgr | 585847 | 64.24 | 42 | 36.52 | -0.565 | 0.574 | -1.139 | 0.024 | 0.014 | 0.194 | -5.879 |
| 90m | Tsm | 10716 | 10.59 | 32 | 27.83 | 0.966 | -0.214 | 1.180 | 0.031 | 0.012 | 0.208 | 5.672 |
| | Pzc | 18107 | 17.90 | 23 | 20.00 | 0.111 | -0.026 | 0.137 | 0.043 | 0.011 | 0.233 | 0.588 |
| | pCd | 3846 | 3.80 | 12 | 10.43 | 1.010 | -0.071 | 1.081 | 0.083 | 0.010 | 0.305 | 3.545 |
| | GHlml | 2549 | 2.52 | 5 | 4.35 | 0.546 | -0.019 | 0.565 | 0.200 | 0.009 | 0.457 | 1.235 |
| | GHlo | 64931 | 64.17 | 42 | 36.52 | -0.564 | 0.572 | -1.136 | 0.024 | 0.014 | 0.194 | -5.864 |
| | Tgr | 1034 | 1.02 | 1 | 0.87 | -0.161 | 0.002 | -0.163 | 1.000 | 0.009 | 1.004 | -0.162 |
| Rainfall(mm) | | | | | | | | | | | | |
| 12.5m | 1786.79 - 2434.61 | 1345852 | 25.62 | 19 | 16.52 | -0.439 | 0.115 | -0.554 | 0.053 | 0.010 | 0.251 | -2.207 |
| | 2434.62 - 2930.01 | 1499293 | 28.54 | 15 | 13.04 | -0.783 | 0.196 | -0.979 | 0.067 | 0.010 | 0.277 | -3.537 |
| | 2930.02 - 3539.74 | 1065871 | 20.29 | 16 | 13.91 | -0.377 | 0.077 | -0.454 | 0.063 | 0.010 | 0.269 | -1.686 |
| | 3539.75 - 4225.67 | 710092 | 13.52 | 39 | 33.91 | 0.920 | -0.269 | 1.189 | 0.026 | 0.013 | 0.197 | 6.035 |
| | 4225.68 - 5025.93 | 631492 | 12.02 | 26 | 22.61 | 0.632 | -0.128 | 0.760 | 0.038 | 0.011 | 0.223 | 3.408 |
| 30m | 1786.79 - 2434.61 | 233498 | 25.60 | 19 | 16.52 | -0.438 | 0.115 | -0.553 | 0.053 | 0.010 | 0.251 | -2.203 |
| | 2434.62 - 2930.01 | 260364 | 28.55 | 14 | 12.17 | -0.852 | 0.206 | -1.059 | 0.071 | 0.010 | 0.285 | -3.712 |
| | 2930.02 - 3539.74 | 185119 | 20.30 | 17 | 14.78 | -0.317 | 0.067 | -0.384 | 0.059 | 0.010 | 0.263 | -1.462 |
| | 3539.75 - 4225.67 | 123357 | 13.53 | 39 | 33.91 | 0.919 | -0.269 | 1.188 | 0.026 | 0.013 | 0.197 | 6.031 |
| | 4225.68 - 5025.93 | 109609 | 12.02 | 26 | 22.61 | 0.632 | -0.128 | 0.760 | 0.038 | 0.011 | 0.223 | 3.409 |
| 90m | 1786.79 - 2434.61 | 25797 | 25.50 | 19 | 16.52 | -0.434 | 0.114 | -0.548 | 0.053 | 0.010 | 0.251 | -2.181 |
| | 2434.62 - 2930.01 | 28937 | 28.60 | 14 | 12.17 | -0.854 | 0.207 | -1.061 | 0.071 | 0.010 | 0.285 | -3.721 |
| | 2930.02 - 3539.74 | 20564 | 20.32 | 16 | 13.91 | -0.379 | 0.077 | -0.456 | 0.063 | 0.010 | 0.269 | -1.694 |
| | 3539.75 - 4225.67 | 13715 | 13.55 | 40 | 34.78 | 0.942 | -0.282 | 1.224 | 0.025 | 0.013 | 0.196 | 6.253 |
| | 4225.68 - 5025.93 | 12170 | 12.03 | 26 | 22.61 | 0.631 | -0.128 | 0.759 | 0.038 | 0.011 | 0.223 | 3.406 |
| Land use land cover | | | | | | | | | | | | |
| 12.5m | Agricultural Land | 172063 | 3.28 | 2 | 1.74 | -0.633 | 0.016 | -0.649 | 0.500 | 0.009 | 0.713 | -0.910 |
| | Built Up Area | 4943 | 0.09 | 0 | 0.00 | 0.000 | 0.001 | -0.001 | 0.000 | 0.009 | 0.093 | -0.010 |
| | Forest | 4863000 | 92.58 | 110 | 95.65 | 0.033 | -0.534 | 0.567 | 0.009 | 0.200 | 0.457 | 1.239 |
| | Shrub | 130659 | 2.49 | 3 | 2.61 | 0.048 | -0.001 | 0.049 | 0.333 | 0.009 | 0.585 | 0.083 |
| | Water Bodies | 81935 | 1.56 | 0 | 0.00 | 0.000 | 0.016 | -0.016 | 0.000 | 0.009 | 0.093 | -0.169 |
| 30m | Agricultural Land | 29903 | 3.28 | 2 | 1.74 | -0.634 | 0.016 | -0.650 | 0.500 | 0.009 | 0.713 | -0.911 |
| | Built Up Area | 851 | 0.09 | 0 | 0.00 | 0.000 | 0.001 | -0.001 | 0.000 | 0.009 | 0.093 | -0.010 |
| | Forest | 844305 | 92.58 | 110 | 95.65 | 0.033 | -0.534 | 0.567 | 0.009 | 0.200 | 0.457 | 1.239 |
| | Shrub | 22629 | 2.48 | 3 | 2.61 | 0.050 | -0.001 | 0.051 | 0.333 | 0.009 | 0.585 | 0.088 |
| | Water Bodies | 14259 | 1.56 | 0 | 0.00 | 0.000 | 0.016 | -0.016 | 0.000 | 0.009 | 0.093 | -0.169 |
| 90m | Agricultural Land | 3261 | 3.22 | 2 | 1.74 | -0.617 | 0.015 | -0.632 | 0.500 | 0.009 | 0.713 | -0.886 |
| | Built Up Area | 96 | 0.09 | 0 | 0.00 | 0.000 | 0.001 | -0.001 | 0.000 | 0.009 | 0.093 | -0.010 |
| | Forest | 93764 | 92.67 | 107 | 93.04 | 0.004 | -0.053 | 0.057 | 0.009 | 0.125 | 0.367 | 0.155 |
| | Shrub | 2467 | 2.44 | 5 | 4.35 | 0.578 | -0.020 | 0.598 | 0.200 | 0.009 | 0.457 | 1.308 |
| | Water Bodies | 1595 | 1.58 | 1 | 0.87 | -0.595 | 0.007 | -0.602 | 1.000 | 0.009 | 1.004 | -0.599 |